Reviewer 1.

We thank the reviewer for their careful reading of the manuscript. We address each of the comments in turn below, with the comments first given in bold, followed by the response in normal type, followed by any changes made to the manuscript.

Figure 1: I fully appreciate the challenge in creating efficient and accurate diagrams such as Figure 1 to portray the chemistry of radical cycling. The species in green are described as primary routes for radical formation. I agree with the way that ozone is portrayed given that its role as an initiator as well as a product of the chemistry is shown. Both HONO and HCHO need to be better explained as they are also chemical products. Maybe a line from RO to CH2O acknowledging that CH2O is coming from oxidation (likely most of it) although some is also directly emitted. For HONO, its origin is still not well understood, so maybe this should be acknowledged in the caption by noting that it's abundance cannot be fully explained by formation via OH+NO. In the literature, CH2O and H2O2 are typically described as being responsible for "secondary" radical production rather than "primary" radical sources. While there may be a large primary source of CH2O in this particular environment, the same is not true for H2O2. One potential solution is to avoid the whole use of the word "primary" and simply say that the "green circles represent species that contribute to radical formation."

A line between RO to HCHO has been added, and as suggested by the reviewer the caption has been changed so that the green circles represent species that contribute to radical formation.

Updated figure below:

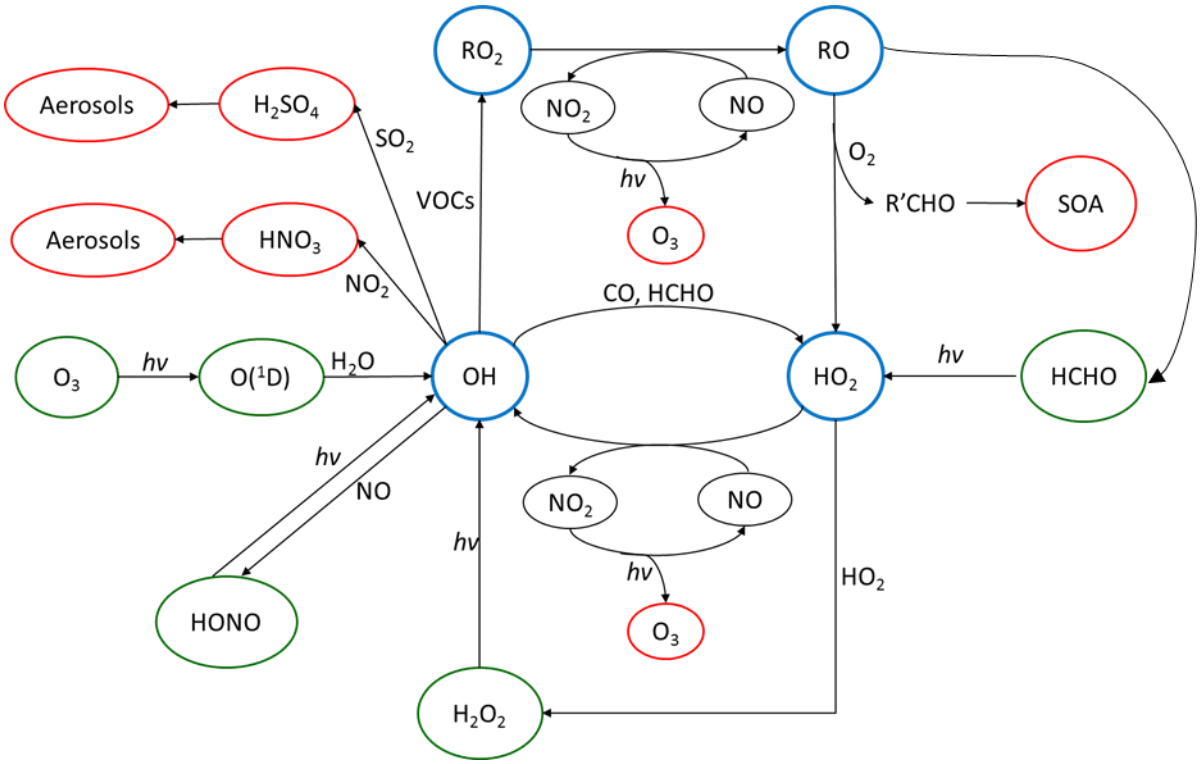

Updated/Modified caption: Figure 1. "The tropospheric photochemical cycle, with the green circles representing species acting as routes for radical formation, the blue circles representing the radical species themselves and the red circles representing the formation of secondary pollutants. The cycle does not show any heterogeneous source (e.g. heterogeneous production of HONO) or loss processes for the radical species. It should be noted the measured HONO abundance cannot be explained by the reaction of OH + NO alone"

Is there a significance to the two additional yellow stars in Figure 2?

No. In order to avoid confusion these have been removed from Figure 2 Please see updated Figure 2 below:

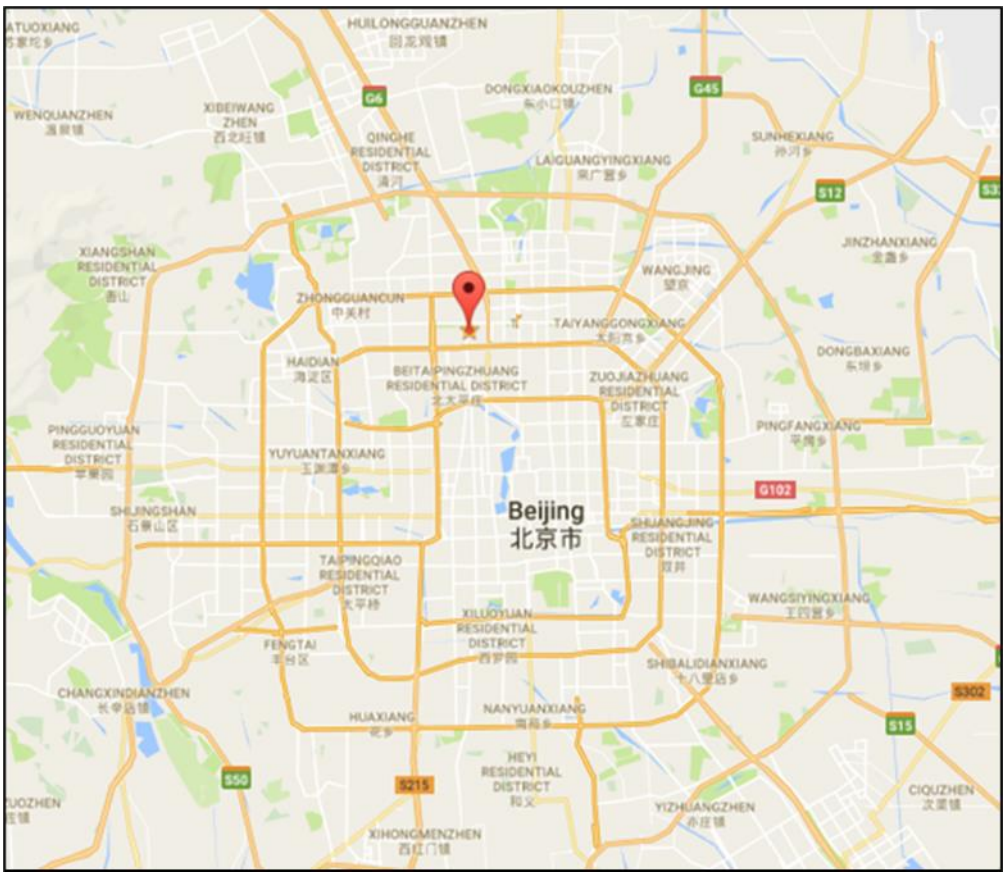

Typo on line 277: O2 should be O3

This has been fixed.

The mention of an AIRPRO project first comes up on line 160. It is mentioned again in the caption of Figure 3, then in Table 4, and again on line 473. Otherwise, all other references in the text, figures, and tables are to APHH. Only in the summary (line 754) do the authors finally say the "APHH AIRPRO campaign". Is AIRPRO an acronym? If so, it is undefined. Is it even necessary to mention AIRPRO? If so, it is crucial to make a clear distinction between what is meant by APHH versus AIRPRO.

We have removed AIRPRO from the paper so that the campaign is just called the APHH campaign.

On line 226, the authors note that the model was constrained by HCHO, but this species is not shown in Figure 4. This may be because it had minimal influence on radical production, but it is also a key outcome from VOC oxidation. While I am not surprised that it is small compared to HONO, I am somewhat surprised that it doesn't seem to be important compared to photolysis of other carbonyl species and alkene ozonolysis. I would like to see HCHO added to Figure 4.

HCHO has been added to Figure 4. See updated figure and caption below:

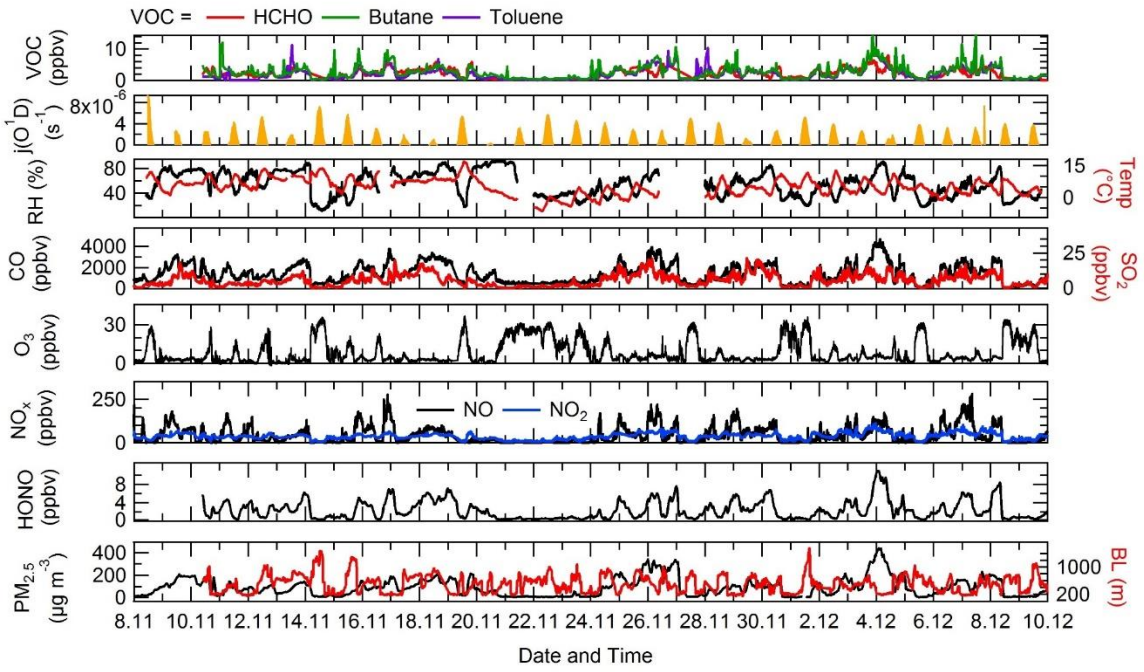

Figure 4. Time-series of $j(O^1D)$, relative humidity (RH), temperature (Temp), CO, SO_2, O_3, NO_x, HONO, boundary layer (BL), $PM_{2.5}$, HCHO, butane and toluene from the 8th of November to 10th December 2016 at Institute of Atmospheric Physics (IAP), Beijing.

As shown in Figure 9 the photolysis of HCHO contribute ~2% to the primary formation of RO_x.

There is no comment about using PAN as a constraint, so was it predicted by the model? How well does it compare? Could it be a radical source at the surface?

PAN was not measured during the winter APHH campaign (only during the summer campaign) thus no comparison could be made between modelled and measured values. Indeed, it may be a radical source at the surface, however, the analysis of production and termination of radicals shown in Figure 9 shows a net-formation of PAN – suggesting that PAN is acting as an overall net RO_2 sink.

Figure 4 would also be improved if a few more things were added. For instance, a couple of VOCs (an alkene and an aromatic would be good). Also, there was a ceilometer at the site. Could mixing height be added to the figure? I expect it would be quite relevant to some of the variability marking the haze periods. While this information does not alter the outcome of the paper, it provides valuable additional context.

HCHO, butane, toluene and boundary layer height have all been added to Figure 4 (see response above for updated version of the Figure 4 and caption), and a short discussion about this has been added.

Modified text related to Figure 4:

"The median diel variation in $j(O^1D)$, relative humidity (RH), temperature, CO, SO_2, O_3, NO,NO_2, HONO, $PM_{2.5,}$ boundary layer height (BL), HCHO, butane and toluene is shown in Figure 4."

"The VOC concentration (HCHO, toluene and butane) track pollution events and each other very well; the mole fraction of the VOCs varied between 0.2 - 11.3 ppbv."

The average diel profile of boundary layer height has also been added to Figure 5, replacing the SO_2 panel, both for inside and outside of haze, along with a short discussion.

Updated version of Figure 5 with the updated caption:

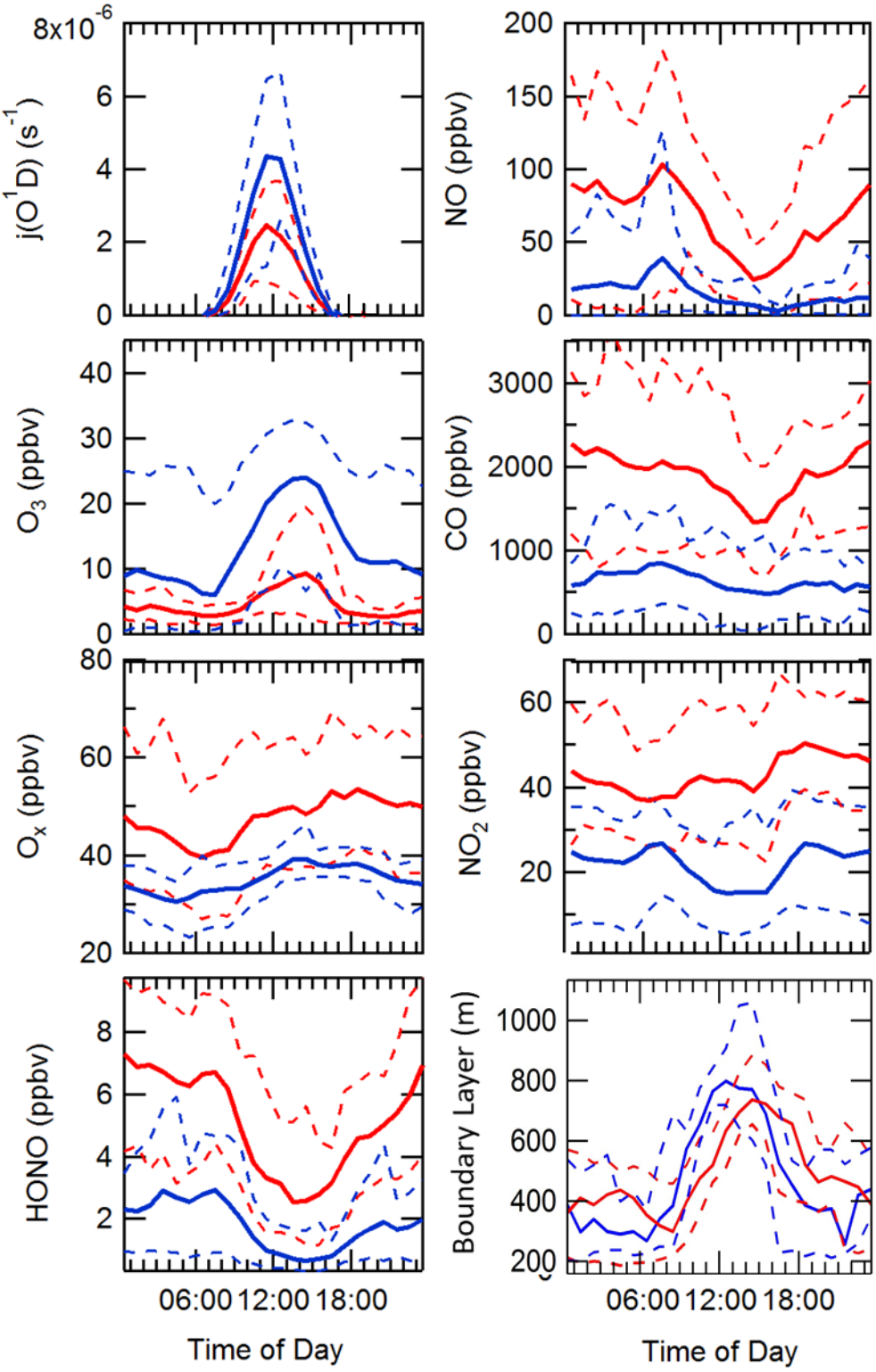

Figure 5. Comparison of the median average diel variation for $j(O^1D)$ (s^{-1}), NO (ppbv), O_3 (ppbv), CO (ppbv), O_x (ppbv), NO_2 (ppbv), HONO (ppbv) and boundary layer height (m) inside and outside haze events; denoted by solid red and blue lines, respectively. The dashed lines represent the interquartile range for the respective species and pollution period.

Modified text relating to Figure 5:

"The boundary layer height (BLH) shows a similar diurnal variation inside and outside of haze, although the maximum BLH in haze is shifted to 14:30 compared to 12:30 outside of haze. The maximum and minimum BLH is similar inside and outside of haze and shows that containment is not the only driving force for pollution periods."

Figure 4: Extra tick marks at irregular intervals on the CO axis appear to be an error.

These have been corrected on Figure 4 (see response above which shows an updated Figure 4).

Figure 5: The panel for J(O1D) shows a small blip after dark for the red curve. I assume that this is an error. If not, what does it signify?

We apologise, this was an error and has been corrected in Figure 5 (see above).

Figure 5: Are the solid lines medians? Would it be better to call the dashed lines the interquartile range rather than confidence intervals? These are after all being used to exhibit real ambient variability in the two populations of data being compared.

The solid lines are indeed the median values and we have changed the caption from confidence intervals to interquartile range.

Modified text: "Comparison of the median average diel variation for $j(O^1D)$ (s^{-1}), NO (ppbv), O_3 (ppbv), CO (ppbv), O_x (ppbv), NO_2 (ppbv), HONO (ppbv) and boundary layer height (m) in and outside haze events; denoted by solid red and blue lines, respectively. The dashed lines represent the interquartile range for the respective species and pollution period."

Some information on mixing depth would also be helpful in the discussion of figure 5. For instance, how important is containment in explaining the high values during the haze periods in addition to wind direction?

A panel showing the boundary layer height inside and outside of the haze has been added to Figure 5 replacing the SO_2 panel (see response above), and shows that containment is not a large factor for explaining the high values observed during haze periods.

Modified text: "The boundary layer height (BLH) shows a similar diurnal variation inside and outside of haze, although the maximum BLH in haze is shifted to 14:30 compared to 12:30 outside of haze. The maximum and minimum BLH is similar inside and outside of haze and shows that containment is not the only driving force for pollution periods."

Line 338: "OH reactivity is discussed further in Section 2.5" (this is a typo that needs to be corrected)

This has been fixed in the revised MS.

Lines 339-341: "Figure 6 shows the steady state calculation for OH between 2/12/2016 to 8/12/2016 where it is compared with the measured OH concentrations. These days were chosen as full data coverage for HONO, NO, j values, radical and k(OH) measurements were available." Referring back to figure 4, it does not appear that HONO measurements are available from 2/12-5/12. Have I missed something? HONO is accounted for in calculations for each day in Figure 6, but this does not seem to track what I see in Figure 4. For instance, the lowest NOx and highest ozone occurs on 5/12, so why does HONO make its greatest contribution on that day? I can't make sense of it.

The HONO dataset shown in Figure 4 was from one HONO instrument only and the HONO used in the steady-state calculation was the HONO concentration recommended by Crilley et al. (2019) based on measurements by several instruments during the campaign, and represents a more complete dataset. The HONO shown in Figure 4 has now been updated to those recommended by Crilley et al. (2019), and are the values that have been used in the steady-state calculation and MCM model. Low NO_x would lead to reduction in recycling from HO_2 + NO, which is the largest source of OH production, and

hence on 5/12 at the lowest NOx, this makes HONO the largest contributor to the rate of OH production. Figure 4 has been updated with the correct HONO dataset, see response above for the updated version of Figure 4 along with the updated caption.

Crilley, L. R., Kramer, L. J., Ouyang, B., Duan, J., Zhang, W., Tong, S., Ge, M., Tang, K., Qin, M., Xie, P., Shaw, M. D., Lewis, A. C., Mehra, A., Bannan, T. J., Worrall, S. D., Priestley, M., Bacak, A., Coe, H., Allan, J., Percival, C. J., Popoola, O. A. M., Jones, R. L., and Bloss, W. J.: Intercomparison of nitrous acid (HONO) measurement techniques in a megacity (Beijing), Atmos. Meas. Tech., 12, 6449–6463, https://doi.org/10.5194/amt-12-6449-2019, 2019.

Lines 343-346: Further discussion of Figure 6 states that "The agreement highlights that the OH budget can be determined by field measurements of the parameters necessary to quantify its rate of production and loss, and is closed to within 10%, well within the 26% error on the OH measurements themselves." I would agree that this plays out in the aggregate, but there is always value in looking at gradients that occur in the time series, and there is a significant discrepancy on 4/12 that falls well outside the 26% error that at least deserves mention if not some investigation or deeper explanation. Even 3/23 exhibits a shift in agreement after the peak that might be able to provide insight. Why does HO2+NO drop so much faster than measured OH on that day? This period on 3/23 requires substantial additional OH sources to make sense.

The steady-state Figure 6 has been revised and has been generated using kOH values from optimised fitting of the OH decays (consideration of the start and end of the decay fit), as used in the MCM modelling comparison. See below for updated version of Figure 6. The diel profile has been separated into haze and non-haze periods as recommended by reviewer 3.

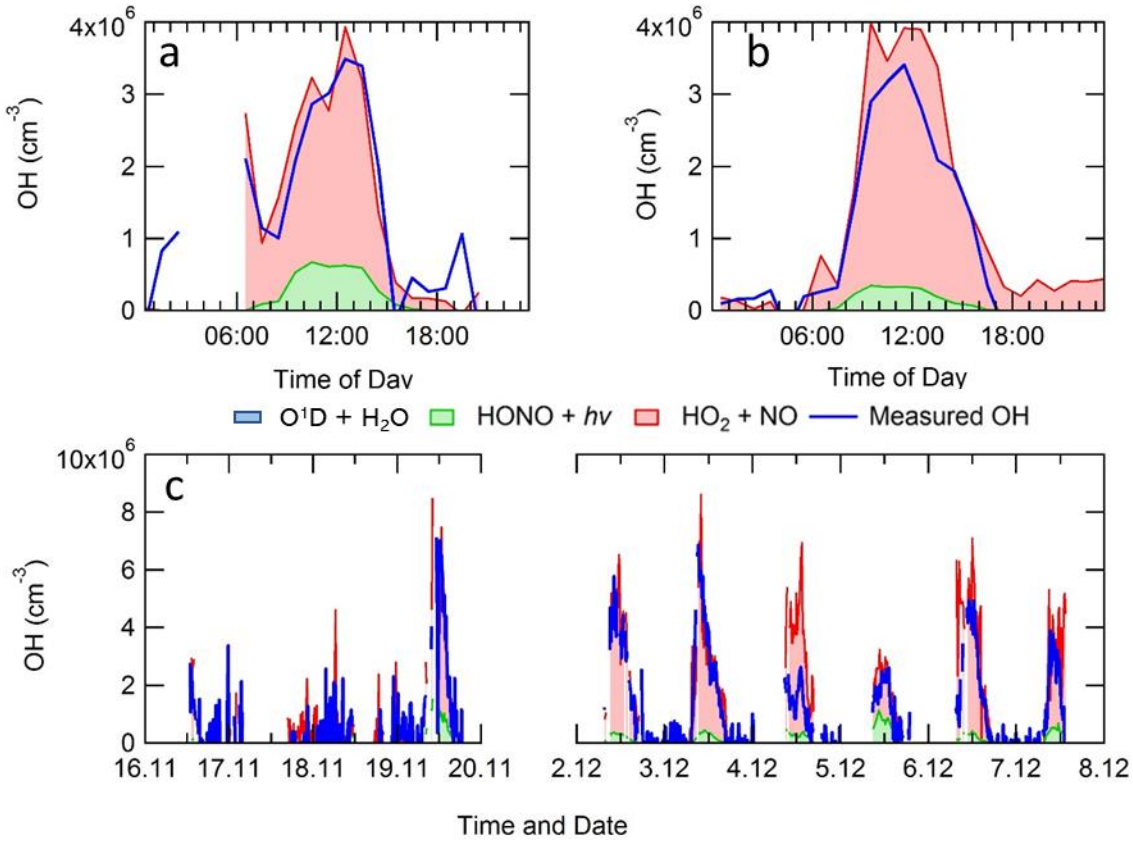

Figure 1. Average diel profile for observed and steady state calculated OH concentrations for: (a) non-haze, and(b) haze periods. Panel (c) shows a comparison time-series for the steady state calculation of OH and measured OH. The OH generated by O^1D+H_2O, although included in the key, is too small to be visible.

Figure S7 below shows that if the measured or modelled kOH is used on the 03/12 the PSS and measured OH agree within error. Although we saw no evidence of OH recycling in the kOH decay curves (no bimolecular behaviour – see response to reviewer 2), the measured kOH was lower than the modelled on the 04/12 and the use of the measured kOH may have caused the PSS to over-estimate OH on this day. However, using the modelled kOH in the PSS calculation does reproduce the PSS calculated OH using the measured kOH and the PSS stills overpredicts the OH by a factor of ~2.4. The large overprediction by the PSS suggests the differences between the PSS and measured OH on the 04/12/2016 stems from measurement problems and could be derived from issues with the OH, HO_2, HONO or NO measurements on this day. On the 3/12, the HO_2 + NO drop is driven by a decrease in NO, however the PSS and measured OH do agree within the error on the OH measurements.

The text in the MS has been modified: "Although on the 04/12/2016 the PSS overpredicts the measured OH by a factor of ~2.5, the differences between the PSS and measured OH could be due to a variety of reason including errors in OH, HO_2, NO, kOH and HONO measurements and NO segregation across the site. A further discussion for the PSS for the 04/12 can be found in the supplementary section S1.6."

The information added to the Supplementary Information is as follows:

"**S1.6 In-depth comparison of measured OH and OH calculated from the PSS on the 04/12 using measured and modelled OH reactivity.**

On the 04/12/2016 the PSS calculation for OH is overpredicted by ~2.5 and the modelled OH reactivity is higher than the measured OH reactivity by an average of ~14 s^{-1}. The modelled OH reactivity was used in the PSS calculation for OH and a comparison between the PSS calculation using measured and modelled kOH and measured OH is shown in Figure S7. Figure S7 shows that whilst using the modelled OH reactivity does reduce the calculated PSS OH, the PSS using modelled kOH still overpredicts the measured OH by a factor of ~2.4. The large overprediction by the PSS suggests the differences between the PSS and measured OH on the 04/12/2016 stems from measurement problems and could be derived from issues with the OH, HO_2, HONO or NO measurements on this day.

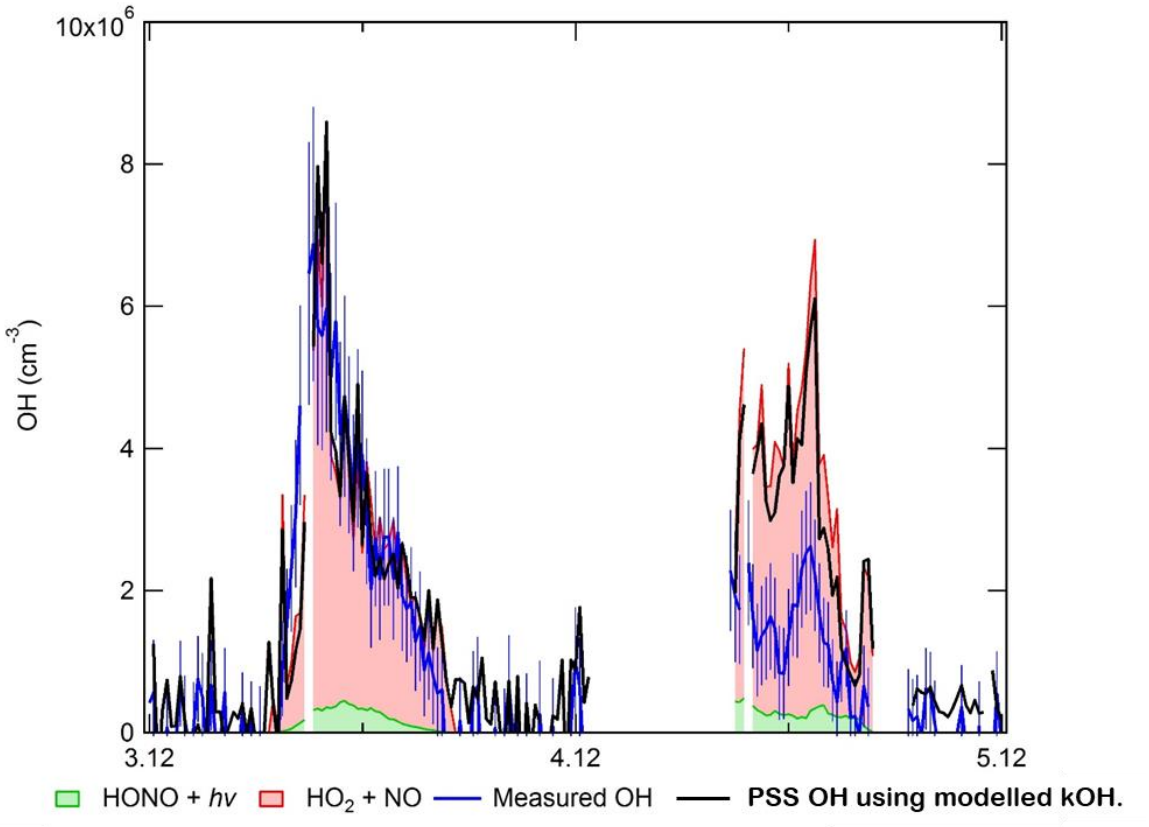

Figure S1. Comparison of measured OH (with errors, blue bars) with OH calculated from a photostationary steady-state (PSS) calculation using measured OH reactivity. The contributions towards OH production from HONO + hv (green) and HO_2 + NO (red) are shown, as well as the OH calculated using the PSS but with modelled OH reactivity (black)."

Lines 364-366: Authors state, "As seen in Figure 7, the measured daily maximum for the radical species varied day-to-day over the range 1 to 8 x 10ˆ6 cm-3, 0.7 to 1.5 x 10ˆ8 cm-3 and 1 to 2.5 x 10ˆ8 cm-3 for OH, HO2 and sum of RO2 respectively." I am again being nitpicky, but precision in your language is important, and I again feel like I am not looking at the same figure that is being described. For instance, which day shows peak OH at 1x10ˆ6? The lowest I see is ~2.5x10ˆ6. For HO2, every day after 2/12 shows peak values well below the stated 0.7x10ˆ8. Similarly, for RO2 I see several days peaking at values less that the stated 1x10ˆ8. These imprecisions lower confidence in the other values you mention regarding over and underprediction of OH, HO2, and RO2 that cannot be deduced as easily from the figure

These inconsistencies have been corrected and the precision in the wording tightened up, and the other values have been checked for accuracy. Originally, we used some values from the first measurement period during 17/12 – 19/12 but then discounted these as no measurements were available at midday for OH. For HO_2, we apologise, the power was given incorrectly, the last day peak is at 0.7 x 10^7. The other values have been checked and are correct.

New range of concentrations: OH – 2.3 – 8 x 10^6 cm^{-3}, HO_2 – 0.07 – 1.5 x 10^8, RO_2 – 0.8 – 2 x 10^8

Modified wording, "As seen in Figure 7, the measured daily maximum for the radical species varied day-to-day over the range 2.5 to 8 x 10^6 cm^{-3}, 0.07 to 1.5 x 10^8 cm^{-3} and 0.8 to 2 x 10^8 cm^{-3} for OH, HO_2 and sum of RO_2 respectively."

In the caption for Figure 7, it is stated that the lines in panel (d) are from the model, but this seems unlikely. Is this a typo?

Yes. This has now been corrected in the caption.

Lines 407-410: The authors state, "The ability of the model to reproduce (to within ~10%) both the OH reactivity and the OH concentration when constrained to measured HO2 (in MCM-cHO2), but not to reproduce RO2 radicals (whether constrained or not to HO2) is suggestive of an incomplete representation of the chemistry of RO2 radicals in the winter Beijing environment." This is somewhat of a throwaway statement. Under the extreme NOx conditions, both OH and its lifetime have very little dependence on RO2. Given the dominance of HO2+NO as a source of OH (80-90%) it is somewhat of a foregone conclusion that the constrained version of the model corrects the OH discrepancy. It is simply the lack of RO2 in the model that indicates missing RO2 chemistry. The bigger problem is explaining the HO2, which is partly derived from RO2. Are there any other notable changes when HO2 is constrained?

We feel this is still an important statement to make as it also highlights that the OH and HO_2 measurements are self-consistent. MCM-cHO2 also increases the RO_2 concentration by a factor of ~3.5 compared to MCM-base, but the RO_2 is still underpredicted by a factor ~7. We have added statement to the paper to make these points as follows.

Modified text: "MCM-cHO2 also increases the RO_2 concentration by ~3.5 compared to MCM-base, but the RO_2 is still underpredicted by a factor ~7."

We agree with the referee that this highlights missing RO_2 chemistry and this is discussed later in the paper.

At this point, it has already been established that the OH abundance is fully consistent with the observed HO2, based on both the photostationary state equation and the MCM-cHO2 model calculations. The latter calculations further demonstrate that the improved representation of OH does almost nothing to close the gap with RO2 observations (figure 8). For this reason, defining ROx as OH+HO2+RO+RO2 does not provide any additional insight. Both production and loss is dominated by OH reactions, which is not where you are looking to solve the problem. If radical production is dominated by HONO photolysis to produce OH and getting OH correct in the model does nothing to rectify RO2, I don't understand how this helps. It is just another way of showing the same thing that you have already shown in Figures 6 and 8. Also, when OH+NO dominates radical loss in the haze period, it isn't really a termination, but more akin to a null cycle for radicals since it will photolyze to return to OH on a short timescale. If you removed this cycling, and only accounted for HONO from other sources, the figure would be more accurate. Nevertheless, the dominance of OH reactions prevents this figure from advancing beyond what has already been demonstrated.

Figure 9 highlights that most of the RO_2 in the model derives from OH sources, and highlights the need for additional primary RO_2 sources, this has clarified this in the paper using the statement below:

Modified text, line 508-509: "Figure 9. Shows that almost all of the RO_2 species in the model are derived from OH sources highlighting the need for additional primary RO_2 sources in the model."

We have also removed the cycling between OH + NO and HONO photolysis as suggested by the referee so now termination is not shown through the OH + NO pathway, and Figure 9 now only accounts for the HONO from other sources. The percentages for termination and production in the paper and Table 5 (which have been removed to the Supplementary Information) have also been updated.

Modified text: "As shown in Figure 9, primary production of new radicals (radicals defined as RO_x = OH + HO_2 + RO + RO_2) via initiation reactions was dominated by the photolysis of HONO (67%, averaged over the campaign), with a small contribution from the photolysis of HCHO (2%), photolysis of carbonyl species (8%) and ozonolysis of alkenes (21%)."

Modified text: "A comparison between the primary production routes observed during the APHH and previous urban winter campaigns can be found in supplementary section S1.2."

Modified text: "OH + NO_2 contributes up to 94% and 65% in haze and non-haze, respectively. Figure 9 shows that during non-haze conditions contribution to termination from the net formation of PAN (~35%) becomes important; but under haze conditions less than 6% of RO_x termination comes from the net formation of PAN."

Updated version of Figure:

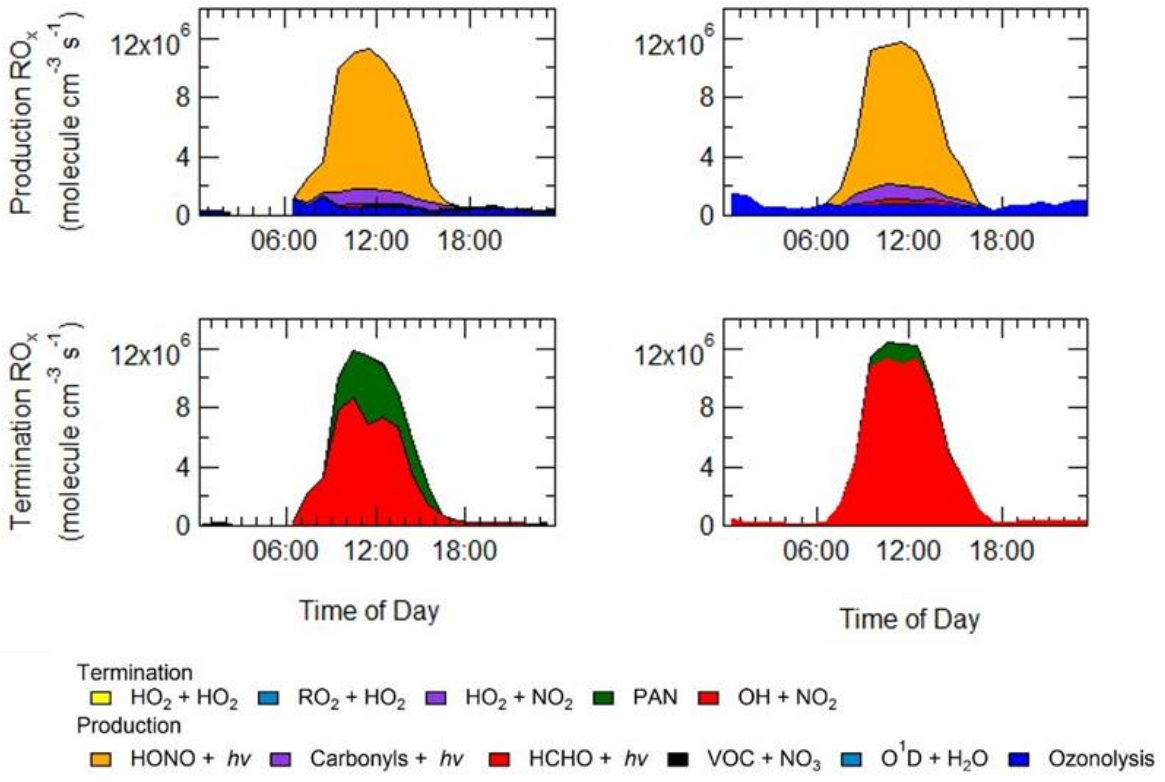

Figure 9. Rates of primary production (top panel) and termination (bottom panel) for RO_x radicals (defined as OH + HO_2 + RO + RO_2) calculated for MCM-base model separated into haze (right) and non-haze (left) periods. The definition of haze is when $PM_{2.5}$ exceeds 75 μm^{-3}. The production from: O^1D + H_2O and VOC + $NO_3$and the termination reactions: RO_2 + HO_2, HO_2 + HO_2, HO_2 + NO_2, although shown in the key, are not visible and contributed <1% of the total production and termination.

The updated table and discussion have been moved in supplementary section S1.2 as follows:

"S1.2 Primary radical production and comparison with previous campaigns.

As summarised in S4 Table 1, several other winter-time campaigns have highlighted the importance of HONO, including the PUMA campaign (Emmerson et al., 2005) in Birmingham; the IMPACT campaign in Tokyo (Kanaya et al., 2007); the NACHTT campaign in Boulder (Kim et al., 2014) and the PMTACS-NY campaign in New York (Ren et al., 2006). These campaigns showed 36.2, 19, 80.4, and 46 % contribution to primary production of ROx from HONO. However, it should be noted that HONO was not measured during the PUMA campaign, so the percentage contribution to the primary production of radicals should be considered a lower limit as it is based upon modelled HONO (where only the reaction of OH + NO was considered), which is often an underestimate (Lee et al., 2015). As shown in Table 5, the Birmingham, Tokyo, New York and Surburban Beijing campaigns all show a high contribution towards RO_x production from ozonolysis, 63, 35, 42 and 28%, respectively, only the campaign in Boulder (5%) showed little contribution, which is similar to the observations made during APHH campaign. The Boulder campaign is the only one that showed a significant contribution (14.9 %) to primary radical production from the reaction of $O(^1D)$ + H_2O, whilst other winter campaigns show a

contribution of less than 1%. The higher contribution from photolysis of O_3 during the Boulder campaign may be due to the campaign taking place in late February (spring) and, as shown in Table 1, photolysis rates, water vapour and temperature were all higher.

	PUMA, Birmingham, UK	IMPACT, Tokyo, Japan	NACHTT, Boulder, USA	PMTACS-NY, New York, USA	BEST-ONE, Suburban Beijing, China	APHH, Central Beijing, China	PKU, Central Beijing, China
Date	Jan – Feb 2000	Jan – Feb, 2004	Late Feb 2011	Jan – Feb, 2001	Jan – March 2016	Nov -Dec, 2016	Jan-Feb, 2017
OH (cm^{-3})	~1.7×10^6	~1.6×10^6	~2.7×10^6	~ 1.4×10^6	3×10^6	2.7×10^6	1.4×10^6
O_3 (ppbv)	37	20	40	20	30	15	10
$j(O^1D)$ (s^{-1})	~1×10^{-5}	~2.8×10^{-5}	~1×10^{-5}	~5×10^{-6}	7×10^{-6}	~3×10^{-6}	-
$j(O_3)$ (%)	0.6	<1	14.7	1.1	<1	<1	<1
j(HONO) (%)	36.2[1]	19	80.4	65.5	46	68	86
Ozonolysis (%)	63.2	35	4.9	42.4	28	21	6
j(Carbonyls) (%)	22	23	-	-	9	8	7%[2]
j(HCHO) (%)	6	10	-	6	9	2	
Reference	Emmerson et al. (2005)	Kanaya et al. (2007)	Kim et al. (2014)	Ren et al. (2006)	Tan et al. (2018)	This work.	Ma et al. (2019)

Table S1. Summary of some previous measurements of OH, HO_2 and RO_2 that have taken place during the winter, and a summary of the major primary radical sources during these campaigns. All values are the noon average for each campaign. [1] This should be considered a lower limit due to no HONO measurements being made during the campaign. [2] Primary production from the sum of j(Carbonyls) and j(HCHO)."

The comparisons given in Table 5 are fine and do not require figure 4, but they are also somewhat of a distraction as you have already determined that the OH can be explained. As a reader, I am expecting you to advance more quickly to the clear questions regarding RO2 established at the end of section 3.

We agree, and so this table and the comparison/discussion with previous campaigns (other than the discussion in the text for BEST-ONE and PKU campaigns) have been moved into the supplementary material. See response above.

Line 462: "As summarized in Table 2" should be "Table 5"

This line is no longer in the paper as it has been moved into the supplementary material, see response above and is now "As summarised in S4 Table 1".

Line 467: "campaign" is misspelled

This has been corrected.

Table 4 and 5: "NCITT" should be "NACHTT"

Corrected in both tables.

Line 539: "as shown in Figure 10" should be "Figure 11"

This has been corrected.

Line 541: "and can almost be reproduced by the model at NO concentrations above 100 ppbv." I do not think this a valuable statement as there is no expectation that the model is getting such an answer for the right reason. Instead, what you are seeing is that NOx reactions effectively suppress complex RO2 concentrations at only a few ppbv in the model, while it appears that in the observations such suppression does not occur until NOx is well above 100 ppbv

We agree and this statement has now been removed from the paper.

Line 545: "degredation" is misspelled and should be "degradation"

This has been corrected.

Section 4.3: It is not clear to me why this section is necessary to the paper. Everything to this point has been about trying to understand the model discrepancies with radical chemistry, especially at high NOx. At this point, I would expect some discussion of what might be pursued in the future to reconcile the problem. The foray into what these oxidants are doing in terms of aerosol formation feels like it belongs in another paper. I would shorten what is already a lengthy manuscript and remove this section.

We still feel that it is an important outcome of higher than expected concentrations of oxidants, namely that the rate of secondary aerosol production is also higher than expected. However, we agree about trying to shorten the manuscript and so have moved this section to the supplementary information, with just a sentence to signpost this in the main paper.

Signposting text in main text: "A discussion on the impact of similar OH concentration inside and outside of haze on the oxidation of SO2 and NO2 can be found in the supplementary section S1.3. "

Section added to the supplementary information shown below:

"**S1.3 NO_2 and SO_2 oxidation during haze events**

Secondary oxidation products, such as nitric acid and sulphuric acid, which partition to the aerosol phase, are major contributors towards the formation of secondary particulate matter (Huang et al., 2014). The OH measurements enable calculation of the rate of SO_2 and NO_2 oxidation *via* reaction with OH, to form gas-phase phase HNO_3 and H_2SO_4.. Figure 4 shows that on average 1.5 ppbv/h and 0.03 ppbv/h of gas-phase NO_2 and SO_2 are oxidised to form acidic species, and that the oxidation increases in these haze periods caused by comparable OH concentration in and out of haze and, as shown in Figure 4, an increase in local NO_2 and SO_2 concentrations. NO_x can also be lost in the atmosphere by the formation of N_2O_5 (Evans, 2005) and subsequent hydrolysis, but this is uninportant in Beijing during winter due to the low levels of O_3. The reaction of OH + SO_2 in the gas-phase is the rate-determining step in the formation SO_4^{-2}, so the H_2SO_4 formed in the gas-phase will partition in the aerosol phase (Barth et al., 2000). H_2SO_4 is effectively a non-volatile gas at atmospheric temperatures, and H_2SO_4 condensation onto pre-exsisiting particles is an irreversible kinetic process (Zaveri et al., 2008). Whilst HNO_3 is a semivolatile species and the gas-particle partitioning is highly sensitive to to meteorological conditions including: temperature, RH, particle size distribution, pH and particle composition. If the realtive humidity is lower than the deliquescence relative humidity (RH_d), then the HNO_3 that is formed in the gas phase reacts with NH_3 to form ammonium nitrate aersol (NH_4NO_3):

$$HNO_3(g) + NH_3(g) \rightleftharpoons NH_4NO_3(s) \qquad \text{S R1}$$

$$HNO_3(g) + NH_3(g) \rightleftharpoons NO_3^-(aq) + NH_4^+(aq)$$ S R2

If the ambient RH exceeds the RH_d then HNO_3 and NH_3 dissolve into the aqueous phase (aq):
To take into account the reversible process, knowledge of the RH_d that marks the transition between the solid and the aqueous phase, and the equilibrium constant, K_p, for the two phase is required (Ackermann et al., 1998). The MADE module (modal aerosol dynamics model for europe) uses these thermodynamic parameters as given by (Mozurkewich, 1993), resulting in:

$$\ln\left(\frac{RH_d}{100}\right) = \frac{618.3}{T} - 2.551$$ S E1

for RH_d and:

$$\ln\left(K_p\right) = 118.87 - \frac{24084}{T} - 6.025\ln(T)$$ S E2

for K_p. SE1 and SE2 shows that nitrate formation is favoured thermodynamically at low temperatures and high relative humidties (Ge et al., 2017). Previous measurements of SO_4^{-2} and NO_3^- made in wintertime Beijing suggests that photochemstry is important in the formation of nitrate aersol, but not the formation of sulphate (Ge et al., 2017; Sun et al., 2013).
Figure S4 also shows that the gas-phase oxidation of NO_2 increases under haze conditions, showing that nitrate formation is driven by photochemistry in haze events despite the lower photolysis rates. Similar conclusions have been made in Lu et al. (2019) from measurements during the BEST-ONE campaign; with SO_4^- aerosol predominantly driven by aqueous-phase chemistry whilst the production of NO_3^- aerosol from gas-phase oxidation of NO_2 with OH is important. The maximum production rate of HNO_3 observed during the BEST-ONE campaign is the same as the one calculated for the APHH campaign (3 ppbv hr^{-1}). The BEST-ONE campaign assumed all the gas-phase HNO_3 formed partitioned into the aerosol-phase due to the high relative humidity observed during the campaign.

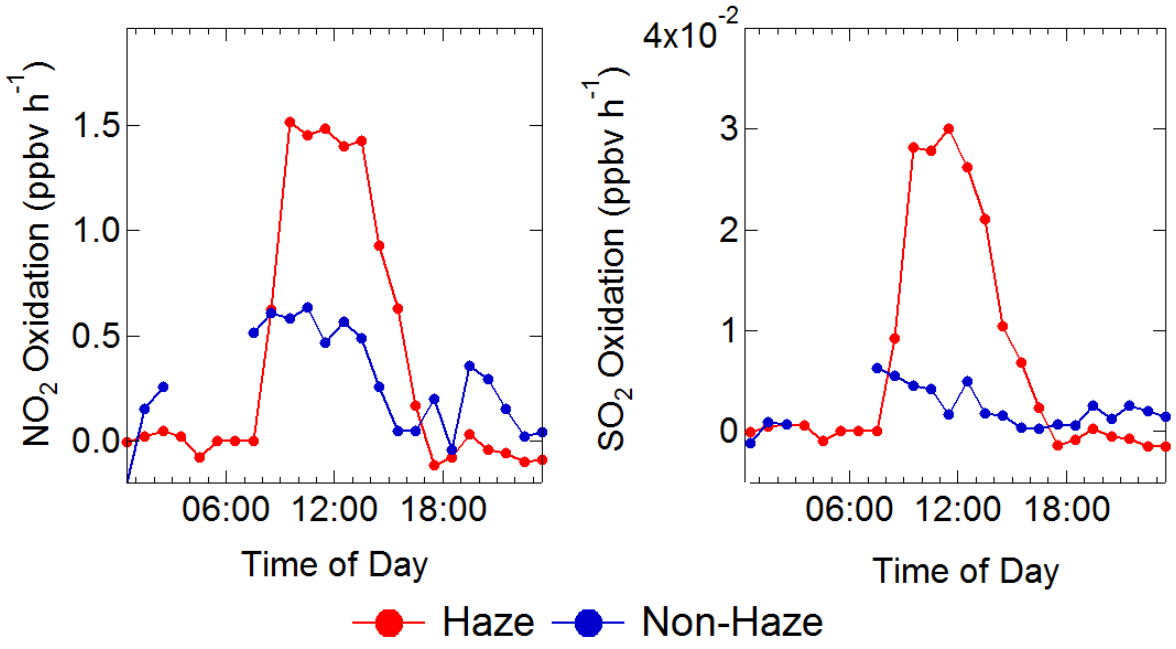

Figure S2 Average diel profiles of the rate of oxidation of NO_2 (left) and SO_2 (right) via reaction with OH in non-haze (blue) and haze (red) conditions.

“

Section 4.4: This section focusing on ozone production only makes sense to include if it attempts to reconcile to calculated rate of production with what is observed. Ozone itself is on the order of only 1-30 ppbv and Ox fluctuations are on the order of 10-15 ppbv per day based on what is shown in Figure 5. Thus, a formation rate of 71 ppb/hr on average would need to be offset by an equally large NOx sink via NO2+OH. Also, with such low ozone, it would seem that radicals play an outsized role in NOx cycling between NO and NO2. Has there been any analysis of NO/NO2 and its consistency with the observed ozone and radical abundances?

We feel that the inclusion of the ozone production rate is important as it highlights how this missing RO_2 chemistry impacts the models ability to predict *in situ* ozone formation.

The Leighton ratio calculated from the measured ozone, NO and NO_2 concentrations from the campaign is generally below 1 indicating that the ratio of NO/NO_2 are not in steady-state during the winter campaign and so it is not possible to estimate a peroxy radical concentration from this.

Also, a comparison between measured O_3 and ozone production rate is difficult as the changes in measured ozone will be controlled by transport and dilution which the box model does not take into account. In the case of this work the ozone concentration is likely reduced by mixing with O_3 depleted air – such as air from the nearby large roads in Beijing. Here were are showing that the instantaneous rate of ozone production is underestimated by the model compared with measured levels of HO_2 and RO_2 are used.

Line 765: "2.7.0" please fix this typo

Fixed

Reviewer 2.

We thank the reviewer for their careful reading of the manuscript. We address each of the comments in turn below, with the comments first given in bold, followed by the response in normal type, followed by any changes made to the manuscript.

I agree with reviewer one on the possibility of shortening the paper which, at the current status, feels more as a description of the observation (with some model run) but does not really try and push for suggesting possible explanations for the finding or even looking in explanations given in the past (segregation for example or Cl2 chemistry) to check if they would help the situation in this campaign.

As outlined in the responses to Reviewer 1, we have now shortened the manuscript by either shortening or completely removing Tables, Figures and Sections, and moving these to the Supplementary Material.

Unfortunately, there were no $ClNO_2$ measurements during the winter campaign, and hence it was not possible to calculate a time series for Cl atoms formed from photolysis of $ClNO_2$ and to assess any additional RO_2 radicals generated. Using the model run where an additional RO_2 source was added to reconcile the measurements and the model, a rough calculation has shown that the $ClNO_2$ concentration would have to be of the order of ~5800 ppbv in order to close the gap between modelled and measured RO_2. Previous measurements of $ClNO_2$ in suburban Beijing has shown a peak of ~2.9 ppbv (Wang et al. 2017) which is ~3 orders of magnitude smaller than the $ClNO_2$ concentration required, suggesting other additional primary sources are needed in the model besides Cl chemistry.

Added statement to paper about chlorine chemistry (page 28, line 615 – 619): "Although the $ClNO_2$ concentration required to bridge the gap between model and measurements would be ~5800 ppbv on average (see supplementary section S1.8 for details). Previous measurements in China in suburban Beijing have shown $ClNO_2$ peaking at 2.9 ppbv (Wang et al. 2017), however, and suggests other additional primary source are needed in the model besides Cl chemistry."

This section has been added into the supplememtary material:

"

S1.8 $ClNO_2$ and Cl concentration required to bridge the gap between measured and modelled total RO_2

Unfortunately, there were no $ClNO_2$ measurements during the winter campaign, and hence it was not possible to calculate a time series for Cl atoms formed from photolysis of $ClNO_2$ and to assess any additional RO_2 radicals generated. Using the model run where additional RO_2 source was added to reconcile the measurements and the model a rough calculation has shown that the $ClNO_2$ concentration would have to be on average ~5800 ppbv in order to close the gap between modelled and measured RO_2. Figure S10 shows the average diel of the calculated $ClNO_2$ and Cl concentration with peak at 1.4 x 10^4 ppbv and 1.6 x 10^6 molecule cm^{-3}, respectively. The $ClNO_2$ and Cl concentration have been calculated using SE3 – SE5:

$$P'RO_2 = k_{VOC+Cl}[VOC][Cl] \quad \text{S E3}$$

$$[Cl] = \frac{P'RO_2}{k_{VOC+Cl}[VOC][Cl]} \quad \text{S E4}$$

$$[ClNO_2] = \frac{k_{VOC+Cl}[VOC][Cl]}{jClNO_2} \quad \text{S E5}$$

where $k_{\mathrm{VOC+Cl}}$ is a generic rate constant to represents the reaction of all VOCs with Cl which in this case is 4 x 10^{-12} molecule^{-1} cm^3 s^{-1}, [VOC] is the sum of the measured VOC concentration for the campaign and P'RO_2 is the calculated additional RO_2 used in MCM-PRO2 (see main paper section 4.2 for more details). The $ClNO_2$ required to bridge the gap between measured and modelled of RO_2 is ~3 orders of magnitude greater than the peak $ClNO_2$ concentration measured in suburban Beijing (2.9 ppbv) by Wang et al. (2018) suggesting that other additional primary source are needed in the model besides Cl chemistry .

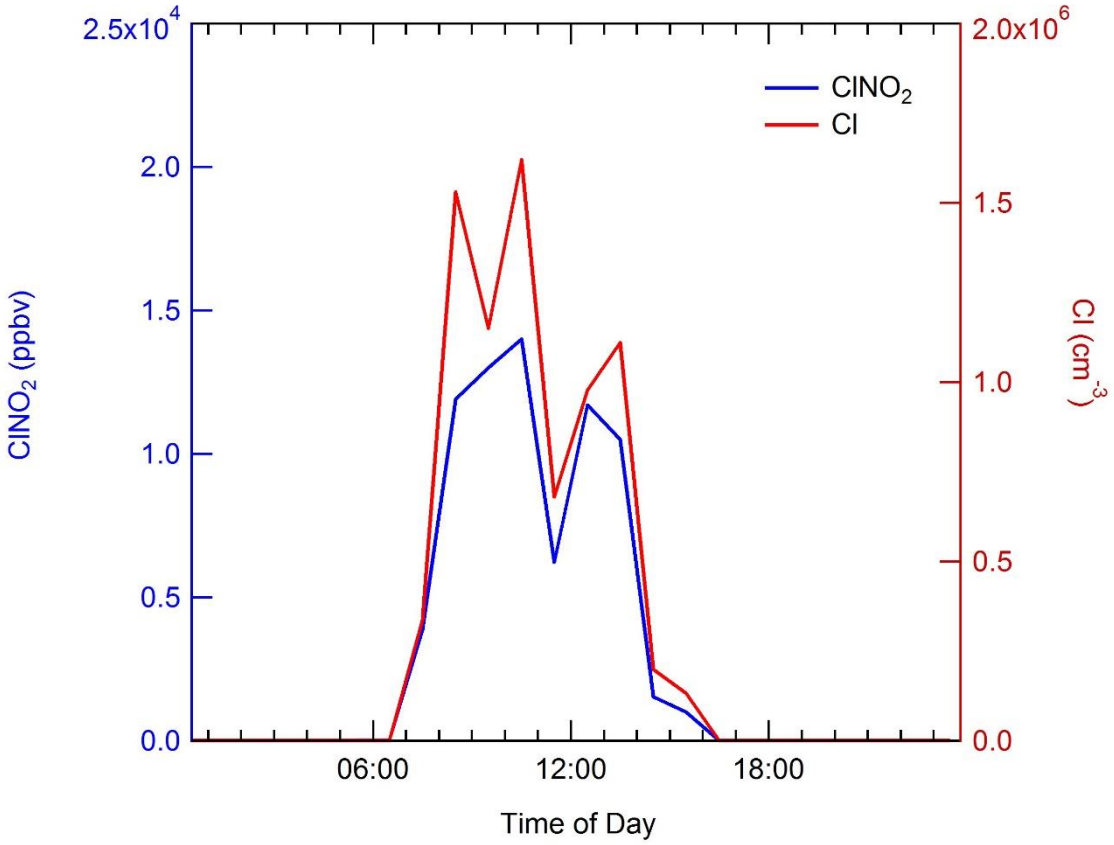

Figure S10 Average diel of the $ClNO_2$ and Cl atom concentration required to bridge the gap between measured and modelled RO_2. The $ClNO_2$ and Cl concentrations have been calculated from the additional primary source of RO_2 added to the MCM-PRO2 model run, see section 4.2 in the main paper for more details.

"

Wang, X., Wang, H., Xue, L., Wang, T., Wang, L., Gu, R., Wang, W., Tham, Y.J., Wang, Z., Yang, L. and Chen, J., 2017. Observations of N2O5 and ClNO2 at a polluted urban surface site in North China: High N2O5 uptake coefficients and low ClNO2 product yields. *Atmospheric environment*, *156*, pp.125-134.

Regarding segregation, there were several instruments for NO measurements located at different positions around the field-site and there were no obvious differences between the measurements, and so we feel that NO segregation between the instruments cannot account for the differences between the measured and modelled RO_2. We have made a statement in the text (page 25, line 563-564) regarding this: ". There were several instruments for NO measurements located around the site and no differences in concentrations were observed, hence no evidence of any obvious segregation"

I would suggest trying and making better use of the complex and simple RO2 concentrations. Measurement of RO2 or scarce to start with and here several time the measurement of simple and complex RO2 separately is brought up but then the data is not really used. Even when mentioning

that there seems to be a better agreement between the measurement of simple RO2 and model results at high NO (which, by the way, I do not agree with), the discussion stops there and there is no additional use of the data. Why not checking for example if the RO2 measurement is consistent with the VOC load?

We have now included an additional analysis of the complex and simple RO_2 concentrations, and their agreement with the model (see the next comment below). Regarding whether RO_2 simple and RO_2 complex are consistent with the VOC load, the increase is kOH contribution for VOCs from non-haze to haze periods has been assessed. It shows that the increased contribution to kOH (s^{-1}) from VOCs going from non-haze to haze is a factor of: ~10 for aromatics, ~8 for alkenes and alkynes , ~6 for alkanes, ~9 for alcohols and ~2 for aldehydes. The large increase in relative contribution to kOH from aromatics, alkenes and alkynes is consistent with the observation of higher complex RO_2 (compared to simple RO_2) during haze periods compared to non-haze periods.

The statement "The increased contribution to kOH (s^{-1}) from VOCs going from non-haze to haze conditions is a factor of: ~10 for aromatics, ~8 for alkenes and alkynes , ~6 for alkanes, ~9 for alcohols and ~2 for aldehydes. The large increase in the relative contribution to kOH from aromatics, alkenes and alkynes is consistent with the observation of higher complex RO_2 (compared to simple RO_2) during haze periods compared to non-haze periods." has been added to the paper.

The statements: "and can almost be reproduced by the model at NO concentrations above 100 ppbv." Has been removed from the paper as suggested by reviewer 1.

Does the contribution of simple and complex RO2 changes with time? During the day? From non-haze to haze periods? I think this type of analysis could maybe also help understanding a little bit more where the large discrepancy between measurement and model results arises from.

The average diel profile of both measured and modelled complex and simple RO_2 inside and outside of haze has been added to Figure 14, and we have added the following text to the paper. "The measured complex RO_2 radical species peak at similar concentrations inside (4.3×10^7 molecule cm^{-3}) and outside (4.6×10^7 molecule cm^{-3}) of haze. Interestingly, unlike the complex RO_2, the simple RO_2 concentration peaks at a lower concentration inside of haze (3.4×10^7 molecule cm^{-3}) compared with outside of haze (5.5×10^7 molecule cm^{-3}). The complex RO_2 is undepredicted by the model by a factor of ~48 and ~12 inside and outside of haze, respectively, whilst the simple RO_2 is undepredicted by a factor of ~66 and ~5.7 inside and outside of haze, respectively. The sharp increase for the underprediction of both simple and complex RO_2 inside haze events highlights the need of a large additional primary source of both simple and complex RO_2".

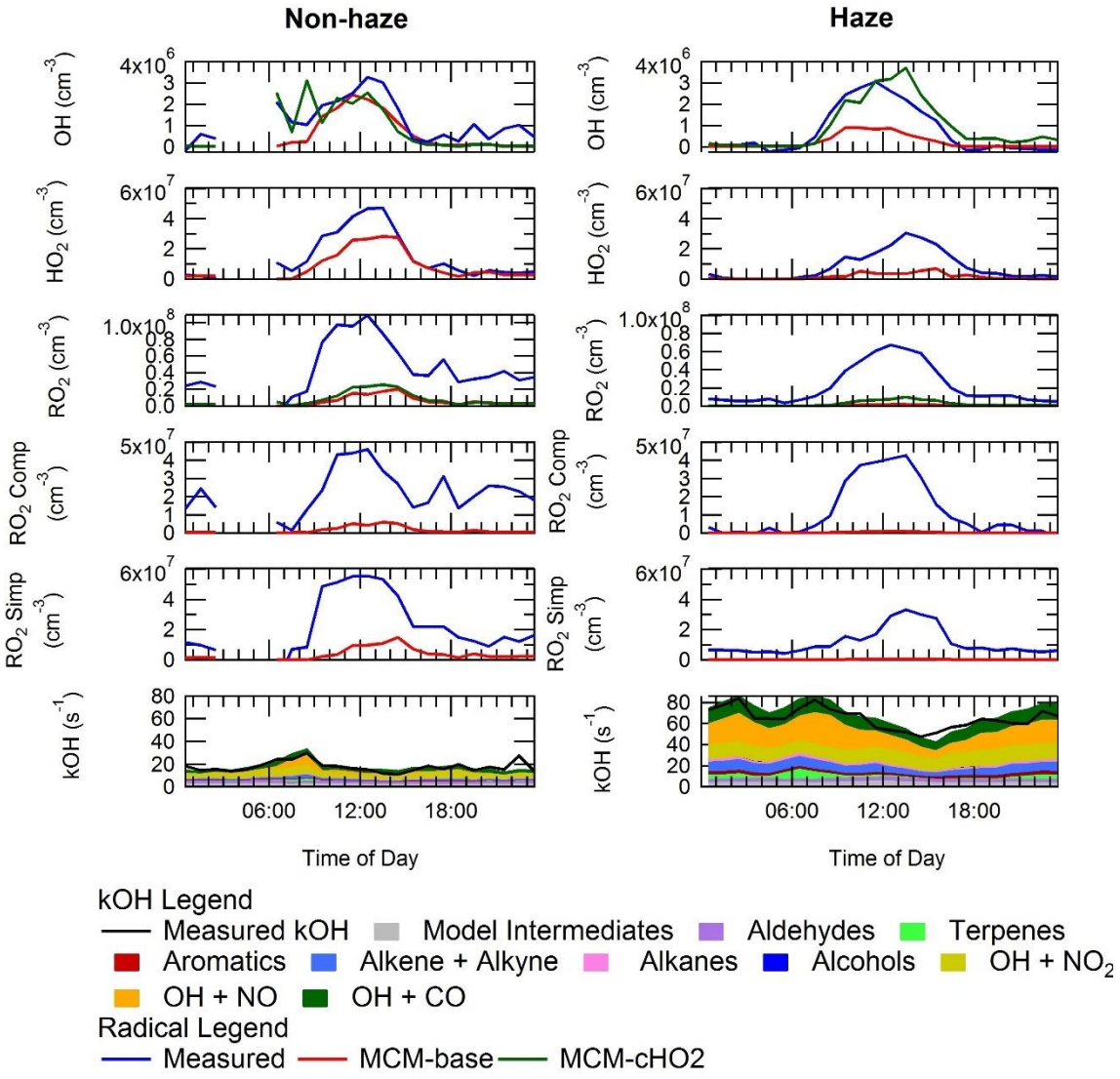

Figure 14. Average diel profiles for measured and modelled OH, HO_2, total RO_2, complex RO_2 (RO_2 comp), simple RO_2 (RO_2 simp) and kOH separated into haze (right) and non-haze (left) periods.

The average diurnal profile of measured and modelled simple and complex RO_2 have been added to Figure.8., and the updated Figure 8. Is shown below:

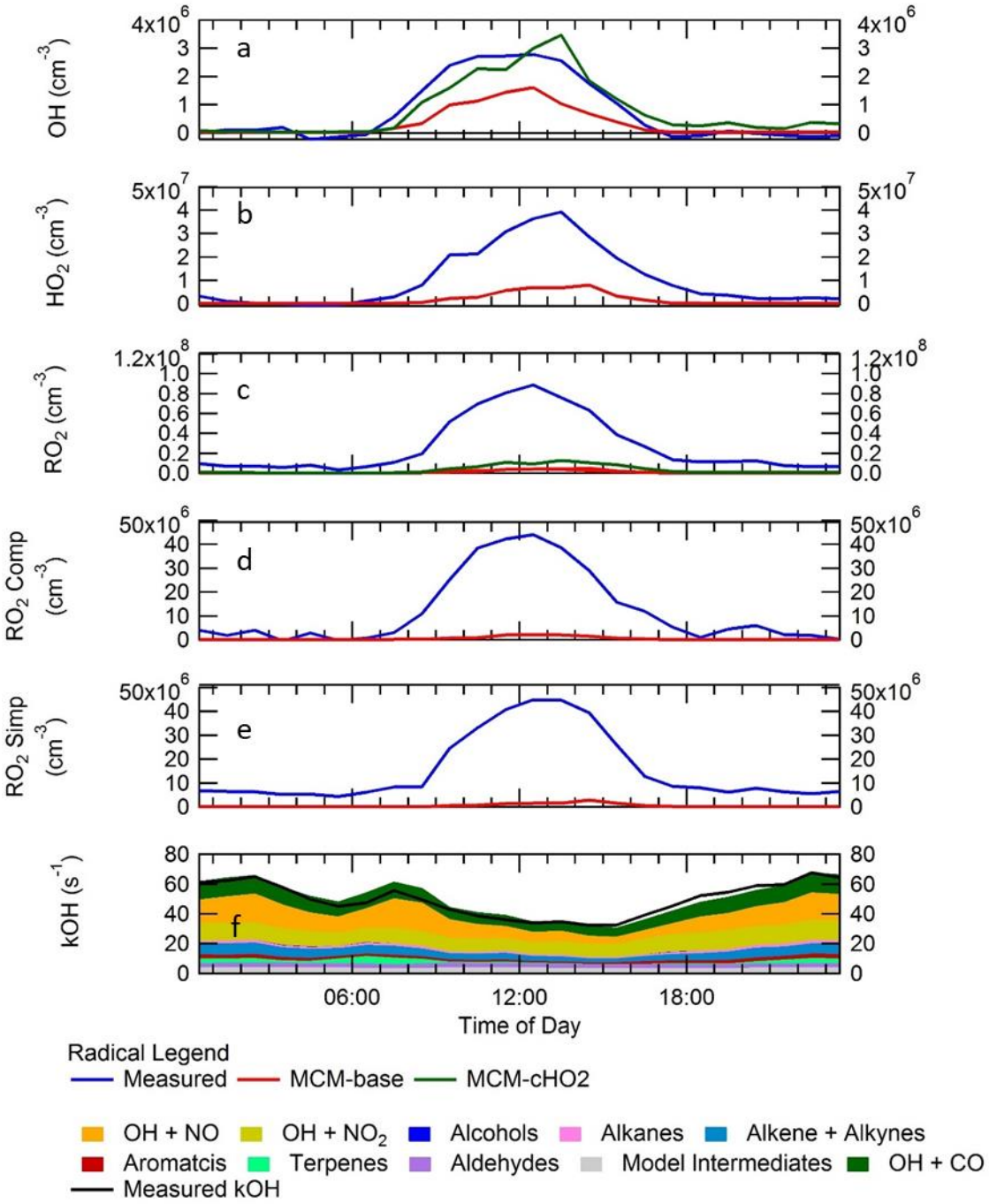

Figure 8. Campaign averaged diel profile of OH (a), HO_2 (b), sum of RO_2 (c), complex RO_2 (d), simple RO_2 (e) for measurements (blue) and box-model calculations: MCM-base (red) and MCM-cHO_2 (green). See text for descriptions of each model scenario. (f) – OH reactivity (s^{-1}) for measurements (black line) and model (stacked plot) with the contribution to reactivity from different measured species and modelled intermediates shown in the key.

Along with a small discussion on the variability during the day. The new text is as follows:.

"The complex and simple RO_2 show a very similar diurnal profile both peaking at 12:30 at a concentration of 4.4 x 10^7 molecule cm^{-3} and 4.5 x 10^7 molecule cm^{-3}, respectively. The model underpredicts the simple and complex RO_2 at 12:30 by a factor of 30 and 22, respectively. The large underprediction of both simple and complex RO_2 highlights the needs for additional primary sources

forming both simple and complex species in the model. Section 4.2 explores the impact of additional primary source of RO_2 added into the model on OH and HO_2

I am missing a small but useful description of all the measurements used within the model and which instrumentation (with accuracy and precision) was used for the different trace gases. It does not have to go too much in details but there is no mentioning of how NO, which is extremely important for the radicals chemistry, was measured. . .or O3 or anything.

We have added a Table (Table 2) which describes the methods used for some of the key species which are used to constrain the model. For many of the other species used to constrain the model, details are given in Shi et al 2018, and we have made a clear reference to that paper.

Modified wording "The accuracy and precision of trace gas species can be found in Table 2, details on the HONO measurements used in the modelling scenarios can be found in Crilley et al.(2019). Details for other measurements can be found in Shi et al.(2018)"

The following table has been added to the manuscript:

Instrument	Technique	2σ Uncertainty / %	2σ Precision/ ppbv
O_3, TEi49i	UV absorption	4.04	0.28[1]
NO, TEi42i-TL	Chemiluminescence via reaction with O_3	4.58	0.03[1]
SO_2, TEi43i	UV fluorescence	3.12	0.03[1]
NO_2, CAPS, T500U	Cavity enhanced absorption spectroscopy	5.72	0.04[1]
HONO	LOPAP x2, BBCEAS x 2, ToF-CIMS and SIFT-MS	9 – 22%	0.025 – 0.130

Table 2. Instruments and techniques used to measure key model constraints. 2σ uncertainties for the measured trace gas species used in the modelling scenarios are quoted. [1]Precision is given for 15-minute averaging time. For details of the HONO measurements please see Crilley et al.(2019).

In addition to this, there is no description of how the OH reactivity was measured and how much of a deviation from the mono-exponential decay could be expected for values of NO reaching up to 250 ppbv. What is the accuracy of the kOH measured at high NO? Could this represent a lower limit? This should be discuss appropriately and it could add an additional explanation of why the model is largely underestimating the RO2 and HO2 concentrations (lack of some primary VOCs).

The kOH decays show no biexponential behaviour suggesting that recycling from HO_2 + NO was not observed and all decays were fitted with a single exponential decay. Details of the OH reactivity instrument have been added to the instrumental details section, and relevant citations are given. The total uncertainty in the ambient measurements of OH reactivity is ~ 6% (Stone et al. 2016). The new text describing the method is as follows:

"OH reactivity measurements were made using the laser flash photolysis pump-probe technique and the instrument is described in detail in Stone et al. (2016). Ambient air was drawn into the reaction cell (85 cm in length, 5 cm in diameter) at 12 SLM. Humidified ultra-high purity air (Messer, Air Grade Zero 2) passed a low-pressure Hg lamp at 0.5 SLM to generate ~ 50 ppbv of O_3 which was mixed with the ambient air. The O_3 was photolyzed at 266 nm to generate a uniform OH concentration across the reaction cell. The change in the OH radical concentration from pseudo-first-order loss with species present in ambient air was monitored by sampling the air from the reaction cell into a FAGE detection cell at ~1.5 Torr. The 308 nm probe laser (same as the FAGE laser describe above) was passed across the gas flow in the FAGE cell to excite OH radicals, and then detected the fluorescence signal at ~ 308

nm detected by a gated channel photomultiplier tube. The OH decay profile owing to reactions with species in ambient air was detected in real time. The decay profile was averaged for 5-mins and fitted with a first-order rate equation to find the rate coefficient describing the loss of OH (k_{loss}), with k_{OH} determined by subtracting the physical loss of OH (k_{phys}). The OH reactivity data were fitted with a mono-exponential decay function as no bi-exponential behaviour was observed, even at the highest NO concentrations, and hence there was no evidence for recycling from HO_2 + NO impacting on the retrieved values The total uncertainty in the ambient measurements of OH reactivity is ~ 6% (Stone et al. 2016). ”

Page2 line46: “. . .quality are of serious concern. . .”

This has been fixed

Page2 line49: “. . . of the world fastest. . .”

This has been fixed.

Page2 line51: I would drop the number after the comma and round the percentages

We agree and this has been done.

Page2 line 59: NOx, SO2 and VOCs have not been defined

We have now defined these, and added the following text:

“The reaction of OH with primary pollutant emissions (particularly NO_x ($NO+NO_2$), SO_2 and VOCs (volatile organic carbon)) can form secondary pollutants such as HNO_3, H_2SO_4 and secondary oxygenated organic compounds (OVOCs).”

Chapter 2.1 More information on the specific of the campaign site would be beneficial. Was the site on the street? On a platform? On the roof of the building? What was the distance between different instruments? I understand there is a specific paper on the topic but just two lines with a little bit information would suffice.

We have added a brief description of the field site as follows:

“The instruments were housed in containers and located on the ground at the IAP site on a grassed area, the distance between the Leeds and York container (VOC and trace gas measurements) was ~3 m.”

Chapter 2.2.2 Here as well more details on the sensitivity towards the different RO2 is needed. The different concentrations of RO2 are used later on to justify some of the conclusions on the discrepancies between model and measurements so it is important to mention how well know is the separation in two classes of RO2 and which sensitivity is applied for which classes.

A more detailed description of the ROxLIF instrument has been added which explains how the two different classes of RO_2 are measured and discusses what the sensitivity towards different RO_2 is and how this is determined.

The new text is as follows:

”The ROxLIF flow reactor (83 cm in length, 6.4 cm in diameter) was coupled to the second FAGE detection cell to allow for detection of RO_2 (total, complex and simple) using the method outlined by Fuchs et al. (2008). The flow reactor was held at ~30 Torr and drew ~7.5 SLM through a 1 mm pinhole ID (in-diameter). The flow reactor was operated in two mode: in the first (HO_x mode) 125 sccm of CO (Messer, 10% in N_2) was mixed with ambient air close to the pinhole to convert OH to HO_2. In the second (RO_x mode), 25 sccm of NO in N_2 (Messer, 500 ppmv) was also added to the CO flow to convert RO_2 into OH. The CO present during RO_x mode rapidly converts the OH formed into HO_2. The air from

the RO_xLIF flow reactor was drawn (5 SLM) into the FAGE fluorescence cell (held at ~1.5 Torr) and NO (Messer, 99.9%) was injected into the fluorescence cell to convert HO_2 to OH. In HO_x mode a measure of OH + HO_2 + cRO_2 (complex RO_2) was obtained; whilst RO_x measured OH + HO_2 + ΣRO_2. sRO_2 (simple RO_2) concentration was determined by subtracting the concentration of cRO_2, HO_2 and OH from RO_x.

In previous laboratory experiments the sensitivity of the instrument to a range of different RO_2 was investigated and can be found in Whalley et al.(2018). Similar sensitivities were determined for a range of RO_2 species that were tested and agreed well with model-determined sensitivities. For comparison of the modelled RO_2 to the observed RO_2-total, RO_2-complex and RO_2-simple, the RO_xLIF instrument sensitivity towards each RO_2 species in the model was determined by running a model first under the RO_xLIF reactor and then the RO_xLIF FAGE cell conditions (NO concentrations and residence times) to determine the conversion efficiency of each modelled RO_2 species to HO_2. "

Page8 line212: Is there really no difference between the accuracy of OH, HO2 and RO2 accounting that HO2 requires conversion into OH and RO2 requires a minimum of 2 NO steps?

Although detection of OH is direct, detection of HO_2 is via conversion to OH via addition of NO, and RO_2 is via conversion to HO_2, and then the HO_2 is converted to OH in the FAGE (requiring two steps as the reviewer points out), because the instruments are calibrated separately using known concentrations of OH, HO_2 and RO_2, the accuracy of the measurement is the same as this depends on the calibration accuracy. The latter is controlled mainly by the accuracy in determining the product of the lamp intensity, the water vapour (in air) and photolysis time (which makes OH and HO_2), which is determined using chemical actinometry. Other factors such as absorption cross-sections, rate coefficients and quantum yields to make OH and HO_2, and the conversion efficiency of OH to the relevant RO_2 (which is quantitative) have very low uncertainties. In addition, the flow of NO is very reproducible.

Page9 line 239: What is the concentration of H2 to 500 ppbv included in the model needed for?

H_2 can react with OH and thus constitutes part of the OH reactivity, although a very minor contribution, and is also a source of HO_2. However, the inclusion of H_2 does not change the modelled reactivity or HO_2 (< 0.1%) much but is included in the model for completeness, as is normally the case in field studies of radicals and comparison with models.

Page 9 line241: What was the time resolution of the GC data?

The time resolution for the GC data was 1 hr and has been interpolated at 15 min intervals for the model. A sentence about this has been added to the paper as follows:

" The time resolution for the GC-FID data was 1 hr and has been interpolated to 15-min for the model input."

Page 11 line290: Is the diel variation shown the mean or the median of the data?

It is the median and this has been added to the caption of Figure 5.

"Comparison of the median average diel variation for $j(O^1D)$ (s^{-1}), NO (ppbv), O_3 (ppbv), CO (ppbv), O_x (ppbv), NO_2 (ppbv), HONO (ppbv) and boundary layer height (m) inside and outside haze events; denoted by solid red and blue lines, respectively. The dashed lines represent the interquartile range for the respective species and pollution period."

Page 11 line300: O3 does not react with high levels of NO but with a high concentration of NO

Thanks, this has been fixed.

Page 21 Section 4.1: I assume that here only the results from the model are shown but this is not clear from reading the text.

Yes, only the results from the model are shown here, and text to make this clear has been added to caption of Figure 9.

"Figure 9. Rates of primary production (top panel) and termination (bottom panel) for RO_x radicals (defined as OH + HO_2 + RO + RO_2) calculated for MCM-base model separated into haze (right) and non-haze (left) periods. The definition of haze is when $PM_{2.5}$ exceeds 75 μm^{-3}. The production from: $O^1D + H_2O$ and VOC + NO3 and the termination reactions: $RO_2 + HO_2$, $HO_2 + HO_2$, $HO_2 + NO_2$, are shown in the key, although many are not visible and contributed <1% of the total production and termination."

Page 24 Lines516-521: Has the possibility of segregation of air been investigated and ruled out or why this is mentioned here but there is no discussion on how this could have had an impact on this specific site? It could be worth discussing if this could help bringing measurements and model results in agreement.

As noted in the response to reviewer 1, various NO measurements were made at ground level around the site via multiple instruments and which might have pointed to any segregation of NO owing to local point source. A sentence has been added to paper as follows:

"There were several instruments for NO measurements located around the site and no differences in concentrations were observed, hence no evidence of any obvious segregation."

Page 24 line539: Assuming that figure 10 is actually figure 11 (where in the caption of the figure the model line is the red one (?)), I do not agree with the statement in the paper that the model can reproduce the simple RO2 measured for NO above 100 ppbv. Actually, there is overlap between the model and the measured RO2 95th percentile for the complex RO2. In all honesty, I am not sure this plot tells us much as the model equally predicts pretty much zero RO2 expected at NO above 10 ppbv for both type of RO2. Although I agree that the simple RO2 have been studied more carefully, what would be the difference in rate with NO to justify the observed concentration of RO2 or what type of different chemistry for the most complex RO2 would be needed? There is no discussion in this study about it and some suggestions of what is feasible are needed.

We apologise, Figure 10 is indeed Figure 11 and this has been amended in the text.

Please see the response to Reviewer 1 regarding the model behaviour for the various types of RO_2 at high NO, where there is an amended statement that the model could reproduce simple RO_2 at high NO.

This plot (Figure. 11) is important as it shows that the missing source of RO_2 must form both complex and simple RO_2, as the underprediction of both increases with increasing NO.

The effect on decreasing the kRO2 + NO has been investigated and shows that decreasing the rate constant by a factor ~ 10 cannot reconcile the modelled RO_2 with the measured at high NO (still underpredicted by a factor of 10). Also, whilst the modelled RO_2 is improved by decreasing the rate constant, the increased RO_2 in the model is not recycled into HO_2 and OH and the model underpredictions for these radical species remains. A discussion for these results has been added into the supplementary in section S1.7, and is as follows:

"**S1.7 The effects of the kRO2 + NO rate constant on the modelled radical species**

Other than CH_3O_2 and $C_2H_5O_2$, rate constants for the reaction of many other RO_2 + NO is based on structure activity relationships (SARs) in the MCM and is lumped to kRO2NO and kAPNO (http://mcm.leeds.ac.uk/MCM/). The lumped rate constants kRO2NO and kAPNO were both decreased by a factor of 2 and 10 to investigate the effects on modelled OH, HO_2 and RO_2. The model where the rate constant for RO_2 + NO was decreased by a factor of 2 is titled MCM-kRO2-2, whilst the model where the rate constant was decreased by a factor of 10 is titled MCM-kRO2NO-10.

The comparison of measured values with modelled values (MCM-base, MCM-kRO2-2 and MCM-kRO2-10) is shown in Figure S8. Figure S8 shows that on certain days (e.g. 19/11, 5/12 and 9/12) when the model (MCM-base) could not reproduce the measured values of RO_2 the discrepancy between the measurements and the MCM-kRO2NO-10 model is almost reconciled. On these days the MCM-kRO2NO-10 does not really change the OH or HO_2 concentration from the base model. On all days the MCM-base underpredicts the RO_2 concentration, and MCM-kRO2NO-10 does decrease the gap between measurements and modelled, compared to MCM-base. MCM-kRO2NO-2 does not significantly increase the total RO_2 concentration from MCM-base, unlike MCM-kRO2NO-10. Since changing the rates of RO_2 + NO will be very dependent on the NO concentration, the ratio of measured:modelled radical concentration has been binned against the log of NO for MCM-base, MCM-kRO2NO-2 and MCM-kRO2NO-10 in Figure S9. Figure S9 shows similar results to the timeseries where at the lower concentration of NO (19/11, 5/12 and 9/12) the MCM-kRO2NO-10 can reproduce the RO_2 concentration. The results at higher [NO] show that decreasing the rate of RO_2 + NO improves the agreement between measured:modelled RO_2, especially for MCM-kRO2NO-10, but the observed RO_2 concentration is still underpredicted beyond 30 ppbv.

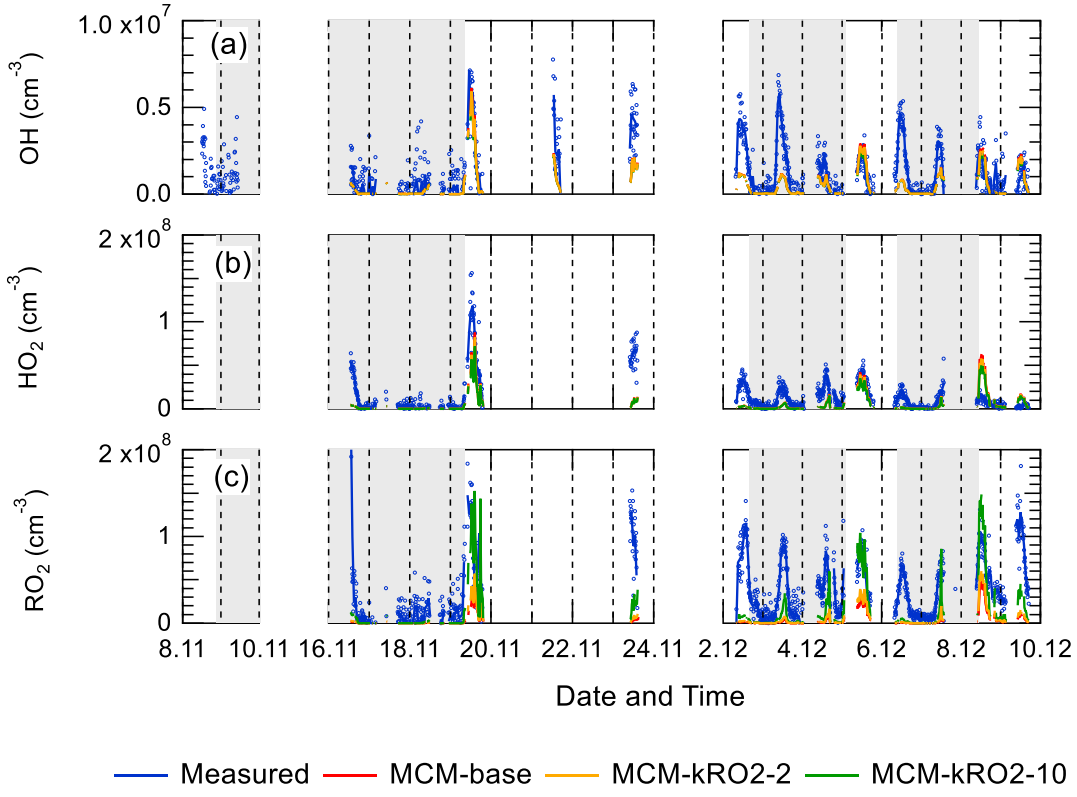

Figure S8. (a) Time-series comparison of measured values of OH with modelled OH concentrations from MCM-base, MCM-kRO23NO-2 and MCM-kRO2-10. (b) Time-series comparison of measured values of HO_2 with modelled HO_2 concentrations from MCM-base, MCM-kRO23NO-2 and MCM-kRO2-10. (c) Time-series comparison of measured values of total RO_2 with modelled total RO_2 concentrations from MCM-base, MCM-kRO23NO-2 and MCM-kRO2-10. The data sets are 15-minutes averaged.

The fact that the OH and HO_2 modelled concentrations do not change significantly for the models with reduced RO_2 + NO rate constant highlights that the enhanced RO_2 radicals (in MCM-kRO2-10) are not recycling into HO_2 or OH, even though the agreement for the RO_2 concentration is improved for these models (MCM-kRO2NO-2 and MCM-krO2NO-10). The lack of RO_2 recycling highlights that the RO_2 and RO radicals are terminating rather than propagating in the model.

This work highlights alternative chemistry and solutions must be applied for the two different NO regimes observed during the Beijing wintertime campaign. At high [NO] (above 10 ppbv) further reductions in the RO_2+NO rate constant would be required to reconcile the model with observations. However, at NO mixing ratios below 10 ppbv, further reductions in the RO_2+NO rate constant would lead to the model overpredicting the RO_2 concentration.

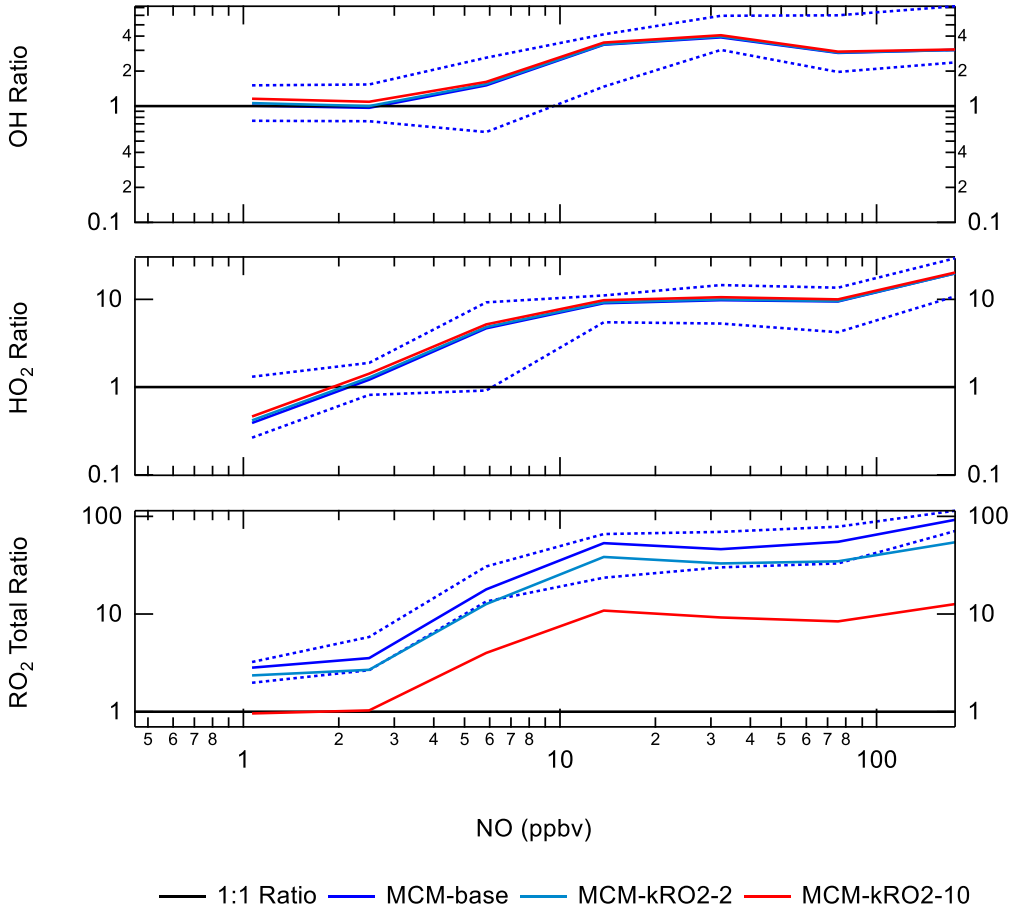

Figure S9. The ratio of measurement/model for OH (a), HO_2 (b) and RO_2 (c) across various NO concentrations for daytime values only ($j(O^1D) > 1 \times 10^{-6}$ s^{-1}). Light blue represents for results from MCM-kRO2NO-2, dark blue represents results from MCM-base and red represents results from MCM-kRO2NO-10.

"

A reference in the paper to this section has been added "The effect on reducing the RO_2 has been investigated and is shown in S1.7 in the supplementary material. The results show that reducing the rate constant by a factor ~10 does improved the modelled to measurements agreement by a factor of 8.3 for total RO_2. However, RO_2 is still underpredicted by a factor of ~12 at the highest NO. Also the increased RO_2 in the model does not recycle into HO_2 or OH efficiently. This work highlights that uncertainties in the rate constant for RO_2 + NO for different RO_2 cannot be the only explanation for the underprediction of RO_2 in the model."

Page 27 line 570-573: What would be the concentration of CL2 and/or ClNO2 needed to justify such a production of RO2? This could tell us if it could be possible at all.

Unfortunately, there were no $ClNO_2$ measurements during the winter campaign, and hence it was not possible to calculate a time series for Cl atoms formed from photolysis of $ClNO_2$ and to assess any

additional RO_2 radicals generated. Using the model run where an additional RO_2 source was added to reconcile the measurements and the model a rough calculation has shown that the $ClNO_2$ concentration would have to be of the order of ~5800 ppbv in order to close the gap between modelled and measured RO_2. Previous measurements of $ClNO_2$ in suburban Beijing has shown a peak of ~2.9 ppbv (Wang et al. 2017) which is ~3 orders of magnitude smaller than the $ClNO_2$ concentration required, suggesting other additional primary sources are needed in the model besides Cl chemistry.

Added statement to paper about chlorine chemistry (page 28, line 615 – 619): "Although the $ClNO_2$ concentration required to bridge the gap between model and measurements would be ~5800 ppbv on average (see supplementary section S1.8 for details). Previous measurements in China in suburban Beijing have shown $ClNO_2$ peaking at 2.9 ppbv (Wang et al. 2017), however, and suggests other additional primary source are needed in the model besides Cl chemistry."

This section has been added into the supplememtary material:

"

S1.8 $ClNO_2$ and Cl concentration required to bridge the gap between measured and modelled total RO_2

Unfortunately, there were no $ClNO_2$ measurements during the winter campaign, and hence it was not possible to calculate a time series for Cl atoms formed from photolysis of $ClNO_2$ and to assess any additional RO_2 radicals generated. Using the model run where additional RO_2 source was added to reconcile the measurements and the model a rough calculation has shown that the $ClNO_2$ concentration would have to be on average ~5800 ppbv in order to close the gap between modelled and measured RO_2. Figure S10 shows the average diel of the calculated $ClNO_2$ and Cl concentration with peak at 1.4 x 10^4 ppbv and 1.6 x 10^6 molecule cm^{-3}, respectively. The $ClNO_2$ and Cl concentration have been calculated using SE3 – SE5:

$$P'RO_2 = k_{VOC+Cl}[VOC][Cl] \quad \text{S E3}$$

$$[Cl] = \frac{P'RO_2}{k_{VOC+Cl}[VOC][Cl]} \quad \text{S E4}$$

$$[ClNO_2] = \frac{k_{VOC+Cl}[VOC][Cl]}{jClNO_2} \quad \text{S E5}$$

where k_{VOC+Cl} is a generic rate constant that represents the reaction of all VOCs with Cl which in this case is 4 x 10^{-12} $molecule^{-1}$ cm^3 s^{-1}, [VOC] is the sum of the measured VOC concentration for the campaign and $P'RO_2$ is the calculated additional RO_2 used in MCM-PRO2 (see main paper section 4.2 for more details). The $ClNO_2$ required to bridge the gap between measured and modelled of RO_2 is ~3 orders of magnitude greater than the peak $ClNO_2$ concentration measured in suburban Beijing (2.9 ppbv) by Wang et al. (2018) suggesting that other additional primary source are needed in the model besides Cl chemistry.

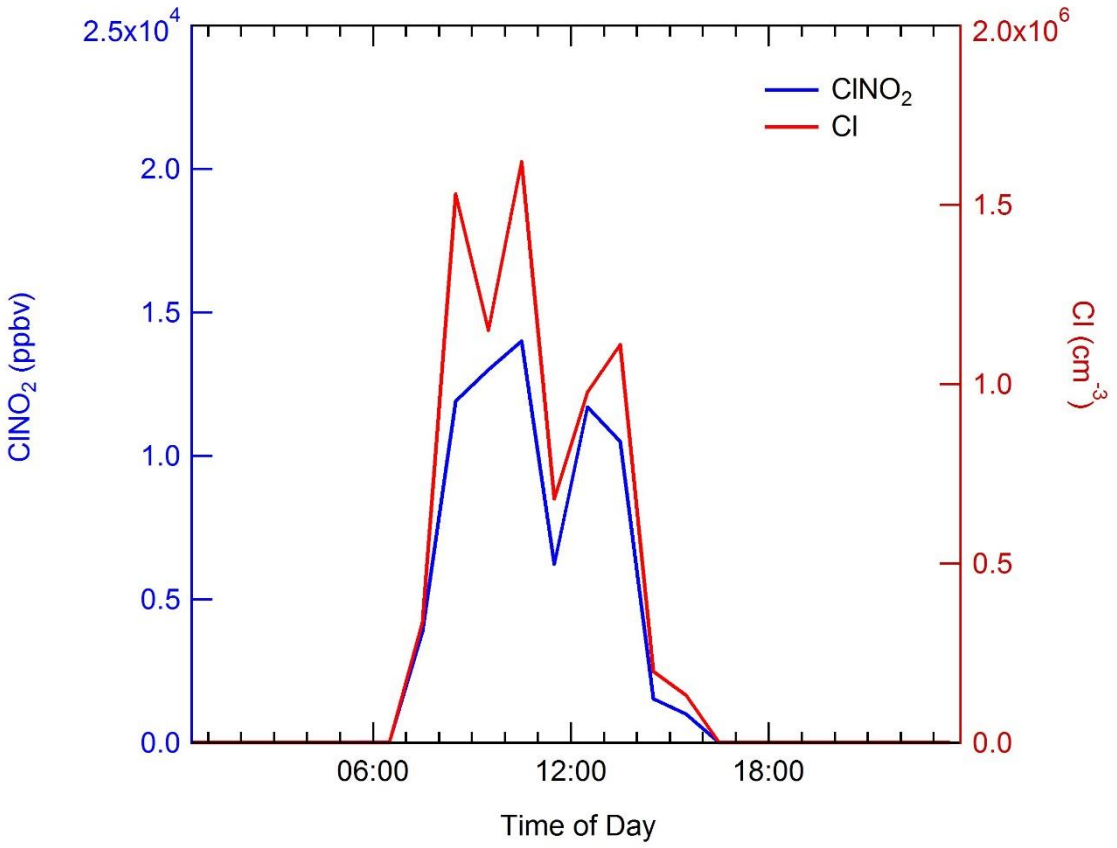

Figure S10 Average diel of the $ClNO_2$ and Cl atom concentration required to bridge the gap between measured and modelled RO_2. The $ClNO_2$ and Cl concentrations have been calculated from the additional primary source of RO_2 added to the MCM-PRO2 model run, see section 4.2 in the main paper for more details.

“

Wang, X., Wang, H., Xue, L., Wang, T., Wang, L., Gu, R., Wang, W., Tham, Y.J., Wang, Z., Yang, L. and Chen, J., 2017. Observations of N2O5 and ClNO2 at a polluted urban surface site in North China: High N2O5 uptake coefficients and low ClNO2 product yields. *Atmospheric environment*, *156*, pp.125-134.

Reviewer 3.

We thank the reviewer for their careful reading of the manuscript. We address each of the comments in turn below, with the comments first given in bold, followed by the response in normal type, followed by any changes made to the manuscript.

While the title and main conclusions of the paper refer to wintertime haze events, the main modeling of the results summarized in Figure 8 appears to include both haze and non-haze events, while the brief discussion in section 4.3 separates the model analysis to haze and non-haze events, with Figure 14 showing the base model agreement worse under haze events. While the model appears to underestimate the measured RO2 concentration similarly for both events, the agreement of the predicted OH and HO2 concentrations with the measurements is better for the non-haze events. It appears from Figure 7 that the number of haze and non-haze events were roughly equal. As a result, it is not clear whether some of the main conclusions of the paper would be applicable to the haze events. It would be useful to illustrate in Figure 6, 8, and 13 how the different models in Table 1 are able to reproduce the radical measurements for haze and non-haze events. Is the estimation of the missing source different for the haze and non-haze events? Are the model results/conclusions different for the different events? While they may not be significant, any differences between the events should be discussed in more detail.

The reviewer makes a good point and we have now updated some figures to include separate comparisons for haze and non-haze events and introduced a more detailed discussion. In Figure 8 we do include diel profiles for both haze and non-haze events, and we have now updated Figure 14 to include modelling results from MCM-base, MCM-cHO2 as well as the measured values (including speciated RO_2 concentrations) for both haze and non-haze events, and we have included an additional discussion on the differences in model performance for the haze and non-haze periods for each of these species. The modified text is as follows:

"The measured complex RO_2 radical species peak at similar concentration inside (4.3 x 10^7 molecule cm^{-3}) and outside (4.6 x 10^7 molecule cm^{-3}) of haze. Unlike the complex RO_2, the simple RO_2 concentration peaks at a lower concentration inside of haze (3.4 x 10^7 molecule cm^{-3}) compared with outside (5.5 x 10^7 molecule cm^{-3}). The complex RO_2 is undepredicted by a factor of ~48 and ~12 inside and outside of haze, respectively. Whilst the simple RO_2 is undepredicted by a factor of ~66 and ~5.7 inside and outside of haze, respectively. The sharp increase for the underprediction of both simple and complex RO_2 inside of haze highlights the need of a large additional source of both simple and complex RO_2, especially under haze conditions. The increased contribution to kOH (s^{-1}) from VOCs from non-haze to haze conditions is a factor of: ~10 for aromatics, ~8 for alkenes and alkynes, ~6 for alkanes, ~9 for alcohols and ~2 for aldehydes. The large increase in relative contribution to kOH from aromatics, alkenes and alkynes is consistent with observation of higher complex RO_2 (compared to simple RO_2) during haze periods compared to non-haze periods. " and the updated Figure 14 is shown below:

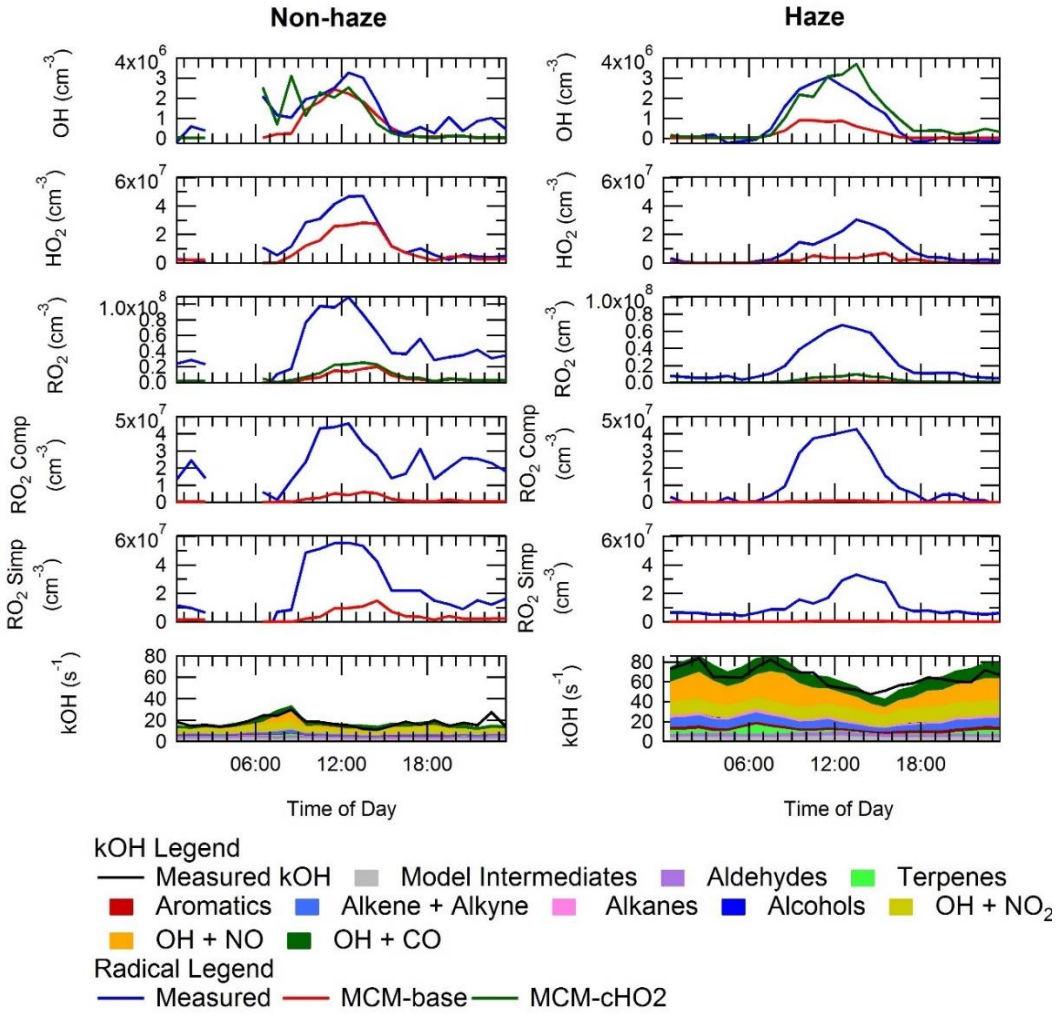

Figure 14. Average diel profiles for measured and modelled OH, HO_2, total RO_2, complex RO_2 (RO_2 comp), simple RO_2 (RO_2 simp) and kOH separated into haze (right) and non-haze (left) periods.

Figure 6, which shows the results of the photo-stationary state (PSS) expression for OH together with measurements of OH, has also been updated to include separation into haze and non-haze events. The PSS has been separated into haze and non-haze events and shows that during haze events the PSS captures the OH concentration, although the PSS does overpredict the OH concentration by ~1.35 between 09:30 – 14:30 in haze events. The overprediction by the PSS in haze events is highly influenced by the overprediction on the 04/12/2016. Whilst under non-haze conditions the PSS captures the OH concentration very well throughout the day. The production of from HONO increases in non-haze (~19%) compared with haze events (~7%). The updated text is as follows:

"The PSS has been separated into haze and non-haze events and shows that during haze events the PSS captures the OH concentration, although the PSS does overpredict the OH concentration by ~1.35 between 09:30 – 14:30 in haze events. However, the overprediction by the PSS in haze events is highly influenced by the overprediction on the 04/12/2016. Whilst under non-haze conditions the PSS captures the OH concentration very well throughout the day. The production of from HONO increases in non-haze (~19%) compared with haze events (~7%). " and the updated Figure 6 is shown below:

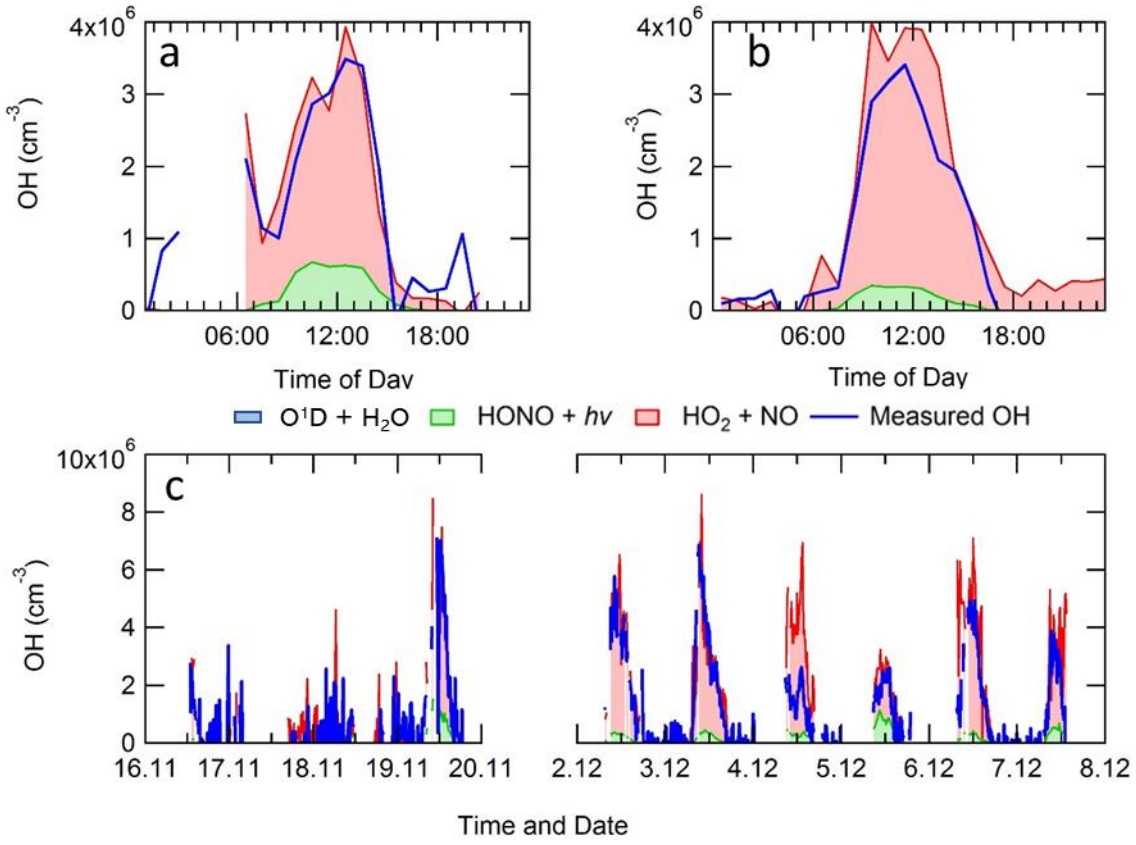

Figure 6. Average diel profile for observed and steady state calculated OH concentrations for: (a) non-haze, and(b) haze periods. Panel (c) shows a comparison time-series for the steady state calculation of OH and measured OH. The OH generated by O^1D+H_2O, although included in the key, is too small to be visible.

Figure 12 which shows the additional primary production required to bridge the gap between measured and modelled RO_2 and Figure 13 have been merged in an effort to shorten the manuscript. The merged graph (now Figure.12) has been separated into haze and non-haze events. The $P'RO_2$ is higher in the updated version of Figure 12 (see below) as the original Figure 12 had not been filtered for when measured data was available.

Figure 13 is now separated into haze and non-haze events too. A discussion has been added for the new graph.

Modified text :" The additional primary production of RO_x ($P'RO_x$) radicals required to bridge the gap between measured and modelled total RO_2 was found to peak at an average of 3.5 $x10^8$ molecule cm^{-3} s^{-1} at 08:30 non-haze events. Under haze conditions, the gap between measured and modelled total RO_2 was found to peak at an average of 4 x 10^8 molecule cm^{-3} s^{-1} at 13:30 as shown in Figure 12, calculated from Eq. 3 (Tan et al., 2018):

$$P'(RO_x) = k_{HO2+NO}\,[HO_2]\,[NO\ \ ] - P(HO_2)_{prim} - P(RO_2)_{prim} - k_{VOC}[OH] + L(HO_2)_{term} + L(RO_2)_{term} \quad \text{Eq. 3}$$

where $P(HO_2)_{prim}$, $P(RO_2)_{prim}$, $L(HO_2)_{term}$ and $L(RO_2)_{term}$ are the rates of primary production of HO_2, primary production of RO_2, termination of HO_2 and termination of RO_2, respectively. The overall (haze and non-haze) additional primary production peak of ~44 ppbv hr^{-1} (at 10:30) is almost nine times

larger than the additional RO_2 source that was required to resolve the measured and modelled RO_2 during the BEST-ONE campaign (5 ppbv h^{-1} during polluted periods, also calculated using Eq. 3), and is much larger compared to the known noon-average modelled primary production of RO_x during the APHH campaign of 1.7 ppbv hr^{-1}. The additional primary production required in non-haze rises sharply in the morning peaking at 08:30 (3.5 x 10^8 molecule cm^{-3}) and then decreases rapidly; whilst the additional source needed in haze events peaks at 4 x 10^8 molecule cm^{-3} s^{-1}. The additional primary source required during haze events through-out the day is ~7 times higher than that during non-haze events."

Modified text: "However, the MCM-PRO2 run overpredicts the observed HO_2 during haze and non-haze events by a factor of 3.4 and 2.5, respectively, with the large overprediction of HO_2 in haze and non-haze events driving the overprediction of OH by a factor of 2.2 and 2.5. This highlights that the additional primary RO_2 source may be an RO_2 species that does not readily propagate to HO_2, this has also been discussed in Whalley et al. (2020). "

Modified text: "The comparison of MCM-PRO2-SA with both measurements and MCM-PRO2 (see Table 2 for details) is shown in Figure 12 and shows that the uptake of HO_2 only has a small impact <6% and <14% on the modelled levels of OH, HO_2 and RO_2 during haze and non-haze events, respectively."

Updated Figure 13.

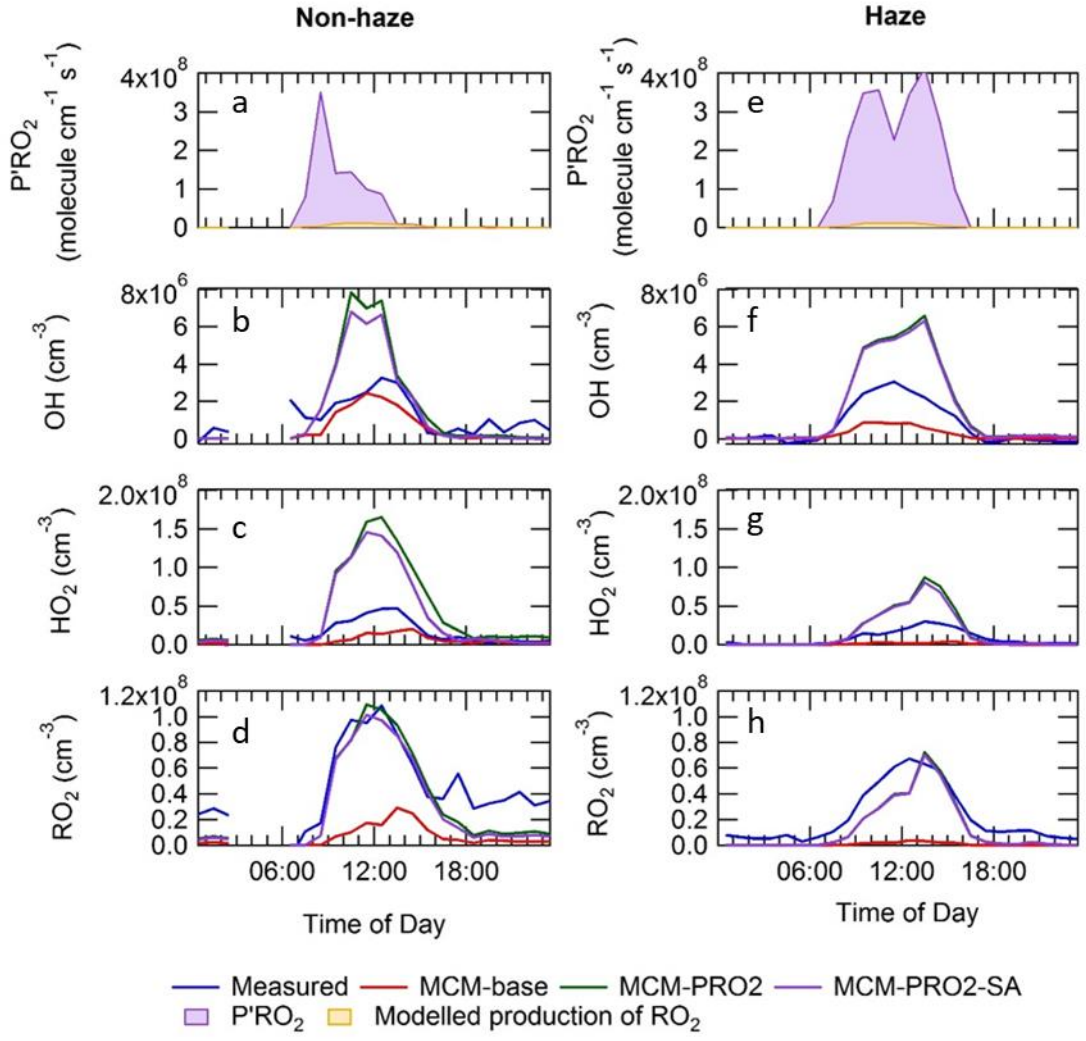

Figure 13. Average diel comparison of measurements of P'RO_2, OH, HO_2 and sum of RO_2 with the MCM-base, MCM-PRO2 and MCM-PRO2-SA box-model runs inside (e – h) and outside (a – d) of haze events. The average diel is from the entire APHH winter campaign. See text and Table 2 for definitions of each of the model runs.

Lisa K Whalley, Eloise J Slater, Robert Woodward-Massey, Chunxiang Ye, James D Lee, Freya Squires, James R Hopkins, Rachel E Dunmore, Marvin Shaw, Jacqueline F Hamilton, Alastair C Lewis, Archit Mehra, Stephen D Worrall, Asan Bacak, Thomas J Bannan, Hugh Coe, Bin Ouyang, Roderic L Jones, Leigh R Crilley, Louisa J Kramer, William J Bloss, Tuan Vu, Simone Kotthaus, Sue Grimmond, Yele Sun, Weiqi Xu, Siyao Yue, Lujie Ren, W. Joe F Acton, C. Nicholas Hewitt, Xinming Wang, Pingqing Fu, and Dwayne E Heard : Evaluating the sensitivity of radical chemistry and ozone formation to ambient VOCs and NOx in Beijing, *Atmos. Chem. Phys Disc*, 2020.

2) The authors should clarify their definition of OHwave and OHchem on pages 6-7. The current description suggests that OHchem is the on-line background measurement including interferences, while OHwave is the off-line background measurement. However, Figure 3 compares the measured OH concentration determined using chemical modulation (signal – OHchem background) with that determined by spectral modulation (signal – OHwave background), not a comparison of the background signal measured by both methods.

The definition of OHwave and OHchem and the discussion surrounding Figure 3 has been tightened up in the paper, and the modified sections of text are as follows:

Modified text

"OHchem is the online OH signal – OHchem background and OHwave is the OH online signal – Ohwave background."

3) Related to this, the authors state that the spectral modulation measurements were also corrected for laser-generated OH from ozone photolysis + H2O (page 7). Based on the Woodward-Massey et al. (2020) paper, it appears that the interference was calculated based on laboratory measurements of the interference as a function of ozone, water and laser power. This should be clarified. Since this interference would be measured by chemical modulation, a comparison of the measured interference with that calculated would provide additional confidence in the OHChem measurement as well as the accuracy of the interference estimate.

OHwave data were indeed corrected for the known interference from O_3 + H_2O, with further details available from Woodward-Massey et al. (2020). The O_3 + H_2O interference calculated was very small (median ~8.5 x 10^3 molecule cm^{-3}) due to the low concentrations of H_2O and O_3.

Modified text: " OHwave data were corrected for the known interference from O_3 + H_2O, see Woodward-Massey et al. (2020) for further details. The O_3 + H_2O interference calculated was very small (median ~8.5 x 10^3 molecule cm^{-3}) due to the low concentration of H_2O and O_3. All figures and calculation from now on have used OHwave as it is the most extensive time-series (12 days compared to 5 days)."

Woodward-Massey, R., Slater, E. J., Alen, J., Ingham, T., Cryer, D. R., Stimpson, L. M., Ye, C., Seakins, P. W., Whalley, L. K., and Heard, D. E.: Implementation of a chemical background method for atmospheric OH measurements by laser-induced fluorescence: characterisation and observations from the UK and China, Atmos. Meas. Tech., 13, 3119–3146, https://doi.org/10.5194/amt-13-3119-2020, 2020.

4) There is little discussion of the HO2, HO2*, and RO2 experimental measurement conditions, except that it appears that the conditions were similar to that in the ClearfLo study. The paper would

benefit from a brief discussion of the experimental conditions employed in this study. It appears that only a single NO flow was used in the HOx detection cell for these measurements, in contrast to the use of two NO flows used to measure HO2 and HO2* (RO2i) during ClearfLo (Whalley et al., 2018). Instead it appears that HO2* was measured using the ROxLIF detection cell. While it is stated that the ROxLIF method is described "in detail below" (page 5), the paper again references Whalley et al. (2018) instead of providing details. Given the high concentrations of NOx in this study, how did the authors account for potential interferences from the decomposition of HO2NO2 and CH3O2NO2? More details on the experimental measurements are needed. In addition the authors should clarify how the simple RO2 and complex RO2 were derived from the measurements. It appears that complex RO2 was obtained from the difference between the HO2* ROxLIF measurements and the FAGE HO2 measurements, while the simple RO2 were obtained from the difference between the ROxLIF RO2 and HO2*measurements. Much of this information could go into the Supplement.

- Description of the RO_xLIF instrument and the running conditions has been added to the paper. The text is as follows:

"The ROxLIF flow reactor (83 cm in length, 6.4 cm in diameter) was coupled to the second FAGE detection cell to allow for detection of RO_2 (total, complex and simple) using the method outlined by Fuchs et al. (2008). The flow reactor was held at ~30 Torr and drew ~7.5 SLM through a 1 mm pinhole ID (in-diameter). The flow reactor was operated in two mode: in the first (HO_x mode) 125 sccm of CO (Messer, 10% in N_2) was mixed with ambient air close to the pinhole to convert OH to HO_2. In the second (RO_x mode), 25 sccm of NO in N_2 (Messer, 500 ppmv) was also added to the CO flow to convert RO_2 into OH. The CO present during RO_x mode rapidly converts the OH formed into HO_2. The air from the RO_xLIF flow reactor was drawn (5 SLM) into the FAGE fluorescence cell (held at ~1.5 Torr) and NO (Messer, 99.9%) was injected into the fluorescence cell to convert HO_2 to OH. In HO_x mode a measure of OH + HO_2 + cRO_2 was obtained; whilst RO_x measured OH + HO_2 + ΣRO_2. sRO_2 concentration was determined by subtracting the concentration of cRO_2, HO_2 and OH from RO_x.

In previous laboratory experiments the sensitivity of the instrument to a range of different RO_2 was investigated and can be found in Whalley et al.(2018). Similar sensitivities were determined for a range of RO_2 species that were tested and agreed well with model-determined sensitivities. For comparison of the modelled RO_2 to the observed RO_2-total, RO_2-complex and RO_2-simple, the RO_xLIF instrument sensitivity towards each RO_2 species in the model was determined by running a model first under the RO_xLIF reactor and then the RO_xLIF FAGE cell conditions (NO concentrations and residence times) to determine the conversion efficiency of each modelled RO_2 species to HO_2. "- The values of RO_2 (simple, complex and total) in the paper have not been corrected for the decomposition of HO_2NO_2 and $CH_3O_2NO_2$ but an estimation has been added to the supplementary material and shows the correction from the decomposition of HO_2NO_2 and $CH_3O_2NO_2$ is ~6 %, ~8 % and 4 % for total, complex and simple RO_2, respectively.

Signposting text has been added in the main paper to the supplementary material discussion for HO_2NO_2 and $CH_3O_2NO_2$ decomposition. Modified text: "The potential interference in the RO_2 measurements from HO_2NO_2 and $CH_3O_2NO_2$ has been explored in the supplementary material in section S1.4, however the data presented through-out the paper are the uncorrected data since the correction is small (correction from the decomposition of HO_2NO_2 and $CH_3O_2NO_2$ is ~6 %, ~8 % and 4 % for total, complex and simple RO_2, respectively.)"

Information added to the supplementary material:

"**S1.4 Estimating the contribution of HO_2NO_2 and $CH_3O_2NO_2$ to the RO_2 signal**

In the main paper we do not apply a correction for a possible contribution of pernitric acid (PNA, HO_2NO_2) and methyl peroxy nitric acid (MPNA, $CH_3O_2NO_2$). The MPNA decomposition will contribute

to the simple RO_2 and total RO_2 whilst the PNA contributes to the complex and total RO_2 measurements. The concentration of HO_2NO_2 and $CH_3O_2NO_2$ was modelled using the MCM-base model, then in agreement with the work by Fuchs et al.(2008) 0.43 % and 9 % of the HO_2NO_2 and $CH_3O_2NO_2$ is calculated to decompose and contribute to the RO_2 signal. The rate of decomposition in the Julich and Leeds RO_xLIF reactors is expected since the design and residence time (~1 second) are similar. The comparison of the measured total, simple and complex RO_2 with the corrected values is shown in Figure S5. Figure S5 shows that the correction from the decomposition of HO_2NO_2 and $CH_3O_2NO_2$ is ~6 %, ~8 % and 4 % for total, complex and simple RO_2, respectively.

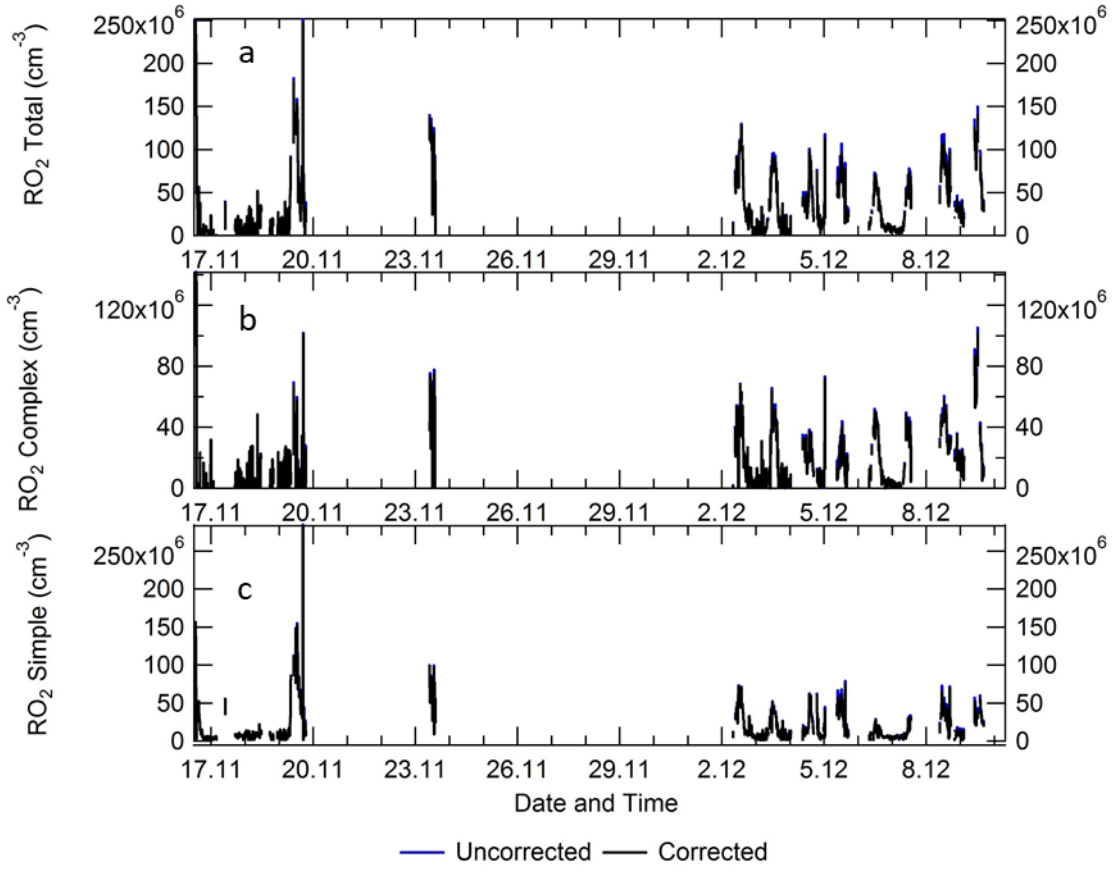

Figure S5 a) Timeseries comparison for measured total RO_2 (blue) and total RO_2 corrected (black) for the decomposition from HO_2NO_2 and $CH_3O_2NO_2$. b) Timeseries comparison for measured complex RO_2 (blue) and complex RO_2 corrected (black) for the decomposition from HO_2NO_2. c) Timeseries comparison for measured simple RO_2 (blue) and simple RO_2 corrected (black) for the decomposition from $CH_3O_2NO_2$.

“

Fuchs, H., Holland, F. and Hofzumahaus, A., 2008. Measurement of tropospheric RO_2 and HO_2 radicals by a laser-induced fluorescence instrument. *Review of Scientific Instruments*, *79*(8), p.084104.

Whalley, L. K., Stone, D., Dunmore, R., Hamilton, J., Hopkins, J. R., Lee, J. D., Lewis, A. C., Williams, P., Kleffmann, J., and Laufs, S.: Understanding in situ ozone production in the summertime through radical observations and modelling studies during the Clean air for London project (ClearfLo), Atmospheric Chemistry and Physics, 18, 2547-2571, 2018.

5) Similarly, there is no discussion of the experimental method used to measure total OH reactivity. From the information given in Figure 7, it appeared that the OH reactivity was calculated based on

the measured OH sinks, but it is clear from Figure 8 that total OH reactivity was measured. Is the measured OH reactivity shown in Figure 7?

Measured OH reactivity is shown in Figure 7 and represented by the black line, and the caption has been updated to make this clear:

Updated Figure 7. caption :" Time-series of OH, b) HO_2, c) total RO_2, d) partly-speciated RO_2 and e) Measured (black) and modelled (stacked plot) OH Reactivity. For (a)-(c), the raw measurements (6-min data acquisition cycle) are blue open circles with 15 min average represented by the solid blue line. The 15 min model output in a-c is represented by the red line for OH, HO_2 and RO_2. The partly-speciated RO_2 is separated into simple (gold open circles) and complex (purple open circles). The individual contributions of the model to the OH reactivity is given below the graph. The grey shaded areas show the haze periods when $PM_{2.5}$ > 75 μg m^{-3}."

A section has also been added describing the OH reactivity method, modified text is shown below copied from response to reviewer 2: "OH reactivity measurements were made using the laser flash photolysis pump-probe technique and the instrument is described in detail in Stone et al. (2016). Ambient air was drawn into the reaction cell (85 cm in length, 5 cm in diameter) at 12 SLM. Humidified ultra-high purity air (Messer, Air Grade Zero 2) passed a low-pressure Hg lamp at 0.5 SLM to generated ~ 50 ppbv of O_3 which was mixed with the ambient air. The O_3 was photolyzed at 266 nm to generate a uniform OH concentration across the reaction cell. The change in the OH radical concentration from pseudo-first-order loss with species present in ambient air was monitored by sampling the air from the reaction cell into a FAGE detection cell at ~1.5 Torr. The 308 nm probe laser (same as the FAGE laser describe above) was passed across the gas flow in the FAGE cell to excite OH radicals, and then detected the fluorescence signal at ~ 308 nm detected by a gated channel photomultiplier tube. The OH decay profile owing to reactions with species in ambient air was detected in real time. The decay profile was averaged for 5-mins and fitted with a first-order rate equation to find the rate coefficient describing the loss of OH (k_{loss}), with k_{OH} determined by subtracting the physical loss of OH (k_{phys}). The OH reactivity data were fitted with a mono-exponentially decaying function as no bi-exponential behaviour was observed, even at the highest NO concentrations, and hence there is no evidence for recycling from HO_2 + NO impacting on the retrieved values The total uncertainty in the ambient measurements of OH reactivity is ~ 6% (Stone et al. 2016). "

Stone, D., Whalley, L.K., Ingham, T., Edwards, P., Cryer, D.R., Brumby, C.A., Seakins, P.W. and Heard, D.E., 2016. Measurement of OH reactivity by laser flash photolysis coupled with laser-induced fluorescence spectroscopy. *Atmospheric Measurement Techniques*, pp.2827-2844.

brief description of the measurement technique should be included. Given the high mixing ratios of NO that were observed, did interference from the HO2+NO reaction impact the OH reactivity measurements?

The kOH decays show no biexponential behaviour suggesting that recycling from HO_2 + NO was not observed and all decays were fitted with a single exponential decay. Details of the OH reactivity instrument have been added to the instrumental details section, and relevant citations are given. The total uncertainty in the ambient measurements of OH reactivity is ~ 6% (Stone et al. 2016). The new text describing the method is as follows:

"OH reactivity measurements were made using the laser flash photolysis pump-probe technique and the instrument is described in detail in Stone et al. (2016). Ambient air was drawn into the reaction cell (85 cm in length, 5 cm in diameter) at 12 SLM. Humidified ultra-high purity air (Messer, Air Grade Zero 2) passed a low-pressure Hg lamp at 0.5 SLM to generated ~ 50 ppbv of O_3 which was mixed with the ambient air. The O_3 was photolyzed at 266 nm to generate a uniform OH concentration across the reaction cell. The change in the OH radical concentration from pseudo-first-order loss with species present in ambient air was monitored by sampling the air from the reaction cell into a FAGE detection

cell at ~1.5 Torr. The 308 nm probe laser (same as the FAGE laser describe above) was passed across the gas flow in the FAGE cell to excite OH radicals, and then detected the fluorescence signal at ~ 308 nm detected by a gated channel photomultiplier tube. The OH decay profile owing to reactions with species in ambient air was detected in real time. The decay profile was averaged for 5-mins and fitted with a first-order rate equation to find the rate coefficient describing the loss of OH (k_{loss}), with k_{OH} determined by subtracting the physical loss of OH (k_{phys}). The OH reactivity data were fitted with a mono-exponentially decaying function as no bi-exponential behaviour was observed, even at the highest NO concentrations, and hence there is no evidence for recycling from HO_2 + NO impacting on the retrieved values The total uncertainty in the ambient measurements of OH reactivity is ~ 6% (Stone et al. 2016). ."

Abstract: There have been previous measurements of radicals at similar NO levels in Mexico City (Shirley et al., ACP, 2006; Dusanter et al., ACP, 2009).

We thank for the reviewer for pointing this out. The abstract has been corrected as follows:

"Wintertime *in situ* measurements of OH, HO_2 and RO_2 radicals and OH reactivity were made in central Beijing during November and December 2016. Exceptionally elevated NO was observed on occasions, up to ~250 ppbv."

The caption in Figure 3 states that the gray points represent an acquisition cycle of 6 min, but the legend states that they are 4 min averages.

The average stated in the legend is for the OH measurement period only, while the overall data acquisition is for the whole measurement period (including 2 minutes of HO_2 measurements).

The caption has been updated, and now reads as follows:

"Overall intercomparison of OHwave and OHchem observations from the winter 2016 APHH campaign. Grey markers represent raw data (6 min acquisition cycle, 4 minutes and 2 minutes for the OH and HO_2 measurements), with 1 h averages (±2 standard error, SE) in red. The thick red line is the orthogonal distance regression (ODR) fit to the hourly data, with its 95% confidence interval (CI) bands given by the thin red lines; fit errors given at the 2σ level. For comparison, 1:1 agreement is denoted by the blue dashed line. OHwave data were corrected for the known interference from $O_3 + H_2O$. Taken from (Woodward-Massey et al., 2020) where further details can be found."

While the VOC measurements used to constrain their model are given in Table 1, the paper would benefit from additional information on the instruments used to measure the other model constraints. Even though this information may be provided in a separate campaign paper, a table similar to that in Whalley et al. (2018) could be included in the Supplement.

This has been covered in response to reviewer 2, and the response to reviewer 2 is copied below:

We have added a Table (Table 2) which describes the methods used for some of the key species which are used to constrain the model. For many of the other species used to constrain the model, details are given in Shi et al 2018, and we have made a clear reference to that paper.

Modified wording "The accuracy and precision of trace gas species can be found in Table 2, details on the HONO measurements used in the modelling scenarios can be found in Crilley et al.(2019). Details for other measurements can be found in Shi et al.(2018)"

The following table has been added to the manuscript:

Instrument	Technique	2σ Uncertainty / %	2σ Precision/ ppbv
O_3, TEi49i	UV absorption	4.04	0.28[1]
NO, TEi42i-TL	Chemiluminescence via reaction with O_3	4.58	0.03[1]
SO_2, TEi43i	UV fluorescence	3.12	0.03[1]
NO_2, CAPS, T500U	Cavity enhanced absorption spectroscopy	5.72	0.04[1]
HONO	LOPAP x2, BBCEAS x 2, ToF-CIMS and SIFT-MS	9 – 22%	0.025 – 0.130

Table 2. Instruments and techniques used to measure key model constraints. 2σ uncertainties for the measured trace gas species used in the modelling scenarios are quoted. [1]Precision is given for 15-minute averaging time. For details of the HONO measurements please see Crilley et al.(2019).

It appears from Figure 4 that HONO measurements were not available between 2/12 and 5/12, but the steady-state calculations shown in Figure 6 include data between 2/12-8/12 and were chosen "as full data coverage for HONO, NO, j values, radical and k(OH) measurements were available." Was HONO available on all these days?

This has been covered in response to reviewer 1, the response to reviewer 1 is copied below:

The HONO dataset shown in Figure 4 was from one HONO instrument only and the HONO used in the steady-state calculation was the HONO recommended by Crilley et al. (2019) based on measurements by several instruments during the campaign, and represents a more complete dataset. The HONO shown in Figure 4 has now been updated to those recommended by Crilley et al. (2019), and are the values that have been used in the steady-state calculation and MCM model. Low NO_x would lead to reduction in recycling from HO_2 + NO, which is the largest source of OH production, and hence on 5/12 at the lowest NOx, this makes HONO the largest contributor to the rate of OH production. Figure 4 has been updated with the correct HONO dataset, see response above for the updated version of Figure 4 along with the updated caption.

Crilley, L. R., Kramer, L. J., Ouyang, B., Duan, J., Zhang, W., Tong, S., Ge, M., Tang, K., Qin, M., Xie, P., Shaw, M. D., Lewis, A. C., Mehra, A., Bannan, T. J., Worrall, S. D., Priestley, M., Bacak, A., Coe, H., Allan, J., Percival, C. J., Popoola, O. A. M., Jones, R. L., and Bloss, W. J.: Intercomparison of nitrous acid (HONO) measurement techniques in a megacity (Beijing), Atmos. Meas. Tech., 12, 6449–6463, https://doi.org/10.5194/amt-12-6449-2019, 2019.

See updated figure and caption below:

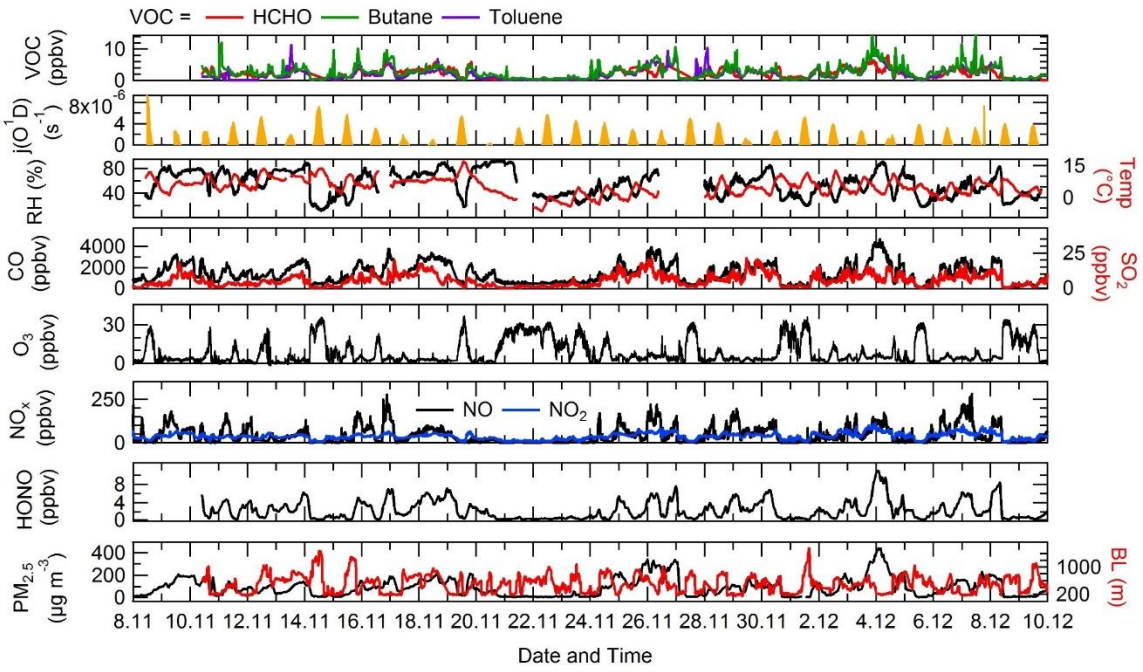

Figure 4. Time-series of $j(O^1D)$, relative humidity (RH), temperature (Temp), CO, SO_2, O_3, NO_x, HONO, boundary layer (BL), $PM_{2.5}$, HCHO, butane and toluene from the 8th of November to 10th December 2016 at Institute of Atmospheric Physics (IAP), Beijing.

Page 16 and Table 4: The text and table state that the average OH maximum was 2.7 E6 cm-3, but a value of 3.03 E6 cm-3 is stated on page 18.

We apologise for the inconsistency. The correct value is 2.7 x 10^6 molecule cm^{-3}, and this has been corrected on page 18.

Page 19: I am not sure late February/March would be considered mid-summer in Boulder, but rather late winter/early spring.

Indeed, that is true. We have used the words 'closer to spring' instead.

Figure 9: The authors should clarify whether this is an experimental radical budget or one derived from the model.

The caption now explicitly states that the radical budget is calculated from the model.

New caption for Figure 9. "Rates of primary production (top panel) and termination (bottom panel) for RO_x radicals (defined as OH + HO_2 + RO + RO_2) calculated for MCM-base model separated into haze (right) and non-haze (left) periods. The definition of haze is when $PM_{2.5}$ exceeds 75 μm^{-3}. The production from: $O^1D + H_2O$, VOC + NO_3, carbonyls + *hv* and the termination reactions: $RO_2 + HO_2$, $HO_2 + HO_2$, $HO_2 + NO_2$, although shown in the key, are not visible and contributed <1% of the total prodcution and termination."

Given the importance of HONO to radical initiation, how sensitive was the model to the systematic differences in the HONO measurements as described in Crilley et al. (2019)?

Rather than show the impact of different HONO concentrations using the MCM model, we have demonstrated the impact of different HONO measurements using a sensitivity analysis of the PSS calculation for OH. The model was not used since the effect would be small as the underprediction of the radicals derives from the RO_2 chemistry which does not lead to any terms in the PSS equation. The sensitivity of the results of the PSS calculation towards the HONO concentration has been included in

the supplementary material, and shows the PSS can be perturbed up to 17% when the HONO measurement is increased/decreased by 40%.

Some new text has been added to the supplementary material as follows:

"**S1.5 Exploring the sensitivity of the photostationary steady-state OH calculation to the HONO concentration.**

The HONO concentration used to constrained both the model and the photostationary steady-state calculation was the suggested value by Crilley et al.(2019). During the campaign there was several HONO measurement present and, although the measurements agreed on temporal trends and variability (r^2>0.97), the absolute concentration diverged between 12 – 39%, the value suggested by Crilley et al. (2019) was the mean of the measurements. Since HONO is a primary source of OH the impact of the variable HONO concentration has been explored by increasing and decreasing the HONO by 40%, the results are shown in Figure S6. Figure S6 shows that the variation observed in the HONO measurements can increase/decrease the PSS up to 17% which is smaller than the error on the measured OH of ~26%.

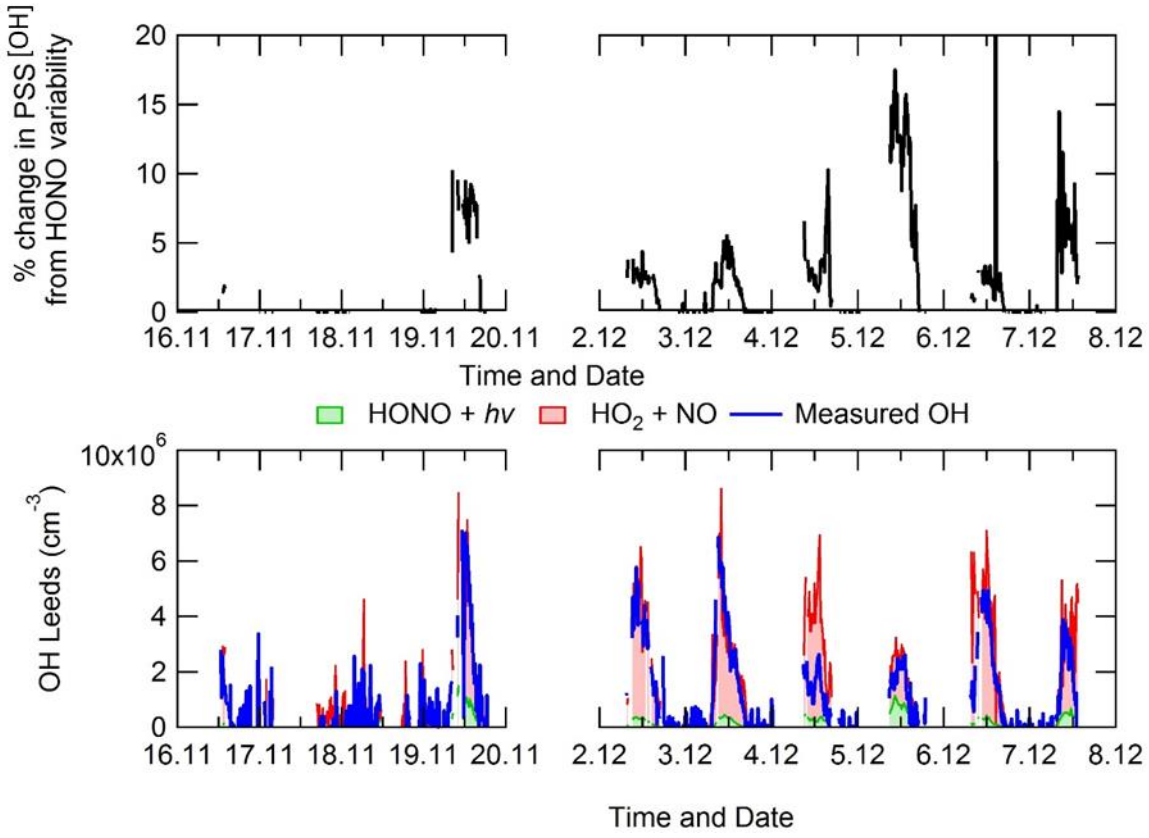

Figure S6 Top – Percentage change in the OH calculated from the PSS when the HONO is varied by 40%. Bottom – Comparison of the measured OH and the OH calculated from the PSS using the mean suggested value by Crilley et al. (2019).

"

and a sentence has been added to the main paper regarding the conclusions of this sensitivity analysis, as follows:

"The different HONO measurements present during the APHH campaign varied up-to ~40%, the sensitivity of the PSS on measured HONO is shown in the supplementary material section S1.5."

Page 26: There appears to be a problem with the signs in Equation 3 (see the corresponding equation in Tan et al. (2018))

This has now been fixed.

Page 26, line 560: Here it is stated that the P'(ROx) is 1.2 E8 cm-3 s-1, but on page 27 line 575 states that it is 1.01 E8 cm-3 s-1.

We apologise for the inconsistency. The $P'RO_2$ is higher in the updated version of Figure 12 (see above) as the original Figure 12 had not been filtered for when measured data was available only.

The correct value is 3×10^8 cm^{-3} s^{-1} and has been corrected in both instances.

Elevated levels of OH observed in haze events during wintertime in central Beijing

Eloise J. Slater[1], Lisa K. Whalley[1,2], Robert Woodward-Massey[1,a], Chunxiang Ye[1,a], James D Lee[3,4], Freya Squires[4], James R. Hopkins[3,4], Rachel E Dunmore[4], Marvin Shaw[3,4], Jacqueline F. Hamilton[4], Alastair C Lewis[3,4], Leigh R. Crilley[5,b], Louisa Kramer[5], William Bloss[5], Tuan Vu[5], Yele Sun[6], Weiqi Xu[6], Siyao Yue[6], Lujie Ren[6], W. Joe F. Acton[7], C. Nicholas Hewitt[7], Xinming Wang[8], Pingqing Fu[9] and Dwayne E. Heard[1]

[1]School of Chemistry, University of Leeds, Leeds, LS2 9JT, UK

[2]National Centre for Atmospheric Science, University of Leeds, Leeds, LS2 9JT, UK

[3]National Centre for Atmospheric Science, University of York, Heslington, York, YO10 5DD, UK

[4]Wolfson Atmospheric Chemistry Laboratories, Department of Chemistry, University of York, Heslington, York, YO10 5DD, UK

[5]School of Geography, Earth and Environmental Sciences, University of Birmingham, B15 2TT, Birmingham, UK

[6]State Key Laboratory of Atmospheric Boundary Layer Physics and Atmospheric Chemistry, Institute for Atmospheric Physics, Chinese Academy of Sciences, 40 Huayanli, Chaoyang District, Beijing 100029, China

[7]Lancaster Environment Centre, Lancaster University, Lancaster, LA1 4YW, UK

[8]State Key Laboratory of Organic Geochemistry, Guangzhou Institute of Geochemistry, Chinese Academy of Sciences, 511 Kehua Street, Wushan, Tianhe District, Guangzhou, GD 510640 , China

[9] Institute of Surface-Earth System Science, Tianjin University, Tianjin 300072, China

[a]Now at: College of Environmental Sciences and Engineering, Peking University, Beijing, 100871, China

[b]Now at Department of Chemistry, Faculty of Science, York University, 4700 Keele Street, Toronto ON, M3J 1P3, Canada

Correspondence to: Dwayne Heard (d.e.heard@leeds.ac.uk) and Lisa Whalley (l.k.whalley@leeds.ac.uk)

Abstract

Wintertime *in situ* measurements of OH, HO_2 and RO_2 radicals and OH reactivity were made in central Beijing during November and December 2016. Exceptionally elevated NO was observed on occasions, up to ~250 ppbv~~, believed to be the highest mole fraction for which there have then co-located radical observations.~~ The daily maximum mixing ratios for radical species varied significantly day-to-day over the range 1 - 8 x 10^6 cm^{-3} (OH), 0.2 - 1.5 x 10^8 cm^{-3} (HO_2) and 0.3 - 2.5 x 10^8 cm^{-3} (RO_2). Averaged over the full observation period, the mean daytime peak in radicals was 2.7 x 10^6 cm^{-3}, 0.39 x 10^8 cm^{-3} and 0.88 x 10^8 cm^{-3} for OH, HO_2 and total RO_2, respectively. The main daytime source of new radicals *via* initiation processes (primary production) was the photolysis of HONO (~83 %), and the dominant termination pathways were the reactions of OH with NO and NO_2, particularly under polluted, haze conditions. The Master Chemical Mechanism (MCM) v3.3.1 operating within a box model was used to simulate the concentrations of OH, HO_2 and RO_2. The model underpredicted OH, HO_2 and RO_2, especially when NO mixing ratios were high (above 6 ppbv). The observation-to-model ratio of OH, HO_2 and RO_2 increased from ~ 1 (for all radicals) at 3 ppbv of NO to a factor of ~3, ~20 and ~91 for OH, HO_2 and RO_2, respectively, at ~200 ppbv of NO. The significant underprediction of radical concentrations by the MCM suggests a deficiency in the representation of gas-phase chemistry at high

NO_x. The OH concentrations were surprisingly similar (within 20 % during the day) inside and outside of haze events, despite $j(O^1D)$ decreasing by 50% during haze periods. These observations provide strong evidence that gas-phase oxidation by OH can continue to generate secondary pollutants even under high pollution episodes, despite the reduction in photolysis rates within haze.

1. Introduction

In China, especially its capital city, Beijing, air pollution and air quality are serious concerns (Tang et al., 2017). Beijing can experience severe haze episodes (Hu et al., 2014; Lang et al., 2017) with high particulate matter loadings during winter months, and high ozone episodes during the summer (Cheng et al., 2016; Wang et al., 2015). China has one of the ~~world's~~world's fastest expanding economies and has rapidly increased its urban population to form numerous megacities. From 1980 to 2005, the fraction of the population living in urban areas of China increased from ~~19.6~~20 to ~~40.5~~40 %. China's economic growth has led to an increase in energy consumption, with 50% of the global demand for coal accounted for by China in 2016 (Qi et al., 2016). The Chinese government have been implementing air quality controls in China (Zhang et al., 2016a) and emission and concentrations of primary pollutants have been decreasing nationwide, however, secondary pollutants still remain a major concern (Huang et al., 2014).

The OH radical mediates virtually all oxidative chemistry during the daytime, and converts primary pollutants into secondary pollutants, as shown in Figure 1. The reaction of OH with primary pollutant emissions (particularly NO_x ($NO+NO_2$), SO_2 and VOCs (volatile organic carbon)) can form secondary pollutants such as HNO_3, H_2SO_4 and secondary oxygenated organic compounds (OVOCs).~~The reaction of OH with primary pollutant emissions (particularly NO_x, SO_2 and VOCs) can form secondary pollutants such as HNO_3, H_2SO_4 and secondary oxygenated organic compounds (OVOCs).~~ These secondary pollutants can lead to the formation of secondary aerosol and contribute to the mass of $PM_{2.5}$. During the photochemical cycle initiated by OH, NO can be oxidised to form NO_2 via reaction with HO_2 and organic peroxy radicals, RO_2, and the subsequent photolysis of NO_2 can lead to the net formation of ozone. It has been shown in previous field campaigns that measured mixing ratios of radicals have a strong dependence with $j(O^1D)$ (Ehhalt and Rohrer, 2000; Ma et al., 2019; Stone et al., 2012; Tan et al., 2018). Hence, the radical concentrations measured during wintertime are typically expected to be lower than in the summertime due to lower photolysis rates of primary radical sources such as O_3, HONO and HCHO. Here we define primary production as any process which initiates the formation of radicals and hence the photochemical chain reaction. Also, the lower temperatures experienced in the winter lead to lower water vapour concentrations and this is expected to further limit primary OH formation via $(O^1D) + H_2O$ (Heard and Pilling, 2003).

In contrast to the expectation of limited photochemistry in winter, particularly during haze episodes when light levels are reduced, aerosol composition analysis has highlighted that the contribution of secondary aerosol to the total particulate mass increases during pollution events in the North China Plain (NCP) (Huang et al., 2014), suggesting that chemical oxidation still plays an important role in aerosol formation in winter. To fully understand the role of the OH radical during haze events experienced in central Beijing, direct *in situ* measurements of ambient OH concentration are required.

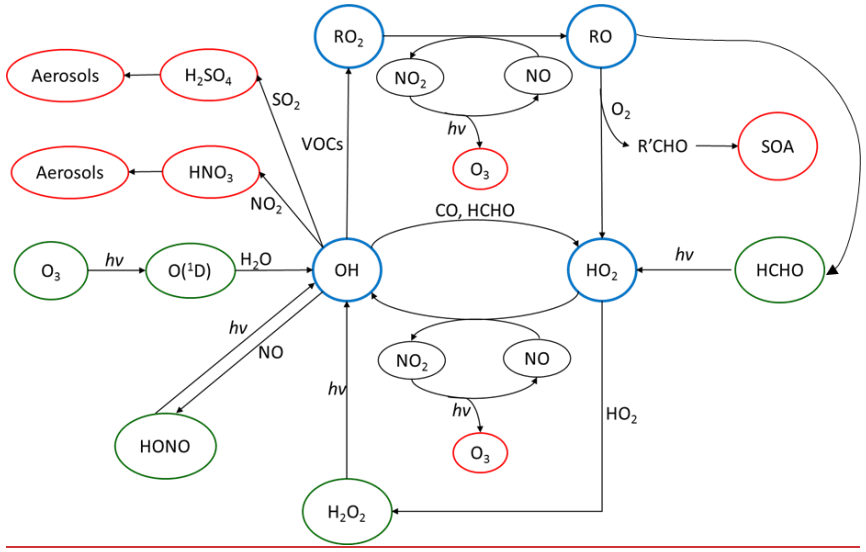

Figure 1. The tropospheric photochemical cycle, with the green circles representing species acting as routes for radical formation, the blue circles representing the radical species themselves and the red circles representing the formation of secondary pollutants. The cycle does not show any heterogeneous source (e.g. heterogeneous production of HONO) or loss processes for the radical species. It should be noted the measured HONO abundance cannot be explained by the reaction of OH + NO alone.

Formatted: Centered

Formatted: Font: Bold

Formatted: Line spacing: Multiple 1.08 li

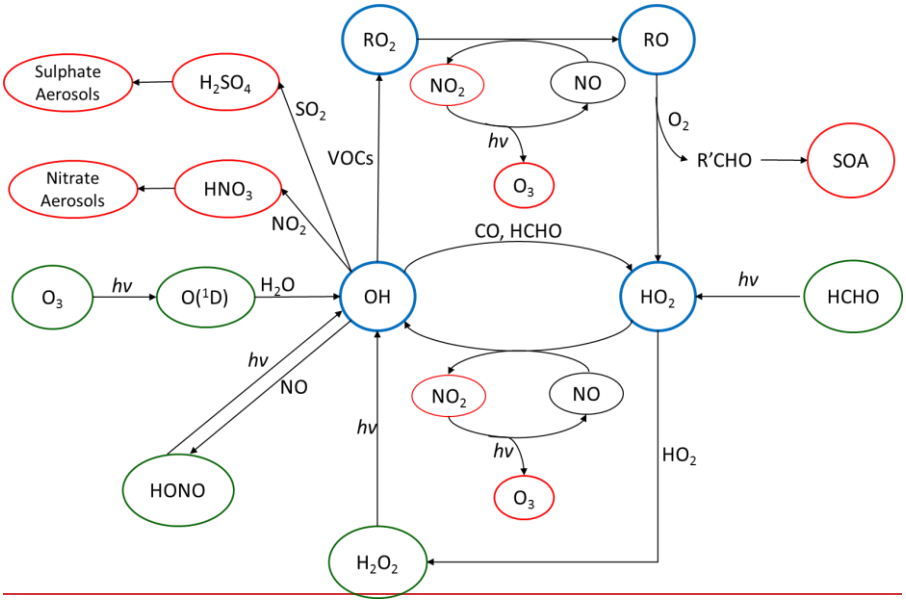

~~***Figure 1.*** The tropospheric photochemical cycle, with the green circles representing species acting as primary routes for radical formation via initiation reactions, the blue circles representing the radical species themselves and the red circles representing the formation of secondary pollutants. The cycle does not show any heterogeneous source or loss processes for the radical species.~~

Formatted: Normal

Measurements of OH and HO_2 in northern China during the wintertime have only recently been made. The first measurements were made during the BEST-ONE campaign (Tan et al., 2017) that took place in January 2016 in Huairou, which is a suburban site 60 km northeast from Beijing. The average daytime maximum concentrations observed during the BEST-ONE campaign for OH, HO_2 and RO_2 were 2.5 x 10^6 cm^{-3}, 0.8 x 10^8 cm^{-3} (3.2 pptv) and 0.6 x 10^8 cm^{-3} (2.4 pptv) respectively. The concentration of OH during the BEST-ONE campaign was an order of magnitude higher than predicted by global models over the North China Plain region (Lelieveld et al., 2016), and is consistent with the increase in secondary aerosol contribution to $PM_{2.5}$ observed during haze events (Huang et al., 2014). The radical measurements during the BEST-ONE campaign were separated into clean and polluted periods (OH reactivity (k_{OH}) > 15 s^{-1}) with an average daily maximum OH concentration for these periods of 4 x 10^6 cm^{-3} and 2.3 x 10^6 cm^{-3}, respectively. The RACM2-LIM1 (Regional Atmospheric Chemistry Model coupled with Leuven Isoprene Mechanism 1) box model was used to simulate the radical concentrations measured during BEST-ONE (Tan et al., 2018) but these could not reproduce the OH concentration observed when NO was above 1 ppbv or below 0.6 ppbv; consistent with previous campaigns when OH was measured and modelled under NO concentrations > 1 ppbv (Emmerson et al., 2005; Kanaya et al., 2007; Lu et al., 2013; Tan et al., 2017; Zhou et al., 2003). More recently, OH

and HO_2 were measured in central Beijing during winter-time at the Peking University (PKU) campus in November/December 2017 (Ma et al., 2019). The radical measurements were simulated using the RACM2-LIM1 box model which highlighted an under-prediction of the OH concentration when NO exceeded 1 ppbv (Ma et al., 2019). Two further campaigns have taken place in northern China during the summertime. The first took place in 2006 at a suburban site in Yufa (Lu et al., 2013), which is 40 km south of Beijing. The second took place in 2014 at the rural site in Wangdu (Tan et al., 2017). In both the Wangdu and Yufa field campaigns, the box model calculations underestimated the OH concentration when NO was below 0.5 ppbv. When NO exceeded 2 ppbv, a missing peroxy radical source was found, leading to a large underestimation of local ozone production by the model.

To try to understand the link between radical chemistry and the extremely high air pollution that is seen during Beijing in the wintertime, a field campaign "Air Pollution and Human Health in Chinese Megacities" (APHH) took place in central Beijing from November to December in 2016. Simultaneous measurements of OH, HO_2, and RO_2 concentrations were performed during the APHH campaign. OH reactivity (k(OH)), which is the sum of the concentration of species (X_i) that react with OH multiplied by the corresponding bimolecular rate coefficient, k_{OH+Xi}, along with other trace gas and aerosol measurements were made alongside the radicals.

In this paper we present the measurements of OH, HO_2, RO_2 and OH reactivity from the winter campaign. The concentrations of the radical species are compared to model results from the Master Chemical Mechanism (MCM3.3.1.) to assess if the radical concentrations can be simulated across the range of measured NO_x, with a particular focus under on the high NO_x conditions that were experienced. The importance of OH-initiated oxidation processes on the formation of ozone and SOA in the wintertime in Beijing are demonstrated.

2 Experimental

2.1 Location of the field measurement site

The observations took place in central Beijing at the Institute of Atmospheric Physics (IAP), which is part of the Chinese Academy of Sciences; the location of the site is shown in Figure 2, and is ~ 6.5 km from the Forbidden City. Beijing is the capital city of China and is located on the northwest border of the North China Plain (NCP). It is surrounded by the Yanshan Mountains in the west, north and northeast (Chan and Yao, 2008). The topography of Beijing allows for the accumulation of pollutants, especially when southerly winds carrying emissions from the industrial regions are experienced. As shown by Figure 2, the measurement site was within 100m of a major road, thus local anthropogenic emissions likely influence the site, although no rush hour was observed from the diel variation of the trace gas measurements (see Figure 5). The site was also close to local restaurants and a petrol station.

More details of the measurement site and instrumentation can be found in the APHH overview paper (Shi et al., 2018). The instruments were housed in containers and located on the ground at the IAP site on a grassed area, the distance between the Leeds and York container (VOC and trace gas measurements) was ~3 m.

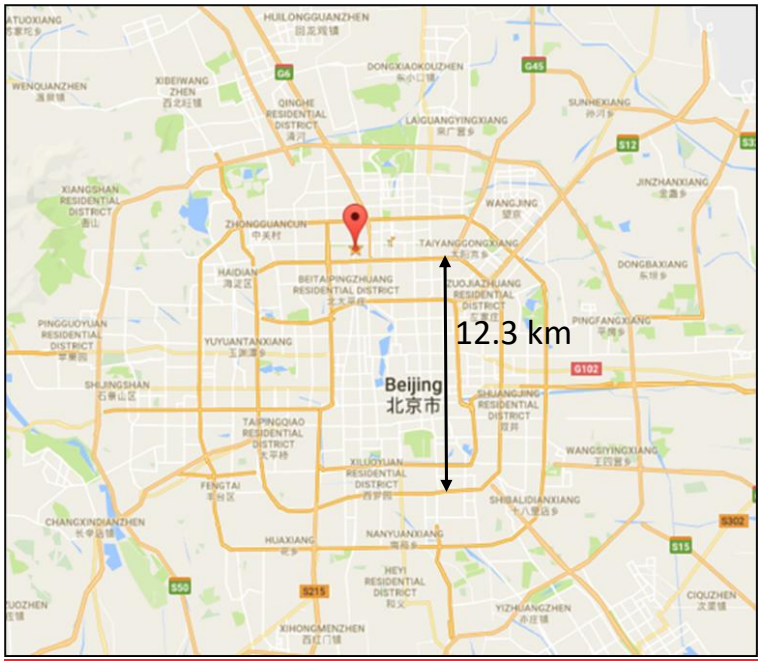

Figure 2. Location of the Institute of Atmospheric Physics, Chinese Academy of Sciences (source: ©Google Maps), the location (39°58′33″ N, 116°22′41″ E) of the APHH campaign.

Formatted: Font: Bold

Formatted: Line spacing: Multiple 1.08 li

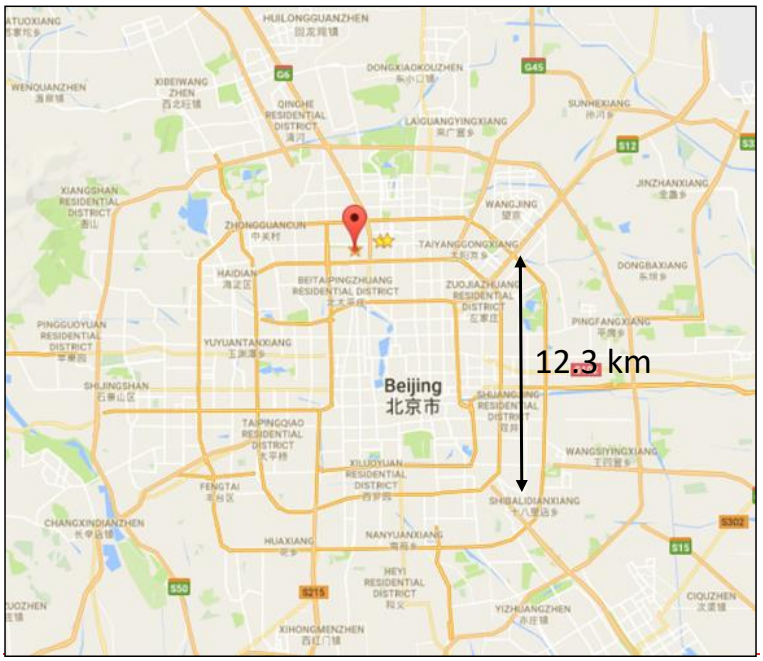

Figure 2. Location of the Institute of Atmospheric Physics, Chinese Academy of Sciences (source: ©Google Maps), the location (39°58′33″ N, 116°22′41″ E) of the APHH campaign.

2.2 Instrumental details

2.2.1 OH, HO_2 and RO_2 measurements

The University of Leeds ground-based FAGE (fluorescence assay by gas expansion) instrument (Whalley et al., 2010) was deployed at the IAP site and made measurements of OH, HO_2 and RO_2 radicals, as well as OH reactivity (k(OH)). A general outline, specific set-up and the running conditions during APHH are described here. Further details on the methodology for sequential measurements of OH and HO_2 that are made in the first fluorescence cell (HO_x) and sequential measurements of HO_2^* and RO_2 using the RO_xLIF method (described in detail below) in the second cell (RO_x) can be found in Whalley et al. (2018). HO_2^* refers to the measurement of HO_2 and complex RO_2 species; complex RO_2 are RO_2 species that are formed from alkene and aromatic VOCs, or VOCs that have a carbon chain greater than C_4 and which under certain conditions are detected together with HO_2 (Whalley et al., 2018). The radical measurements were made from a 6.1 m air-conditioned shipping container which has been converted into a mobile laboratory. The FAGE instrument has two detection cells which are located on top of the shipping container (sampling height of 3.5 metres) within a weather-proof housing. A Nd:YAG pumped Ti:Sapphire laser (Photonics Industries) generated pulsed tuneable near IR radiation at a pulse repetition rate of 5 kHz, which was frequency doubled then tripled using two

Formatted: Justified, Line spacing: Multiple 1.08 li, Don't keep with next

non-linear crystals to produce UV light at 308 nm and used to excite OH via the $Q_1(1)$ transition of the $A^2\Sigma^+$, v′=0 ← $X^2\Pi_i$, v″=0 band.

During the APHH campaign the configuration of the two detection cells was the same as deployed during the ClearfLo campaign in London (Whalley et al., 2018), with the two cells coupled together via a connecting side arm, which enabled the laser light exiting the HO_x cell to pass directly into the RO_x cell. The channel photo-multiplier (CPM) detectors that were used to detect fluorescence previously (Whalley et al., 2018) have been replaced by gated MCPs (micro-channel plates, Photek PMT325/Q/BI/G) and fast gating units, Photek GM10-50B) for the ~~AIRPRO~~ APHH project.

The ROxLIF flow reactor (83 cm in length, 6.4 cm in diameter) was coupled to the second FAGE detection cell to allow for detection of RO_2 (total, complex and simple) using the method outlined by Fuchs et al. (2008). The flow reactor was held at ~30 Torr and drew ~7.5 SLM through a 1 mm pinhole ID (in-diameter). The flow reactor was operated in two mode: in the first (HO_x mode) 125 sccm of CO (Messer, 10% in N_2) was mixed with ambient air close to the pinhole to convert OH to HO_2. In the second (RO_x mode), 25 sccm of NO in N_2 (Messer, 500 ppmv) was also added to the CO flow to convert RO_2 into OH. The CO present during RO_x mode rapidly converts the OH formed into HO_2. The air from the RO_xLIF flow reactor was drawn (5 SLM) into the FAGE fluorescence cell (held at ~1.5 Torr) and NO (Messer, 99.9%) was injected into the fluorescence cell to convert HO_2 to OH. In HO_x mode a measure of OH + HO_2 + cRO_2 (complex RO_2) was obtained; whilst RO_x measured OH + HO_2 + ΣRO_2. sRO_2 (simple RO_2) concentration was determined by subtracting the concentration of cRO_2, HO_2 and OH from RO_x.

In previous laboratory experiments the sensitivity of the instrument to a range of different RO_2 was investigated and can be found in Whalley et al.(2018). Similar sensitivities were determined for a range of RO_2 species that were tested and agreed well with model-determined sensitivities. For comparison of the modelled RO_2 to the observed RO_2-total, RO_2-complex and RO_2-simple, the RO_xLIF instrument sensitivity towards each RO_2 species in the model was determined by running a model first under the RO_xLIF reactor and then the RO_xLIF FAGE cell conditions (NO concentrations and residence times) to determine the conversion efficiency of each modelled RO_2 species to HO_2. The potential interference in the RO_2 measurements from HO_2NO_2 and $CH_3O_2NO_2$ has been explored in the supplementary material in section S1.4, however the data presented through-out the paper are the uncorrected data since the correction is small (correction from the decomposition of HO_2NO_2 and $CH_3O_2NO_2$ is ~6 %, ~8 % and 4 % for total, complex and simple RO_2, respectively.)

2.2.1.3 Inlet Pre Injector

For part of the campaign, an Inlet-pre-injector (IPI) was attached to the HO_x cell. The IPI removes ambient OH by the injection of propane directly above the cell inlet and facilitates a background

Formatted: Line spacing: 1.5 lines

measurement whilst the laser wavelength is still tuned to an OH transition, with this type of OH measurement known as "OHchem". The OHchem background signal will include a signal from laser scattered light, scattered solar radiation and may potentially also include a fluorescence signal from any OH that is generated internally from an interference precursor within the LIF cell. Internally generated OH constitutes an interference, but can be readily identified by comparing the OHchem background signal to the background signal measured when the laser wavelength is tuned away from the OH transition, with this type of OH measurement known as "OHwave". The OHwave background signal is from laser scattered light and solar scattered radiation only. OHchem is the online OH signal – OHchem background and OHwave is the OH online signal – OHwave background.

The Leeds IPI was first implemented during the ICOZA campaign in Norfolk, UK, in the summer of 2015, and is described in further detail elsewhere (Woodward-Massey et al., 2019). During the APHH winter campaign the laser online (wavelength tuned to the OH transition) period lasted 300 seconds for both OHchem and OHwave data acquisition cycles. When the IPI was physically taken off the HO_x fluorescence cell, OH and HO_2 were measured sequentially in this cell with 150 seconds online period each. The other (RO_x) fluorescence cell measured HO_2^* and RO_2 simultaneously with OH and HO_2, respectively, when the IPI was removed. When the IPI was being operated during the APHH campaign OHwave, OHchem and HO_2 were measured in the HO_x cell sequentially for 120, 120 and 60 seconds, respectively. The RO_x cell measured HO_2^* and RO_2 for 240 and 60 seconds, respectively when the IPI was operated. The laser offline period for both data acquisition cycles lasted 30 seconds, with NO injected for the final 15 seconds of this laser offline period. From the 08/11/2016 to 24/11/2016 the HO_x cell was operated without the IPI assembly in place, the IPI was then installed and run on the HO_x cell from 02/12/2016 to 08/12/2016.

The correlation of OHwave and OHchem during the APHH winter campaign is shown in Figure 3. The slope of 1.05±0.07 demonstrates that within the errors in the linear fit no interference was evident during the winter campaign. OHwave data were corrected for the known interference from $O_3 + H_2O$, see Woodward-Massey et al. (2020) for further details. The $O_3 + H_2O$ interference calculated was very small (median ~8.5 x 10^3 molecule cm^{-3}) due to the low concentration of H_2O and O_3. All figures and calculation from now on have used OHwave as it is the most extensive time-series (12 days compared to 5 days). ~~OHwave data were corrected for the known interference from $O_3 + H_2O$, see (Woodward-Massey et al., 2019) for further details.~~ All figures and calculation from now on have used OHwave as it is the most extensive time-series (12 days compared to 5 days).

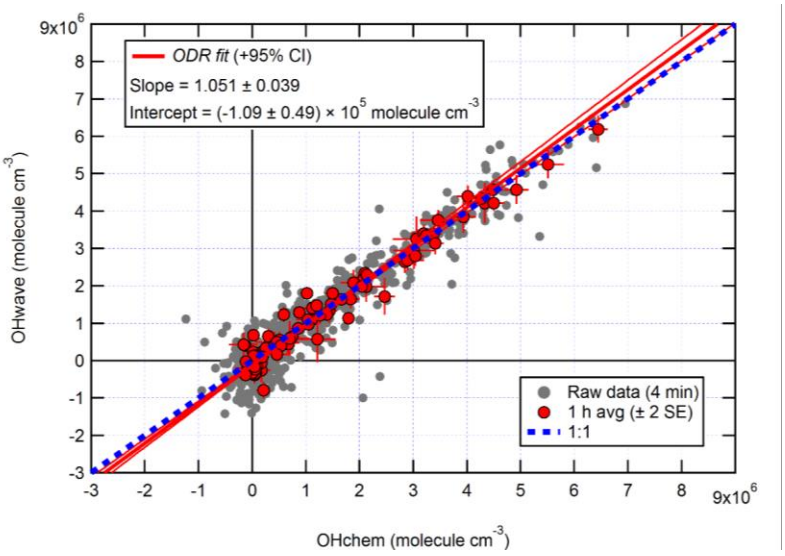

Figure 3. Overall intercomparison of OHwave and OHchem observations from the winter 2016 APHH campaign. Grey markers represent raw data (6 min acquisition cycle, 4 minutes and 2 minutes for the OH and HO_2 measurements), with 1 h averages (±2 standard error, SE) in red. The thick red line is the orthogonal distance regression (ODR) fit to the hourly data, with its 95% confidence interval (CI) bands given by the thin red lines; fit errors given at the 2σ level. For comparison, 1:1 agreement is denoted by the blue dashed line. OHwave data were corrected for the known interference from $O_3 + H_2O$. Taken from (Woodward-Massey et al., 2020) where further details can be found. ~~Overall intercomparison of OHwave and OHchem observations from the winter 2016 AIRPRO campaign. Grey markers represent raw data (6 min acquisition cycle), with 1 h averages (±2 standard error, SE) in red. The thick red line is the orthogonal distance regression (ODR) fit to the hourly data, with its 95% confidence interval (CI) bands given by the thin red lines; fit errors given at the 2σ level. For comparison, 1:1 agreement is denoted by the blue dashed line. OHwave data were corrected for the known interference from $O_3 + H_2O$. Taken from (Woodward-Massey et al., 2019) where further details can be found.~~

Formatted: Font: 11 pt, Not Italic, Font color: Auto

Formatted: Font: 11 pt, Not Italic, Font color: Auto

Formatted: Font: 11 pt, Not Italic, Font color: Auto

Formatted: Font: 11 pt, Not Italic, Font color: Auto

2.2.2 Calibration

The instrument was calibrated approximately every three days by photolysis of a known concentration of water vapour at 185 nm in synthetic air (Messer, Air Grade Zero 2) within a turbulent flow tube to generate equal concentrations of OH and HO_2 as described in Whalley et al. (2018). The product of the photon flux at 185 nm and the water vapour photolysis time, which is required to calculate the concentration of OH and HO_2, was measured using a $N_2O \rightarrow NO$ chemical actinometer (Commane et al., 2010) both before and after the APHH campaign. For calibration of RO_2 concentrations, methane (Messer, Grade 5, 99.99%) was added to the humidified air flow in sufficient quantity to rapidly titrate OH completely to CH_3O_2. For reporting the total concentration of RO_2 the calibration factor for CH_3O_2 was used. More details on the RO_xLIF and calibration, for example the sensitivity of the instrument towards various RO_2 species which is taken into account when comparing RO_2 measurements to model

calculations, can be found in Whalley et al. (2018). The limit of detection (LOD) on average for the APHH campaign was 5.5×10^5 molecule cm^{-3} for OH, 3.1×10^6 molecule cm^{-3} for HO_2 and 6.5×10^6 molecule cm^{-3} for CH_3O_2 at a typical laser power of 11 mW for a 7 minute data acquisition cycle (SNR=2). The field measurements of all species were recorded with 1 s time-resolution, and the precision of the measurements was calculated using the standard errors in both the online and offline points. The accuracy of the measurements was ~ 26 % (2σ), and is derived from the error in the calibration, which derives largely from that of the chemical actinometer (Commane et al., 2010).

2.2.3 OH Reactivity

OH reactivity measurements were made using the laser flash photolysis pump-probe technique and the instrument is described in detail in Stone et al. (2016). Ambient air was drawn into the reaction cell (85 cm in length, 5 cm in diameter) at 12 SLM. Humidified ultra-high purity air (Messer, Air Grade Zero 2) passed a low-pressure Hg lamp at 0.5 SLM to generate ~ 50 ppbv of O_3 which was mixed with the ambient air. The O_3 was photolyzed at 266 nm to generate a uniform OH concentration across the reaction cell. The change in the OH radical concentration from pseudo-first-order loss with species present in ambient air was monitored by sampling the air from the reaction cell into a FAGE detection cell at ~1.5 Torr. The 308 nm probe laser (same as the FAGE laser describe above) was passed across the gas flow in the FAGE cell to excite OH radicals, and then detected the fluorescence signal at ~ 308 nm detected by a gated channel photomultiplier tube. The OH decay profile owing to reactions with species in ambient air was detected in real time. The decay profile was averaged for 5-mins and fitted with a first-order rate equation to find the rate coefficient describing the loss of OH (k_{loss}), with k_{OH} determined by subtracting the physical loss of OH (k_{phys}). The OH reactivity data were fitted with a mono-exponential decay function as no bi-exponential behaviour was observed, even at the highest NO concentrations, and hence there was no evidence for recycling from HO_2 + NO impacting on the retrieved values The total uncertainty in the ambient measurements of OH reactivity is ~ 6% (Stone et al. 2016).

2.2.~~3~~ 4 The Master Chemical Mechanism, MCM

A constrained zero-dimensional (box) model incorporating version 3.3.1 of the Master Chemical Mechanism (MCMv3.3.1) (http://mcm.leeds.ac.uk/MCM/home) was used to predict the radical concentrations and OH reactivity and to compare with the field observations. The MCM is a detailed mechanism that almost explicitly describes the oxidative degradation of ~ 140 VOCs ranging from methane to those containing 12 carbon atoms (C1 – C12). The complete details of the kinetic and photochemical data used in the mechanism can be found at the MCM website (http://mcm.leeds.ac.uk/MCM/home). For this work, the model was run with a sub-set of the MCM

Formatted: Font: Bold

and treated the degradation of simultaneously measured non-methane VOCs, CH_4 and CO following oxidation by OH, O_3 and NO_3, and included 11,532 reactions and 3,778 species. The model was constrained by measurements of NO, NO_2, O_3, CO, HCHO, HNO_3, HONO, water vapour, temperature, pressure and individual VOC species measured by GC-FID (gas chromatography with flame ionisation). The accuracy and precision of trace gas species can be found in Table 2, details on the HONO measurements used in the modelling scenarios can be found in Crilley et al.(2019). Details for other measurements can be found in Shi et al.(2018). The time resolution for the GC-FID data was 1 hr and has been interpolated to 15-min for the model input.

Table 1 shows the different species measured by the GC-FID whose degradation was included in the mechanism used. The model was constrained with the measured photolysis frequencies $j(O^1D)$, $j(NO_2)$ and j(HONO)), which were calculated from the measured wavelength-resolved actinic flux and published absorption cross sections and photodissociation quantum yields. For other species which photolyse at near-UV wavelengths, such as HCHO and CH_3CHO, the photolysis rates were calculated by scaling to the ratio of clear-sky $j(O^1D)$ to observed $j(O^1D)$ to account for clouds. For species which photolyse further into the visible the ratio of clear-sky $j(NO_2)$ to observed $j(NO_2)$ was used. The variation of the clear-sky photolysis rates (j) with solar zenith angle (χ) was calculated within the model using the following expression Eq. 1~~Eq. 1~~:

$$j = l\cos(\chi)^m \times e^{-n\sec(\chi)} \qquad \text{Eq. 1}$$

with the parameters *l, m* and *n* optimised for each photolysis frequency (see Table 2 in Saunders et al. (2003).

A constant H_2 concentration of 500 ppbv was assumed (Forster et al., 2012). The model inputs were updated every 15 minutes, the species that were measured more frequently were averaged to 15 minutes whilst the measurements with lower time resolution were interpolated. The loss of all non-constrained, model generated species by deposition or mixing was represented as a first order deposition rate equivalent to 0.1/MH (MH represent the height of the boundary layer). The effect of changing the deposition rate is minor, as shown in Figure S1 of the Supplementary Information. The model was run for the entirety of the campaign in overlapping 7 day segments. To allow all the unmeasured, model generated intermediate species time to reach steady state concentrations, the model was initialised with inputs from the first measurement day (16th November 2016) and spun-up for 2 days before comparison to measurements were made. The model described above is from now on called MCM-base.

An additional model was run using higher weight VOCs that were measured using a PTR-MS (Proton Transfer Mass Spectrometer) to assess the effect on modelled radical species (OH, HO_2 and RO_2) and

Formatted: Font: Not Italic

modelled OH reactivity, with this model run showing there is <10% effect on the radical concentration and OH reactivity (see Supplementary Information, Figures S2 and S3).

Instrument	Species	Reference
DC-GC-FID	Methane, Ethane, ethylene, propane, propene, isobutane, butane, C_2H_2, trans-but-2-ene, but-1ene, Isobutene, cis-but-2-ene, 2-Methylbutane, pentane, 1,3-butadiene, trans-2-pentene, cis-2-pentene, 2-methylpetane, 3-methypetane, hexane, isoprene, heptane, Benzene, Toluene, m-xylene, p-xylene, o-xylene, methanol, dimethyl ether.	Hopkins et al. (2011)

Table 1. VOC species measured by the DC-GC-FID (dual channel gas-chromatography with flame ionisation detection) that have been constrained in the box-model utilising the Master Chemical Mechanism.

Instrument	Technique	2σ Uncertainty / %	2σ Precision/ ppbv
O_3, TEi49i	UV absorption	4.04	0.28[1]
NO, TEi42i-TL	Chemiluminescence via reaction with O_3	4.58	0.03[1]
SO_2, TEi43i	UV fluorescence	3.12	0.03[1]
NO_2, CAPS, T500U	Cavity enhanced absorption spectroscopy	5.72	0.04[1]
HONO	LOPAP x2, BBCEAS x 2, ToF-CIMS and SIFT-MS	9 – 22%	0.025 – 0.130

Table 2. Instruments and techniques used to measure key model constraints. 2σ uncertainties for the measured trace gas species used in the modelling scenarios are quoted. [1]Precision is given for 15-minute averaging time. For details of the HONO measurements please see Crilley et al.(2019).

Formatted: Font: Bold

The model scenarios involved in this work are summarised in ~~Table 2~~Table 3.

Model Name	Description
MCM-base	The base model described above in Section 2.2.3.
MCM-cHO$_2$	The same as MCM-base, but with the model constrained to the measured value of the HO_2 concentration.
MCM-PRO2	The same as MCM-base, but including an extra primary source of RO_2 species to reconcile the measured total RO_2 with modelled RO_2. Details for this can be found in section 4.2.
MCM-PRO2-SA	The same as MCM-PRO2 but including the uptake of HO_2 to aerosol with an uptake coefficient of γ = 0.2 Jacob et al.(2000).

Table 3. Description of the model scenarios and how they differ from the base model, and the associated name of that model that has been used in the body of this work.

3 Results

3.1 Chemical and Meteorological conditions

During the campaign various chemical and meteorological conditions were observed, as shown in Figure 4, including several haze periods. According to the meteorological standards (QX/T113-2010, Shi et al. (2018)), haze is defined as (i) visibility < 10 km at relative humidity (RH) < 80 % or (ii) if RH is between 80 and 95 %, visibility < 10 km and PM2.5 > 75 μg m^{-3}. For the purpose of this work the periods defined as haze are when $PM_{2.5}$ exceeds 75 μg m^{-3}. The wind rose for the winter 2016 campaign shows the dominant wind direction is from the northwest which coincides with higher wind speeds, also south westerly flows were frequent in the winter APHH campaign (see Shi et al. (2018) for more details). The south-westerly wind direction observed in the winter 2016 campaign had the potential to bring more polluted air from the upwind Hebei province to the observations site in Beijing.

The timeseries of $j(O^1D)$, relative humidity (RH), temperature, CO, SO_2, ~~O_2~~O_3, NO, NO_2, HONO, ~~and~~ $PM_{2.5}$, HCHO, butane and toluene is shown in Figure 4. There were several co-located measurements of HONO made during the APHH campaign, and the HONO mixing ratios shown in Figure 4 and used in the model were values taken from a combination of all measurement at the IAP site, and recommended by Crilley et al. (2019) who provide further details for the methodology for selection of the HONO data. For a given time of day, large variations in $j(O^1D)$ during the campaign were observed, with the reductions caused by decreasing light levels driven by enhanced $PM_{2.5}$. The temperature during the campaign varied between -10°C and +15°C. The relative humidity during the campaign varied between 20 – 80% RH; generally with higher RH coinciding with haze events. The time-series for trace gas species showed high mole fractions for CO (1000-4000 ppbv), SO_2 (5 – 25 pbbv), NO (20 – 250 ppbv) but relatively low O_3 (1 – 30 ppbv). HONO during the campaign was generally quite high reaching up to 10 ppbv (Crilley et al., 2019). Frequent haze events were also observed during the winter campaign, with $PM_{2.5}$ mass concentration reaching up 530 μg m^{-3}. The VOC concentration (HCHO, toluene and butane) track pollution events and each other very well; the mole fraction of the VOCs varied between 0.2 - 11.3 ppbv.

The diel variation for $j(O^1D)$, NO, NO_2, O_3, O_x, HONO, ~~SO_2~~ boundary layer height (BL) and CO separated into haze and non-haze periods is shown in Figure 5; the periods defined as haze are shown in Table 3. During the haze events $j(O^1D)$ decreased by ~50% at midday, as shown in Figure 5. The photo-activity of j(HONO) and $j(NO_2)$ extends further into the visible region of the solar spectrum compared with $j(O^1D)$ and so the reductions in their photolysis rates within haze are less; ~40% for j(HONO) and ~35%

for $j(NO_2)$ as discussed in (Hollaway et al., 2019). During polluted and hazy periods NO on average reached 100 ppbv at 8 am; on some days NO was close to 250 ppbv, some of the highest levels ever recorded during an urban field campaign. On clearer days, the peak NO was ~ 40 ppbv at 8 am (CST). A distinct increase in CO, NO_2 and SO_2 was also observed during haze periods, but no clear diurnal pattern in and outside of haze for these species was observed, as shown in Figure 5. The O_3 during the haze periods reduced on average by a factor of 3, due to titration by reaction with the high ~~levels~~ concentrations of NO observed. NO and O_3 show an anti-correlation during the cleaner periods due to their inter-conversion. The sum of NO_2 and O_3, O_x, increased during pollution periods from 40 ppbv to a maximum of 53 ppbv on average. HONO in both clean and haze periods shows a distinct diel pattern, with a large decrease in the morning from loss through photolysis and a minimum in the afternoon; a large increase in HONO concentration overnight probably originates from heterogeneous sources (i.e. NO_2 converting to HONO on humid surfaces) (Finlayson-Pitts et al., 2003; Lee et al., 2015; Li et al., 2012; Lu et al., 2018; Zhang et al., 2016b; Zhou et al., 2003). The HONO concentration was a factor of 3 higher on average during haze periods at midday than during the clearer periods. The boundary layer height (BLH) shows a similar diurnal variation inside and outside of haze, although the maximum BLH in haze is shifted to 14:30 compared to 12:30 outside of haze. The maximum and minimum BLH is similar inside and outside of haze and shows that containment is not the only driving force for pollution periods.

Haze Event	Local Time	$PM_{2.5}$ (μg m^{-3})	Visibility (km)
Event 1	08/11 21:00 – 10/11 16:00	158 (79 – 229)	4.1 (2.3 – 8)
Event 2	15/11 21:00 – 19/11 08:00	143 (56 – 244)	4.2 (0.6- 8)
Event 3	24/11 12:00 – 27/11 02:00	210 (68 – 363)	4.2 (1.5 -8)
Event 4	02/12 16:00 – 05/12 02:00	239 (58 – 530)	3.9 (0.9 -8)
Event 5	06/12 09:00 – 08/12 10:00	144 (64 – 229)	4.6 (2.2 – 8)

Table 4. The different haze periods observed during the winter campaign. Table recreated from Shi et al. (2018), from which further details can be found.

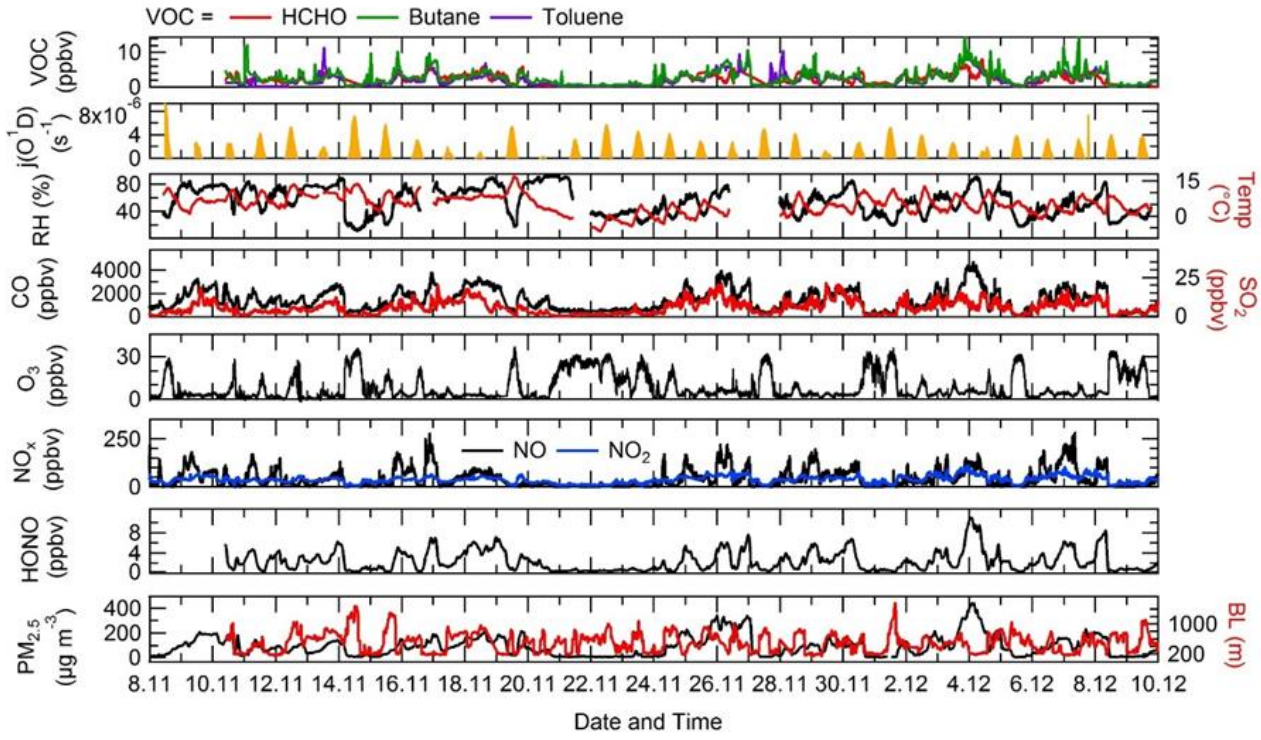

391

392 **Figure 4.** Time-series of $j(O^1D)$, relative humidity (RH), temperature (Temp), CO, SO_2, O_3, NO_x, HONO, boundary layer (BL), $PM_{2.5}$, HCHO, butane and toluene
393 from the 8th of November to 10th December 2016 at Institute of Atmospheric Physics (IAP), Beijing.

Formatted: Font: 11 pt, Bold, Not Italic, Font color:

Formatted: Font: 11 pt, Bold, Not Italic, Font color:

Formatted: Justified

Formatted: Font color: Auto

Formatted: Font: 11 pt, Not Italic, Font color: Auto

Formatted: Font: Not Italic

Formatted: Font: 11 pt, Not Italic

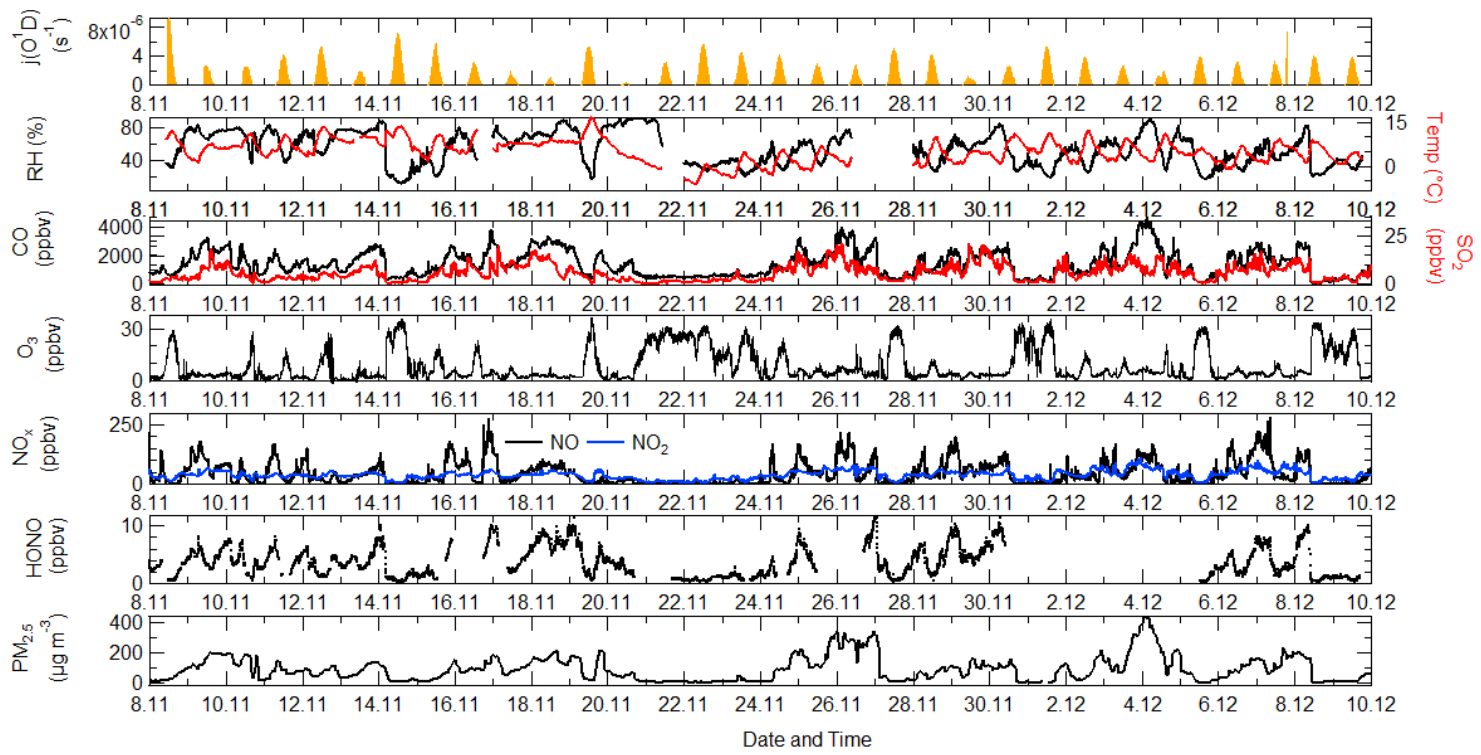

394

395 ~~**Figure 4.** Time-series of $j(O^1D)$, relative humidity (RH), temperature (Temp), CO, SO_2, O_3, NO_x, HONO and $PM_{2.5}$ from the 8th of November to 10th December~~
396 ~~2016 at Institute of Atmospheric Physics (IAP), Beijing.~~

397

Formatted: Centered

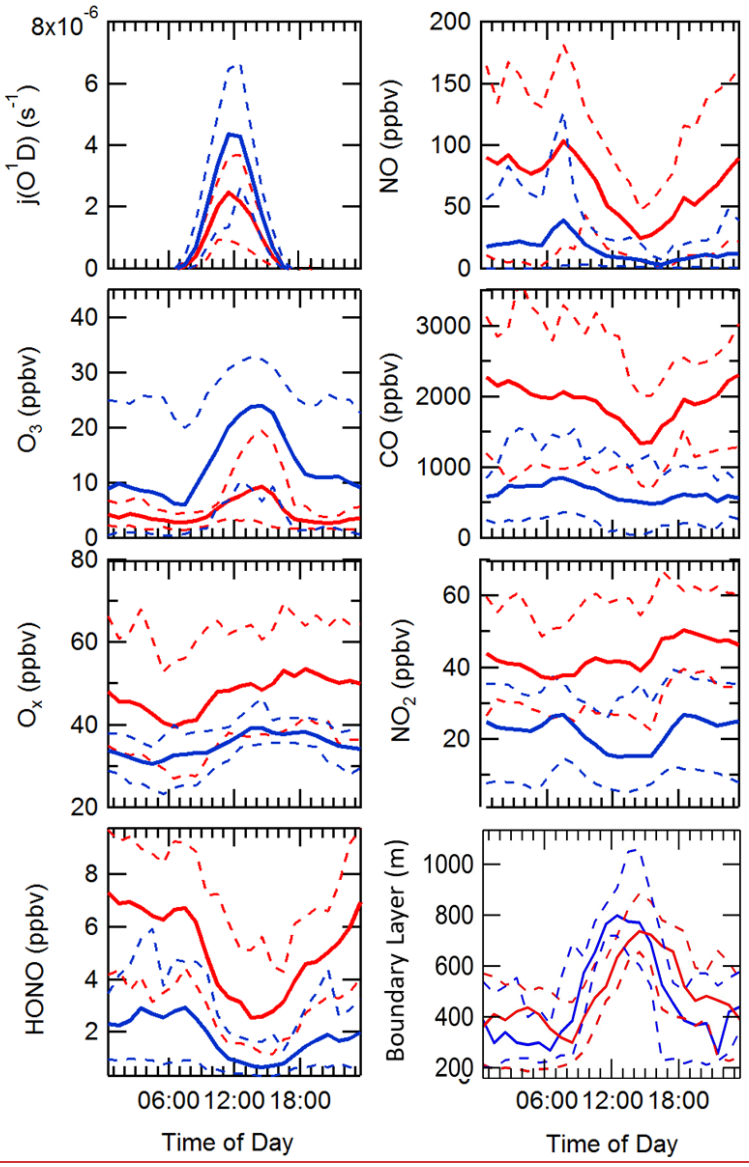

Figure 5. Comparison of the median average diel variation for $j(O^1D)$ (s^{-1}), NO (ppbv), O_3 (ppbv), CO (ppbv), O_x (ppbv), NO_2 (ppbv), HONO (ppbv) and boundary layer height (m) inside and outside haze events; denoted by solid red and blue lines, respectively. The dashed lines represent the interquartile range for the respective species and pollution period.

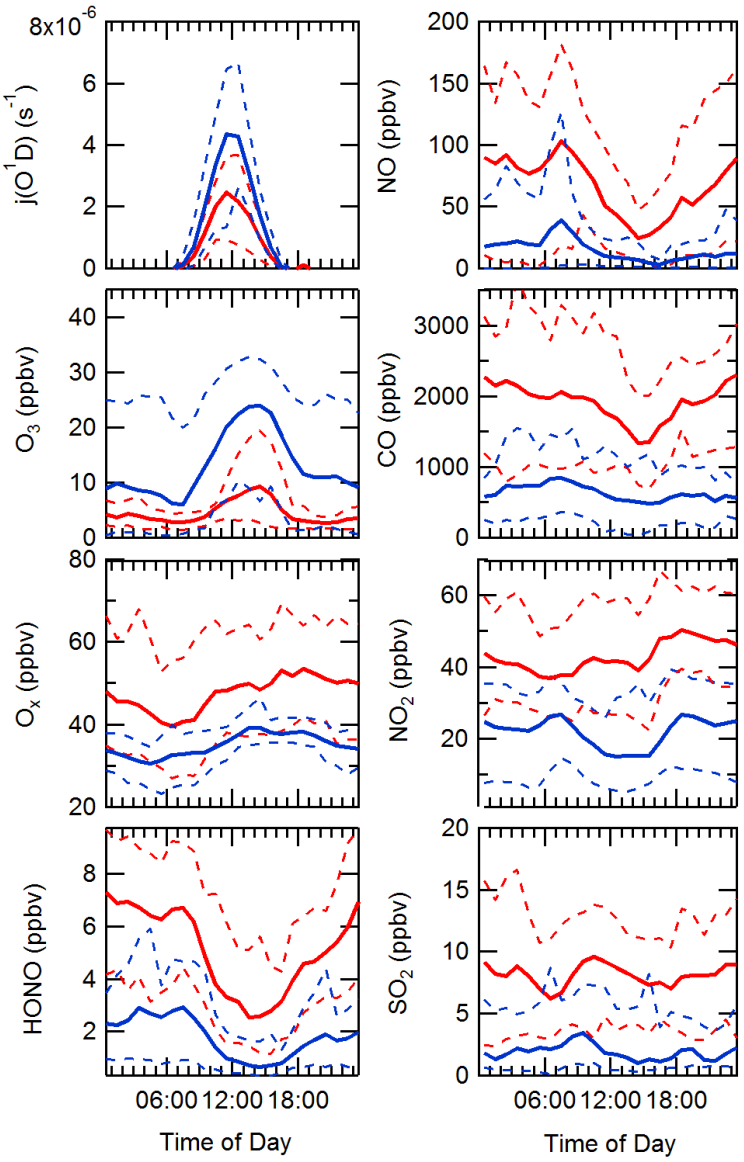

405 **Figure 5.** Comparison of $j(O^1D)$ (s^{-1}), NO (ppbv), O_3 (ppbv), CO (ppbv), O_x (ppbv), NO_2 (ppbv), HONO (ppbv) and SO_2 (ppbv) in and outside haze events; denoted by solid red and blue lines, respectively. The dashed lines represent the 25/75 percent confidence interval for the respective species and pollution period.

3.2 Steady State calculation of OH

Using measured quantities, a steady state approach has been used to calculate the OH concentrations for comparison with measurements, and also to determine the major sources of OH measured during the campaign. The photostationary steady state equation for OH, obtained from $d[OH]/dt = 0$, is given by a balance of the rate of production and the rate of destruction of OH:

$$[OH]_{pss} = \frac{p(OH) + j(HONO)[HONO] + k[HO_2][NO]}{k(OH)} \quad \text{Eq. 2}$$

where p(OH) is the measured rate of OH production from ozone photolysis and the subsequent reaction of $O(^1D)$ with water vapour, k is the rate coefficient for the reaction of HO_2 with NO at the relevant temperature, and k(OH) is the measured OH reactivity. Equation (2) is a simplification, and only takes into account the production of OH from two photolysis sources (O_3 and HONO) and from the reaction of HO_2 + NO. O_3+alkene and HO_2 + O_3 reactions are not included as, owing to the generally low ozone experienced, these were found to contribute < 1 % to the total OH production, as discussed in the MCM modelling section below. The pseudo-first order rate of loss of OH was constrained using the measured OH reactivity during the campaign, and hence includes all loss processes for OH. ~~OH reactivity is discussed further in Section 2.5.~~

Figure 6 shows the steady state calculation for OH between 2/12/2016 to 8/12/2016 where it is compared with the measured OH concentrations. These days were chosen as full data coverage for HONO, NO, j values, radical and k(OH) measurements were available. The agreement between the observed OH and OH calculated by equating the rate of OH produced from HO_2+NO and HONO photolysis and the loss of OH by reaction with all of its sinks, Eq.2, is very good. The agreement highlights that the OH budget can be determined by field measurements of the parameters necessary to quantify its rate of production and loss, and is closed to within 10%, well within the 26% error on the OH measurements themselves. The closure of the experimental budget suggests that measured OH and HO_2 are internally consistent, and that just from measured quantities the rate of production and the rate of destruction are the same within uncertainties. Although on the 04/12/2016 the PSS overpredicts the measured OH by a factor of ~2.5, the differences between the PSS and measured OH could be due to a variety of reason including errors in OH, HO_2, NO, kOH and HONO measurements and NO segregation across the site. A further discussion for the PSS for the 04/12 can be found in the supplementary section S1.6. The reaction of HO_2 and NO is the dominant source of OH (~80 – 90%) for Beijing during wintertime, owing to NO being so high in concentration. The photolysis of HONO is the second most important source producing ~10 – 20% of OH (and a much larger primary source of radicals in general as discussed below). The PSS has been separated into haze and non-haze events and shows that during haze events the PSS captures the OH concentration, although the PSS does

overpredict the OH concentration by ~1.35 between 09:30 – 14:30 in haze events. However, the overprediction by the PSS in haze events is highly influenced by the overprediction on the 04/12/2016. Whilst under non-haze conditions the PSS captures the OH concentration very well throughout the day. The production of from HONO increases in non-haze (~19%) compared with haze events (~7%). Due to low concentrations of O_3 in winter, the photolysis of O_3 and the subsequent reaction of $O(^1D)$ with water vapour is not an important source, being < 1 % of the rate of production. In addition, the reaction of O_3 with alkenes (whose concentrations were elevated in the winter) also contributed < 1% to the rate of OH production. The different HONO measurements present during the APHH campaign varied up-to ~40%, the sensitivity of the PSS on measured HONO is shown in the supplementary material section S1.5.

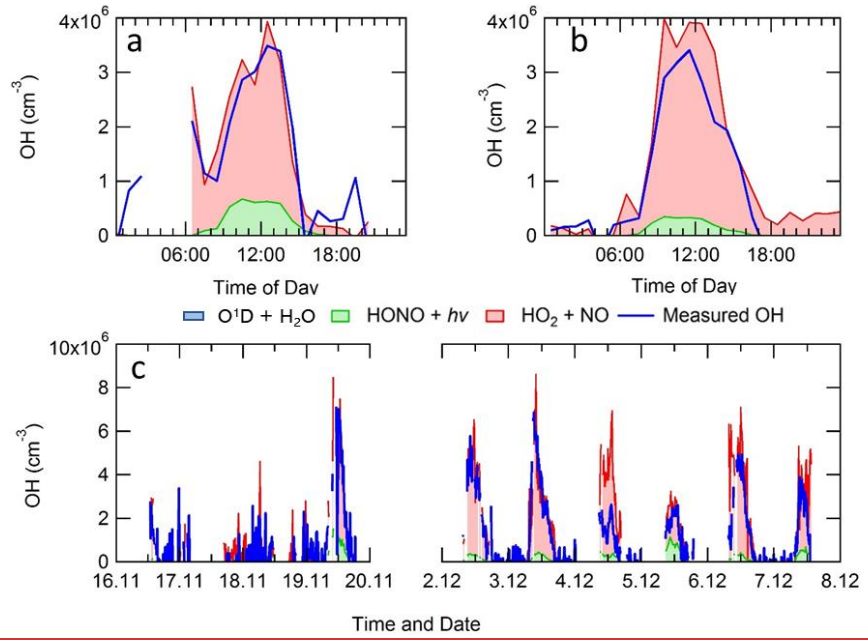

Figure 6. Average diel profile for observed and steady state calculated OH concentrations for: (a) non-haze, and(b) haze periods. Panel (c) shows a comparison time-series for the steady state calculation of OH and measured OH. The OH generated by O^1D+H_2O, although included in the key, is too small to be visible.

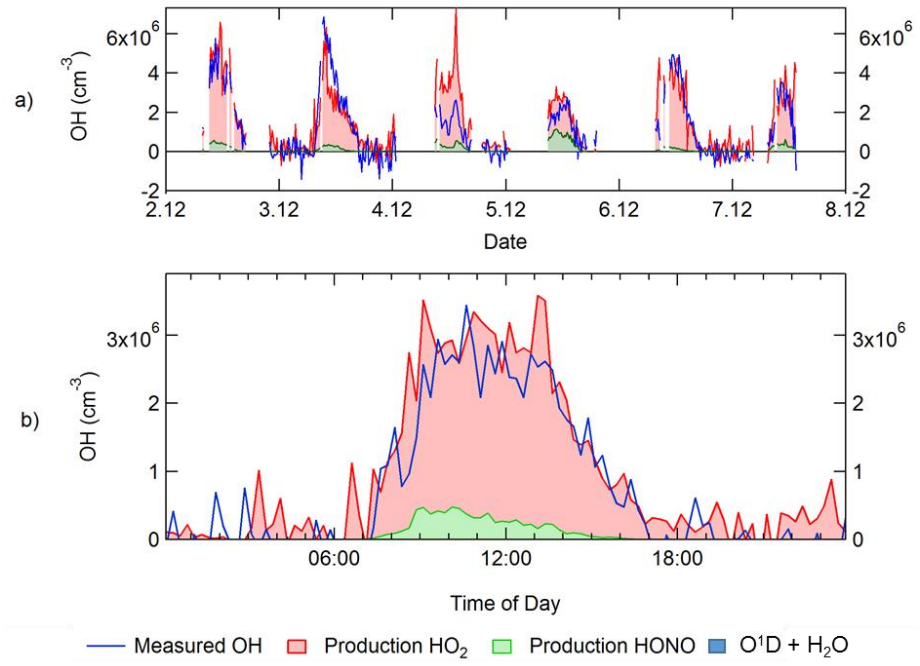

~~**Figure 6.** a) Time series for the steady state calculation of OH using equation (2). b) Average diel profile for observed and steady state calculated OH. Production HO_2 represents the recycling of HO_2 to OH *via* NO, Production HONO represents OH production from HONO photolysis. The OH generated by O^1D+H_2O, although included in the key, is too small to be visible.~~

3.3 Comparison of measured OH, HO_2, RO_2 radical concentrations and OH reactivity with calculations using a box-model and the Master Chemical Mechanism

Figure 7 shows a comparison between measured and modelled (MCM-base, defined in Table 2) OH, HO_2, RO_2 (speciated into simple and complex RO_2, defined in section 2.2.1) and OH reactivity. As seen in Figure 7, the measured daily maximum for the radical species varied day-to-day over the range 2.5 to 8 x 10^6 cm^{-3}, 0.07 to 1.5 x 10^8 cm^{-3} and 0.8 to 2 x 10^8 cm^{-3} for OH, HO_2 and sum of RO_2 respectively. ~~As seen in Figure 7, the measured daily maximum for the radical species varied day-to-day over the range 1 to 8 x 10^6 cm^{-3}, 0.7 to 1.5 x 10^8 cm^{-3} and 1 to 2.5 x 10^8 cm^{-3} for OH, HO_2 and sum of RO_2 respectively.~~ The daily maximum concentration for the sum of simple RO_2 varied between 0.2 to 1.3 x 10^8 cm^{-3}, and the complex RO_2 daily maximum concentration varied between 0.2 and 0.6 x 10^8 cm^{-3}. On average, the model underpredicts the OH, HO_2 and RO_2 concentrations by a factor of 1.7, 5.8 and 25, as shown in Figure 8. Although the underprediction by the model varies day-to-day: for OH, the underprediction varies from a factor of 5.9 to an overprediction of 1.05 (showing good agreement) between the model and measurements; for HO_2 the underprediction varies from a factor of 13.6 to

an over prediction by a factor of 5.3 and for RO_2 the under prediction varies from a factor of 2.1 to an over prediction of 8.0. Figure 8 shows the diel profile of OH, HO_2 and RO_2 averaged over the campaign, with daily average maximum of 2.7 x 10^6 cm^{-3}, 0.39 x 10^8 cm^{-3} and 0.88 x 10^8 cm^{-3} for OH, HO_2 and total RO_2, respectively. The complex and simple RO_2 show a very similar diurnal profile both peaking at 12:30 at a concentration of 4.4 x 10^7 molecule cm^{-3} and 4.5 x 10^7 molecule cm^{-3}, respectively. The model underpredicts the simple and complex RO_2 at 12:30 by a factor of 30 and 22, respectively. The large underprediction of both simple and complex RO_2 highlights the needs for additional primary sources forming both simple and complex species in the model. Section 4.2 explores the impact of additional primary source of RO_2 added into the model on OH and HO_2. The total measured OH reactivity during the campaign was quite large and varied between 10 to 145 s^{-1}. Averaged over the full campaign period the contributions to reactivity came from CO (17.3%), NO (24.9%), NO_2 (22.1%), alkanes (3.0%), alkynes and alkenes (10.8%), carbonyls (5.7%), terpenes (3.7%) and modelled intermediates (6.77%). Unusually, the largest contribution to OH reactivity is from reaction with NO. As shown in Figure 7 and Figure 8, OH reactivity is reproduced within 10% implying that the OH reactivity budget is captured well by the model. The model OH reactivity is the sum of all measured and modelled intermediate species multiplied by the respective rate coefficient for their reaction with OH.

Consistent with the steady state calculation, and as shown also in Figure 8, when the box-model was constrained to the concentrations of HO_2 measured using FAGE in the field (from now on this model scenario is called MCM-cHO_2), the measured and modelled OH concentration are in agreement within 10% which is less than the 26% error on the OH measurements. MCM-cHO2 also increases the RO_2 concentration by ~3.5 compared to MCM-base, but the RO_2 is still underpredicted by a factor ~7. The HO_2 was constrained in the model by inputting the HO_2 concentration at every 15 minute time-step.

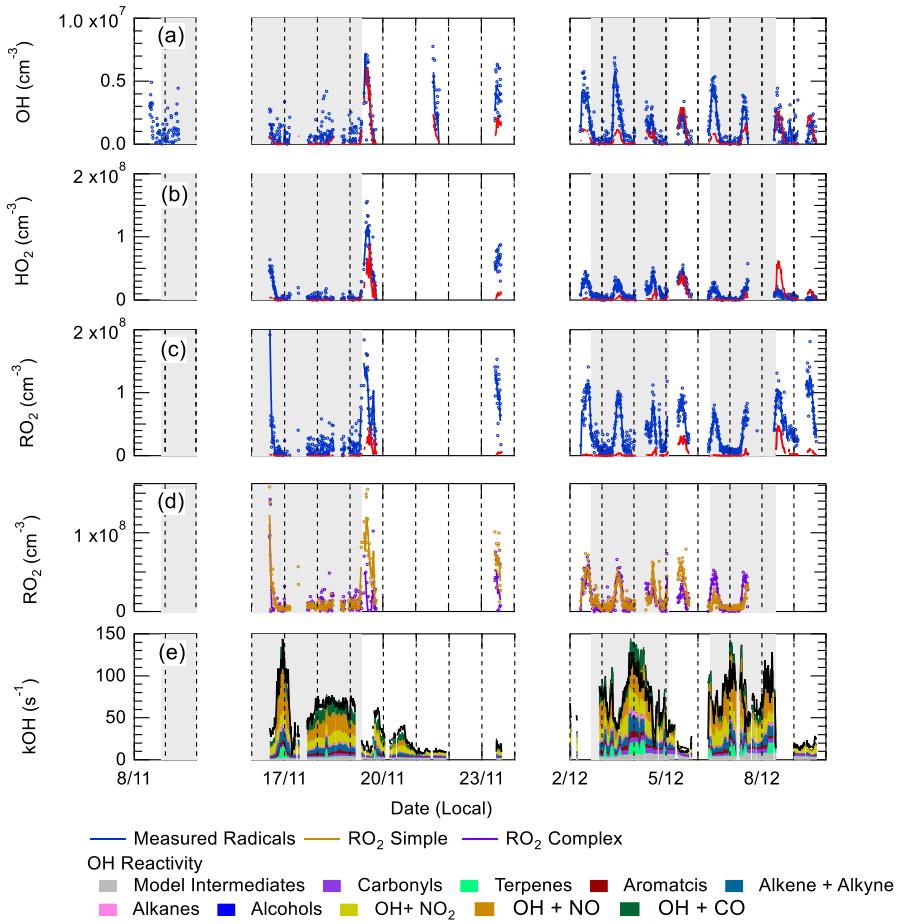

Figure 7. Time-series of OH, b) HO_2, c) total RO_2, d) partly-speciated RO_2 and e) measured (black) and modelled (stacked plot) OH Reactivity. For (a)-(c), the raw measurements (6-min data acquisition cycle) are blue open circles with 15 min average represented by the solid blue line. The 15 min model output in a-c is represented by the red line for OH, HO_2 and RO_2. The partly-speciated RO_2 is separated into simple (gold open circles) and complex (purple open circles)~~), with the model in the same colour (solid line).~~ The individual contributions of the model to the OH reactivity is given below the graph. The grey shaded areas show the haze periods when $PM_{2.5}$ > 75 µg m^{-3}.

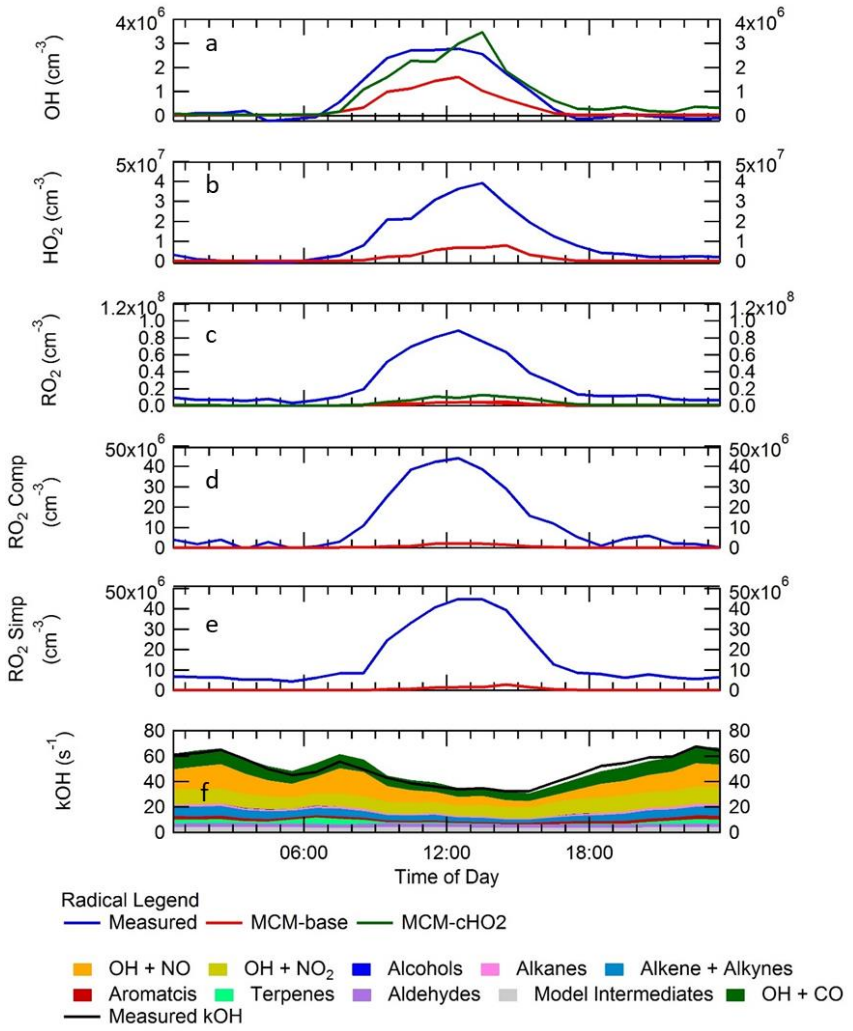

Figure 8. Campaign averaged diel profile of OH (a), HO_2 (b), sum of RO_2 (c), complex RO_2 (d), simple RO_2 (e) for measurements (blue) and box-model calculations: MCM-base (red) and MCM-cHO_2 (green). See text for descriptions of each model scenario. (f) – OH reactivity (s^{-1}) for measurements (black line) and model (stacked plot) with the contribution to reactivity from different measured species and modelled intermediates shown in the key.

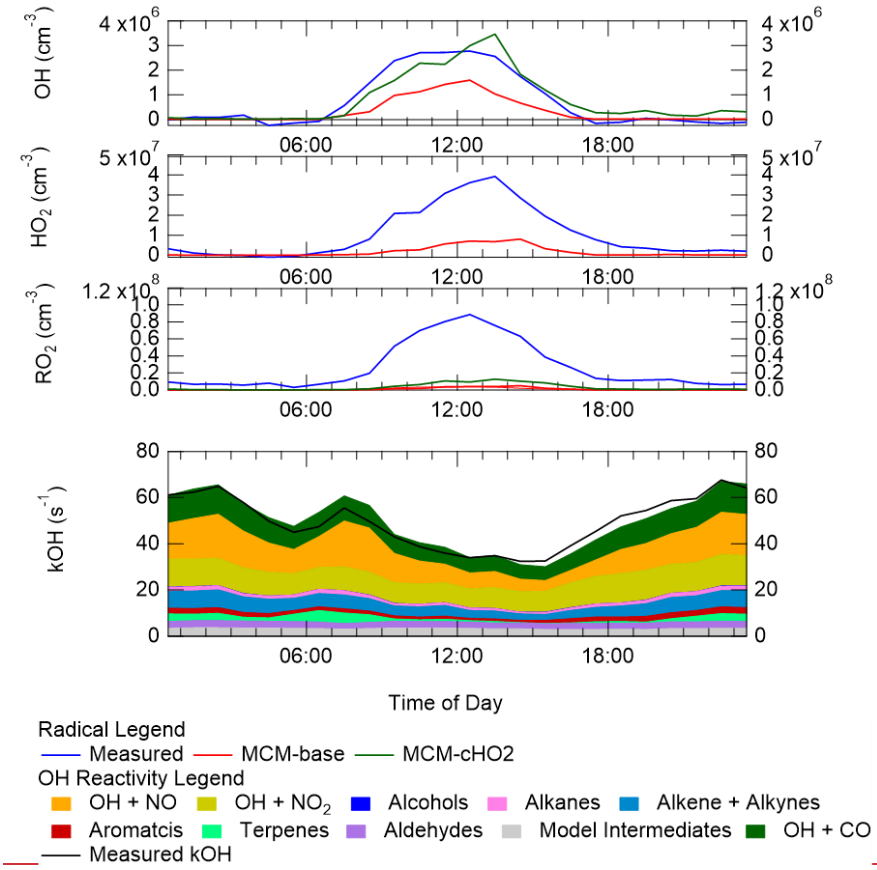

~~**Figure 8.** (a) – Campaign averaged diel profile of OH (top panel), HO_2 (middle panel) and sum of RO_2 (lower panel) for measurements (blue) and box model calculations: MCM-base (red) and MCM-cHO_2 (green) See text for descriptions of each model scenario. (b) – OH reactivity (s^{-1}) for measurements (black line) and model (stacked plot) with the contribution to reactivity from different measured species and modelled intermediates shown in the key.~~

The ability of the model to reproduce (to within ~10%) both the OH reactivity and the OH concentration when constrained to measured HO_2 (in MCM-cHO_2), but not to reproduce RO_2 radicals (whether constrained or not to HO_2) is suggestive of an incomplete representation of the chemistry of RO_2 radicals in the winter Beijing environment. The significant model underprediction of RO_2 implies either that additional sources of RO_2 radicals are required, or that it is inaccuracies in the recycling chemistry within RO_2 species which leads to an overestimate of the loss rate of RO_2 under the high NO_x conditions experienced in central Beijing. The cause of the model underprediction of RO_2 is explored further in section 4.

As summarised in Table 4, previous winter campaigns, where the environment controlling peroxy radicals is generally dominated by NO, have shown a similar underprediction of radical species at high levels of NO_x (above 3 ppbv of NO) (Lu et al., 2013; Ma et al., 2019; Tan et al., 2017; Tan et al., 2018). For the BEST-ONE campaign, which took place in suburban Beijing (~60 km from the centre) it was suggested that in order to reconcile the model with the measurements, an additional source of RO_2 was required.

The OH concentrations measured are surprisingly high for a winter campaign where photolysis rates and RH are low; the average 12:00 OH maximum for the campaign was ~~3.3~~2.7 x 10^6 molecule cm^{-3}. Comparisons with the level of agreement between measured and modelled radicals for other winter field campaigns are given in Table 1. The OH concentration is ~ 3, 2.3, 2, 1.65 and 1.5 times larger than winter measurements in New York (Ren et al., 2006), Beijing (Ma et al., 2019), Tokyo (Kanaya et al., 2007), Birmingham (Emmerson et al., 2005) and the BEST-ONE (Tan et al., 2018) campaigns, respectively, and similar to the campaign in Boulder (Kim et al., 2014). However, it should be noted that the Boulder campaign took place at a time in the year (late February/March) closer to mid-summer when there are higher light levels and water vapour (see Table 5 for details). As shown in Figure 7, the elevated OH concentrations inside haze events, for example up to 6 x 10^6 molecule cm^{-3} of OH was observed on 03/12/2016, suggests gas-phase oxidation is still highly active (this is explored more in section 4.3 and 4.4).

Campaign	Months, Year	NO (ppbv)	O_3 (ppbv)	OH		HO_2		RO_2		Notes	References
				Measured (10^6 cm^{-3})	Obs/ Model	Measured (10^8 cm^{-3})	Obs/ Model	Measured (10^8 cm^{-3})	Obs/ Model		
~~AIRPRO~~APHH, Central Beijing, China	Nov – Dec, 2016	60	12	2.7	0.58	0.39	0.17	0.88	0.04	Average midday.	This work.
BEST-ONE Suburban Beijing, China	Jan – March, 2016	7	30	2.2	0.5	0.5	0.4	0.7	0.2	Campaign Median, midday, polluted period	Tan et al. 2018
~~NCITT~~NACHTT Boulder, USA	Late Feb, 2011	7	37	3	0.9	-	-	-	-	Average midday	Kim et al. (2014)
PUMA, Birmingham, UK	Jan-Feb, 2000	10	13	2	0.50	3	0.49	-	-	Average midday	Emmerson et al. (2005)
IMPACT Tokyo, Japan	Jan-Feb, 2004	8.1	35	1.5	0.93	0.27	0.88	-	-	Average midday	Kanaya et al. (2007)
PMTACS-NY2001 New York, US	Jan–Feb, 2004	25	20	1	0.83	0.17	0.17	-	-	Average midday	Ren et al. (2006)
PKU	Nov – Dec, 2017	30	10	1.4	1.4	0.3	0.13	-	-	Average Midday, Polluted period	Ma et al. (2019)

Table 3. Previous field measurements of OH, HO_2 and RO_2 that have taken place during wintertime in urban areas, together with the campaign average observed to modelled ratio. Modified from Kanaya et al. (2007).

4 Discussion

4.1 Sources and sinks of RO_x radicals

As shown in Figure 9, primary production of new radicals (radicals defined as RO_x = OH + HO_2 + RO + RO_2) via initiation reactions was dominated by the photolysis of HONO (68%, averaged over the campaign), with a small contribution from the photolysis of HCHO (2%), photolysis of carbonyl species (8%) and ozonolysis of alkenes (21%).~~As shown in Figure 9, primary production of new radicals (radicals defined as RO_x = OH + HO_2 + RO + RO_2) via initiation reactions was dominated by the photolysis of HONO (83%, averaged over the campaign), with a small contribution from the photolysis of HCHO (1.1%), photolysis of carbonyl species (4.4%) and ozonolysis of alkenes (10%).~~ An increased rate of production of RO_x radicals is observed during haze events, which is counterbalanced by an increase in the rate of termination. Figure 9 shows that alkene ozonolysis does not play an important role in production of RO_x radicals at night and is reflected by little to no OH observed during night-time as shown in Figure 8 (a). Similarly ozone photolysis does not appear to play an important role for the formation of OH, due to the low O_3 during the campaign, presumably a consequence of local titration via NO, as shown in Figure 4 and Figure 5. In addition, the low temperatures observed during winter caused a low water vapour concentration (~0.5 % mixing ratio), and hence the fraction of O^1D formed from the photolysis of ozone and which reacts with water vapour to form OH compared with collisional quenching (by N_2 and O_2) to form $O(^3P)$ was also low, and varied between 1% to 7% throughout the campaign. Figure 9 shows that almost all of the RO_2 species in the model are derived from OH sources highlighting the need for additional primary RO_2 sources in the model.

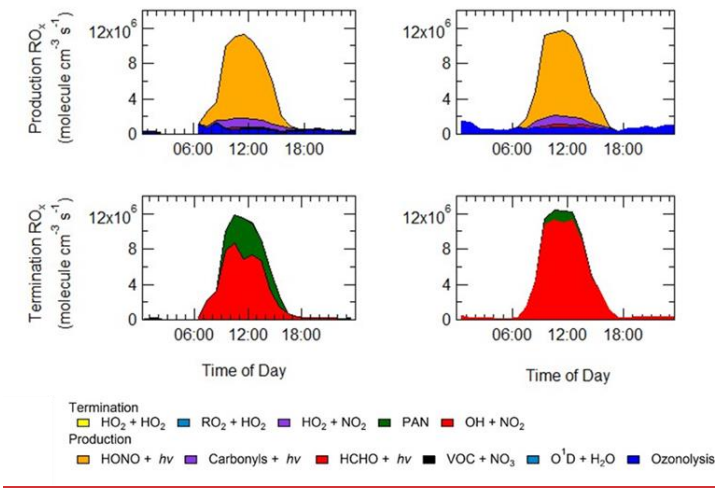

Formatted: Centered

Figure 9. Rates of primary production (top panel) and termination (bottom panel) for RO_x radicals (defined as $OH + HO_2 + RO + RO_2$) calculated for MCM-base model separated into haze (right) and non-haze (left) periods. The definition of haze is when $PM_{2.5}$ exceeds 75 μm^{-3}. The production from: $O^1D + H_2O$ and VOC + $NO_3$and the termination reactions: $RO_2 + HO_2$, $HO_2 + HO_2$, $HO_2 + NO_2$, although shown in the key, are not visible and contributed <1% of the total production and termination.

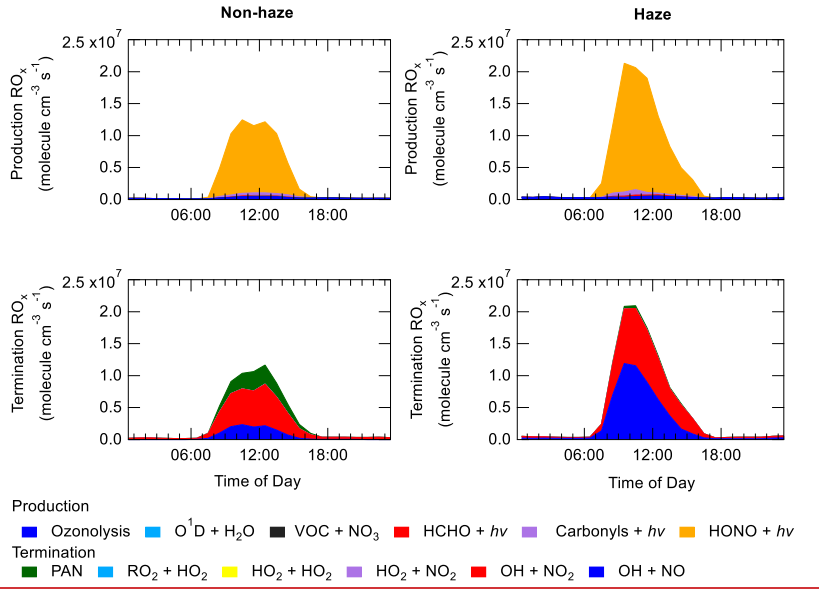

~~**Figure 9.** Rates of primary production (top panel) and termination (bottom panel) for RO_x radicals (defined as $OH + HO_2 + RO + RO_2$) separated into haze (right) and non-haze (left) periods. The definition of haze is when $PM_{2.5}$ exceeds 75 μm^{-3}. The production from: $O^1D + H_2O$, VOC + NO_3, carbonyls + *hv* and the termination reactions: $RO_2 + HO_2$, $HO_2 + HO_2$, $HO_2 + NO_2$, although shown in the key, are not visible and contributed <1% of the total prodcution and termination.~~

The importance of HONO photolysis as a source of OH has been highlighted in several previous studies in both urban and suburban sites as summarised in Table 5.

The BEST-ONE campaign, 60 km north of Beijing, showed HONO produced ~ 46 % of the RO_x during the campaign, although in comparision to the APHH campaign, ozonolysis and carbonyl photolysis in BEST-ONE made up a more significant portion of primary production of radicals, 28 % and 9 %, respectively. The larger contribution to primary production from ozonolysis during BEST-ONE is probably due to higher ozone concentrations (3 times higher at midday, Figure 9). Both the APHH and BEST-ONE campaigns showed that ozone photolysis followed by the reaction of $O(^1D)$ atoms was not an important source of new radicals. A comparison between the primary production routes observed during the APHH and previous urban winter campaigns can be found in supplementary section S1.2.

~~As summarised in Table 2, several other winter-time campaigns have highlighted the importance of HONO, including the PUMA campaign (Emmerson et al., 2005) in Birmingham; the IMPACT campaign in Tokyo (Kanaya et al., 2007); the NCITT campaign in Boulder (Kim et al., 2014) and the PMTACS-NY campaign in New York (Ren et al., 2006). These campaigns showed 36.2, 19, 80.4, and 46 % contribution to primary production of ROx from HONO. However, it should be noted that HONO was not measured during the PUMA camapign, so the percentage contribution to the primary production of radicals should be considered a lower limit as it is based upon modelled HONO (where only the reaction of OH + NO was considered), which is often an underestimate (Lee et al., 2015). As shown in Table 5, the Birmingham, Tokyo, New York and Surburban Beijing campaigns all show a high contribution towards RO_x production from ozonolysis, 63, 35, 42 and 28%, respectively, only the campaign in Boulder (5%) showed little contribution, which is smilar to the observations made during AIRPRO campaign. The Boulder campaign is the only one that showed a significant contribution (14.9 %) to primary radical production from the reaction of $O(^1D) + H_2O$, whilst other winter campaigns show a contribution of less than 1%. The higher contribution from photolysis of O_3 during the Boulder campaign may be due to the campaign taking place in late February (closer to summer) and, as shown in Table 5, photolysis rates, water vapour and temperature were all higher.~~

In both haze and non-haze conditions, the two key reactions which caused a termination of the radical cycling chain reaction ~~were~~ was from~~OH + NO and~~ OH + NO_2. Figure 9 shows that OH + NO_2 contributes up to 94% and 65% in haze and non-haze, respectively. Figure 9 shows that during non-haze conditions contribution to termination from the net formation of PAN (~35%) becomes important; but under haze conditions less than 6% of RO_x termination comes from the net formation of PAN.~~OH + NO contributes up to 53% and 25% of the rate of termination of radicals in haze and non-haze conditions, respectively, and OH + NO_2 contributes up to 44% and 55% , respectively. Figure 9 shows that during non-haze conditions contribution to termination from the net formation of PAN (~19%) becomes important; but under haze conditions less than 2% of RO_x termination comes from the net formation of PAN.~~ In comparision to the BEST-ONE campaign, during the clean periods (clean periods are defined as times when kOH < 15 s^{-1}), the termination reactions of OH + NO_x, net-PAN and peroxy self-reaction contributed ~ 55%, 8%, 30% respectively (Tan et al., 2018). During the polluted periods in the BEST-ONE campaign, the termination reaction of OH + NO_2 increased to 80%, and the net-PAN formation and peroxy self-reaction decreased to ~ 12% annd 6% respectively. The BEST-ONE campaign shows very similar trends to the APHH campaign, except the APHH campaign shows a higher contribution to termination from OH + NO and OH + NO_2 even under cleaner periods. This is potentially due to the higher NO values observed during APHH (located in central Beijing ~6.50 km from Forbidden City) campaign compared to the BEST-ONE campaign. The work that took place at Peking University (PKU)

(Ma et al., 2019) in Beijing (~11 km from the Forbidden City) shows a very smilar trend to the APHH campaign with 86% of the primary production of radicals produced from the photolysis of HONO during the polluted periods . The PKU campaign also showed <1% production from $O^1D + H_2O$, whilst small contribtions from ozonlysis (6%) and photolysis of carbonyls (including HCHO, ~7%) during the polluted periods. Similar to the APHH campaign, the termination of radicals during the PKU campaign during the polluted periods was dominated by the OH + NO (55%) and OH + NO_2 (43%), whilst there was a small contribtuion (~2%) from the net-formation of PAN. The termination trend is very similar to the APHH campaign.

	PUMA, Birmingham, UK	IMPACT, Tokyo, Japan	NCITT, Boulder, USA	PMTACS-NY, New York, USA	BEST-ONE, Suburban Beijing,	APHH, Central Beijing, China	PKU, Central Beijing, China
Date	Jan – Feb 2000	Jan – Feb, 2004	Late Feb 2011	Jan – Feb, 2001	Jan – March 2016	Nov–Dec, 2016	Jan-Feb, 2017
OH (cm^{-3})	~1.7 x 10^6	~1.6 x 10^6	~2.7 x 10^6	~ 1.4 x 10^6	3 x 10^6	3 x 10^6	1.4 x 10^6
O_3 (ppbv)	37	20	40	20	30	15	10
$j(O^1D)$ (s^{-1})	~1 x 10^{-5}	~2.8 x 10^{-5}	~1 x 10^{-5}	~5 x 10^{-6}	7 x 10^{-6}	~3 x 10^{-6}	-
$j(O_3)$ (%)	0.6	<1	14.7	1.1	<1	<1	<1
j(HONO) (%)	36.2[1]	19	80.4	65.5	46	83.3	86
Ozonolysis (%)	63.2	35	4.9	42.4	28	10.0	6
j(Carbonyls) (%)	22	23	-	-	9	4.5	7%[2]
j(HCHO) (%)	6	10	-	6	9	1.1	
Reference	Emmerson et al. (2005)	Kanaya et al. (2007)	Kim et al. (2014)	Ren et al. (2006)	Tan et al. (2018)	This work.	Ma et al.

Table 5. Summary of some previous measurements of OH, HO_2 and RO_2 that have taken place during the winter, and a summary of the major primary radical sources during these campaigns. All values are the noon average for each campaign. [1] This should be considered a lower limit due to no HONO measurements being made during the campaign. [2] Primary production from the sum of j(Carbonyls) and j(HCHO).

4.2 Dependence of radicals concentrations with NO_x

Figure 10 shows the ratio of measured-to-modelled OH, which is close to 1 at or below 10 ppbv of NO; similar to the BEST-ONE campaign. Above 6 ppbv of NO the model underpredicts the OH concentration. As shown in Figure 10, at ~6 ppbv of NO; HO_2 and RO_2 are underpredicted by a factor of 5.4 and 18, respectively; similar peroxy radical under-predictions were reported from the BEST-ONE

campaign (Tan et al., 2017; Tan et al., 2018), with HO_2 and RO_2 being underpredicted by a factor of 5 and 10 at 6 ppbv. Many previous urban campaigns have a more extensive data coverage at lower NO_x values due to the smaller levels of NO_x observed; however, no other campaign with *in situ* measurements of OH has experienced NO values up to 250 ppbv as observed during APHH. Figure 10 shows that the measured-to-modelled ratio for OH, HO_2 and RO_2 increases with NO concentration; for OH the ratio initially increases and then plateaus above 30 ppbv. There have been some suggestions for the origin of the discrepancy that is observed between modelled and measured concentrations of radicals at high concentrations of NO. Dusanter et al., (2009) suggest that poor mixing of a point source of NO with peroxy radicals across a site may cause some of the model to measurement discrepancy observed. There were several instruments for NO measurements located around the site and no differences in concentrations were observed, hence no evidence of any obvious segregation. Tan et al., (2017) suggest that there may be a missing source of peroxy radicals under high-NO_x conditions. Alternatively, the measured-to-modelled discrepancy could be driven by unknown oxidation pathways of the larger, more complex, RO_2 species that are present in these urban environments, whose laboratory kinetics are under-studied.

When the MCM is constrained to the measurements of HO_2 (MCM-cHO_2), the model can replicate the OH measurements to ~10%, within the 26% error of the measurements, as shown in Figure 8. In addition, the MCM-base model can replicate the OH reactivity within 10 % (Figure 8), implying that almost all of the major sources and sinks of OH are captured. The underestimation of HO_2 by the model could be explained by the underestimation of RO_2 by the model, owing to an insufficient rate of recycling of RO_2 to HO_2. Both the ability to replicate OH when the model is constrained to HO_2, along with OH reactivity being captured well by the model, suggests the presence of unknown RO_2 chemistry; either additional sources of RO_2 radicals under high levels of NO_x or unknown chemistry/behaviour of RO_2 under high levels of NO_x. Indeed, many rate coefficients in the MCM for the more complex RO_2 species are based on structure activity relationships (SARs) determined from studies of simpler RO_2 species (http://mcm.leeds.ac.uk/MCM/home, Jenkin et al. (2019)). During the APHH campaign, measurements of partially speciated RO_2 species were made: RO_2 simple (deriving from alkanes up to C_3) and RO_2 complex (deriving from alkanes > C_4, alkene and aromatics), see experimental section 2.2.1 for details on RO_2 speciation and (Whalley et al., 2013). The dependence of the concentration of speciated RO_2 measurements against [NO], as shown in ~~Figure 10~~Figure 11, highlights that the concentration of complex RO_2 species has a steady decrease across the NO range, whilst the concentration of simple RO_2 species starts to decrease rapidly above 2.5 ppbv~~, and can almost be reproduced by the model at NO concentrations above 100 ppbv.~~ The chemistry of the simpler RO_2 species with NO should be well understood, owing to a more extensive laboratory

database of the rate coefficients and product branching, so the model discrepancy for RO_2 species may be due to inaccuracies within the MCM for the ~~degredation~~ degradation of the more complex RO_2 species into these simple RO_2. The degradation pathways of the complex RO_2 species appear not to be well understood, and may be the reason why the real concentration of simple RO_2 species remain high even under high NO_x conditions, whereas the modelled simple RO_2 concentration decreases at high NO. The effect on reducing the RO_2 has been investigated and is shown in S1.7 in the supplementary material. The results show that reducing the rate constant by a factor ~10 does improved the modelled to measurements agreement by a factor of 8.3 for total RO_2. However, RO_2 is still underpredicted by a factor of ~12 at the highest NO. Also the increased RO_2 in the model does not recycle into HO_2 or OH efficiently. This work highlights that uncertainties in the rate constant for RO_2 + NO for different RO_2 cannot be the only explanation for the underprediction of RO_2 in the model.

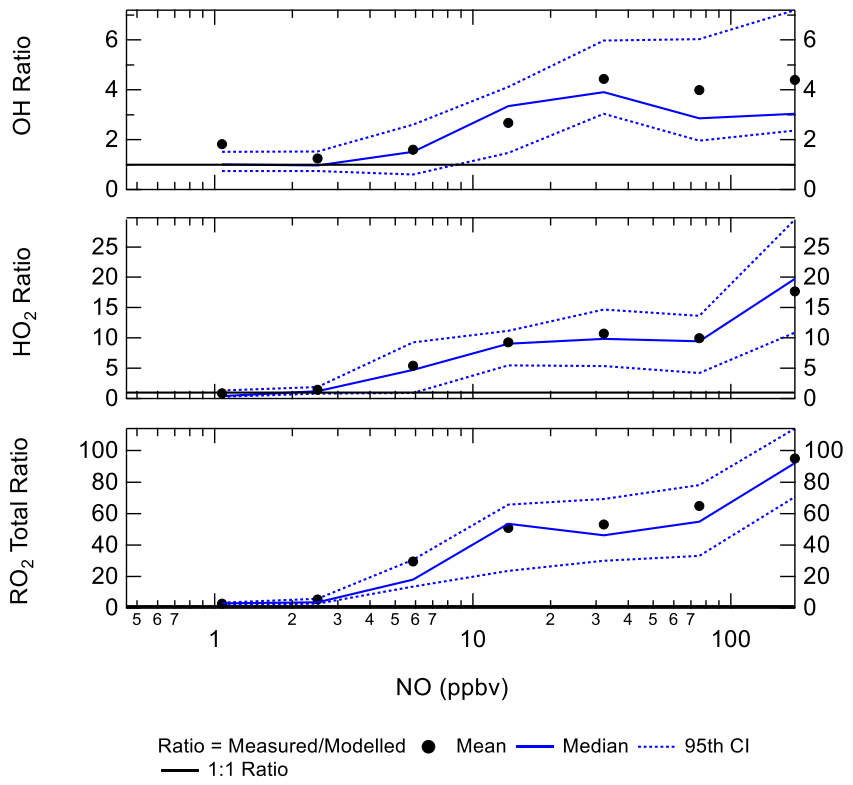

Figure 10. The ratio of measurement/model for OH (top), HO_2 (middle) and total RO_2 (bottom) across the range of NO concentrations experienced, for daytime values only ($j(O^1D) > 1 \times 10^{-6}$ s^{-1}). CI = Confidence Interval.

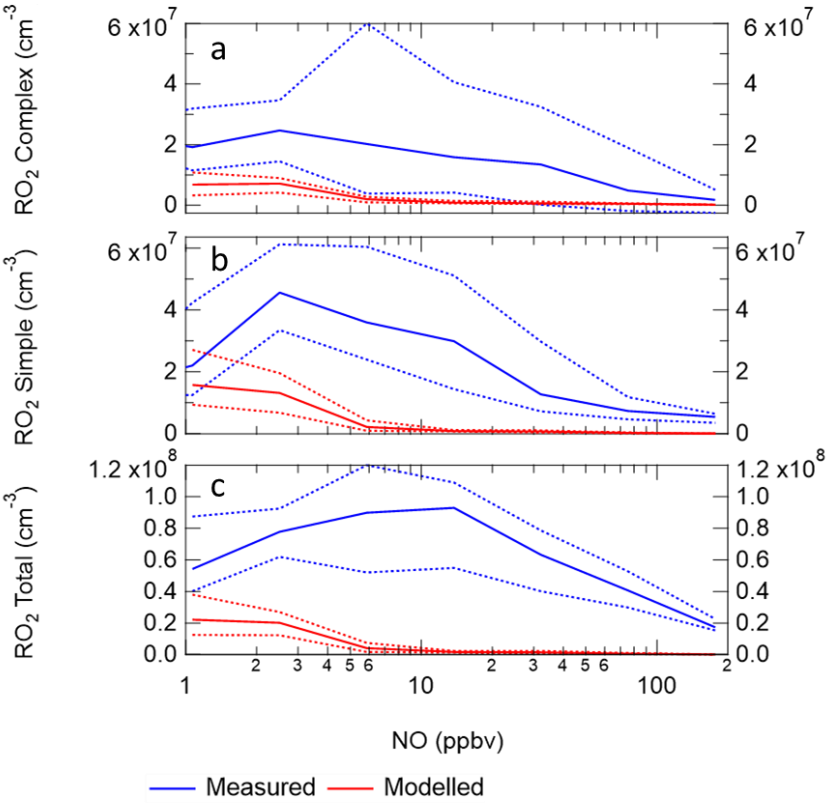

Figure 11. a – Complex RO_2 measurements (blue) and complex RO_2 modelled (black) versus NO. b – Simple RO_2 measurements (blue) and simple RO_2 modelled (black) versus NO. c – Total RO_2 measurements (blue) and total RO_2 modelled (black) versus NO. The points used are for daytime values only ($j(O^1D) > 1 \times 10^{-6}$ s^{-1}). See text for definition of "simple" and "complex" RO_2.

The additional primary production of RO_x ($P'RO_x$) radicals required to bridge the gap between measured and modelled total RO_2 was found to peak at an average of 3.5 x10^8 molecule cm^{-3} s^{-1} at 08:30 non-haze events. Under haze conditions, the gap between measured and modelled total RO_2 was found to peak at an average of 4 x 10^8 molecule cm^{-3} s^{-1} at 13:30 as shown in Figure 12, calculated from Eq. 3 (Tan et al., 2018):

$$P'(RO_x) = k_{HO2+NO}\,[HO_2]\,[NO\ ] - P(HO_2)_{prim} - P(RO_2)_{prim} - k_{VOC}[OH] + L(HO_2)_{term} + L(RO_2)_{term} \quad \text{Eq. 3}$$

where $P(HO_2)_{prim}$, $P(RO_2)_{prim}$, $L(HO_2)_{term}$ and $L(RO_2)_{term}$ are the rates of primary production of HO_2, primary production of RO_2, termination of HO_2 and termination of RO_2, respectively. The overall

Formatted: Line spacing: 1.5 lines

additional primary production peak at ~44 ppbv hr^{-1} (at 10:30) which is almost nine times larger than the additional RO_2 source that was required to resolve the measured and modelled RO_2 during the BEST-ONE campaign (5 ppbv h^{-1} during polluted periods, also calculated using Eq. 3), and is much larger compared to the known noon-average modelled primary production of RO_x during the APHH campaign of 1.7 ppbv hr^{-1}. The additional primary production required in non-haze rises sharply in the morning peaking at 08:30 (3.5 x 10^8 molecule cm^{-3}) and then decreases rapidly; whilst the additional source needed in haze events peaks at 4 x 10^8 molecule cm^{-3} s^{-1}. The additional primary source required during haze events through-out the day is ~7 times higher than that during non-haze events. ~~The additional primary production of RO_x ($P'RO_x$) radicals required to bridge the gap between measured and modelled total RO_2 was found to be on average 1.2 x10^8 molecule cm^{-3} s^{-1} at noon (17 pbbv h^{-1}) as shown in Figure 12, calculated from Eq. *3* (Tan et al., 2018):~~

~~$$P'(RO_x) = k_{HO2+NO}[HO_2][NO] + P(HO_2)_{prim} + P(RO_2)_{prim} + k_{VOC}[OH] - L(HO_2)_{term} - L(RO_2)_{term}$$ Eq. 3~~

~~where $P(HO_2)_{prim}$, $P(RO_2)_{prim}$, $L(HO_2)_{term}$ and $L(RO_2)_{term}$ are the rates of primary production of HO_2, primary production of RO_2, termination of HO_2 and termination of RO_2, respectively. The additional primary source of RO_2, $P'(RO_2)_{prim}$, is almost four times larger than the additional RO_2 source that was required to resolve the measured and modelled RO_2 during the BEST-ONE campaign (5 ppbv h^{-1} during polluted periods, also calculated using Eq. 3), and is much larger compared to the noon-average modelled primary production of RO_x during the APHH campaign of 1.6 ppbv h^{-1}.~~ It has been suggested previously in Tan et al. (2017) that the missing primary radical source originates from the photolysis of $ClNO_2$ and Cl_2 to generate Cl atoms, which can further oxidise VOCs to generate peroxy radicals. However, as no measurements of $ClNO_2$ or Cl_2 measurements were made during the campaign, this route cannot be quantified. However, Cl atom chemistry may only play a minor role, as the inclusion of $ClNO_2$ in a model during a summer campaign in Wangdu (60 km from Bejing) could only close 10 – 30% of the gap between the model and measurements (Tan et al., 2017). Although the $ClNO_2$ concentration required to bridge the gap between model and measurements would be ~5800 ppbv on average (see supplementary section S1.8 for details). Previous measurements in China in suburban Beijing have shown $ClNO_2$ peaking at 2.9 ppbv (Wang et al. 2017), however, and suggests other additional primary source are needed in the model besides Cl chemistry.

Eq.3 has been used to calculate an additional primary source ($P'(RO_x)$) required to reconcile measured and modelled RO_2; on average this peaked at 1.05 x 10^8 molecule cm^{-3} s^{-1}. The calculated additional RO_2 ($P'(RO_x)$) source was included in the model (model run is called MCM-PRO2) as a single species 'A-I' that formed several RO_2 species at the required RO_2 production rate (i.e. k*[A-I] = missing primary production rate, $P'(RO_2)_{prim}$). Using the MCM nomenclature

(http://mcm.leeds.ac.uk/MCM/home), the RO_2 species produced were HOCH2CH2O2, HYPROPO2, IBUTOLBO2, BUTDBO2, OXYBIPERO2, CH3O2 and BUT2OLO2, NBUTOLAO2, and the structures of these RO_2 species are shown in Table 6. The RO_2 species were chosen after a rate of production analysis (ROPA) analysis showed they were highest produced RO_2 species in the model.

The comparison between sum of RO_2 observed and sum of RO_2 modelled from the model run MCM-P'RO_2 demonstrates good agreement in general (Figure 12), although there is a slight overprediction of RO_2 in the afternoon and a slight underprediction of RO_2 in the morning. However, the MCM-PRO2 run overpredicts the observed HO_2 during haze and non-haze events by a factor of 3.4 and 2.5, respectively, with the large overprediction of HO_2 in haze and non-haze events driving the overprediction of OH by a factor of 2.2 and 2.5. This highlights that the additional primary RO_2 source may be an RO_2 species that does not readily propagate to HO_2, this has also been discussed in Whalley et al. (2020). ~~However, the MCM-PRO2 run overpredicts the observed OH and HO_2 by a factor of 1.6 and 2.4, respectively, with the large overprediction of HO_2 driving the overprediction of OH.~~ To investigate whether the uptake of HO_2 onto the surface of aerosols could improve the agreement between measured and modelled HO_2, the MCM-PRO2 modelled was modified to include the uptake of HO_2 with the uptake coefficient set equal to 0.2, as suggested by Jacob (2000), in model run MCM-PRO2-SA. The measured average aerosol surface area peaked at an average of 6.38 x 10^{-6} cm^2 cm^{-3}. The comparison of MCM-PRO2-SA with both measurements and MCM-PRO2 (see Table 2 for details) is shown in Figure 12 and shows that the uptake of HO_2 only has a small impact <6% and <14% on the modelled levels of OH, HO_2 and RO_2 during haze and non-haze events, respectively. ~~The comparison of MCM-PRO2-SA with both measurements and MCM-PRO2 (see Table 2 for details) is shown in Figure 13 and shows that the uptake of HO_2 only has a small impact (< 8%) on the modelled levels of OH, HO_2 and RO_2.~~ The aerosol surface area used in the model may be a lower limit as it was calculated from an Scanning Mobility Particle Sizer (SMPS) that only measured aerosols ranging from 10 nm - 1000 nm. At the high levels of NO encountered, the lifetime of HO_2 is short, and the decrease in HO_2 in MCM-PRO2-SA owing to loss onto aerosols is not enough to reconcile measurements with the model and suggests that an additional primary source of RO_2 may not be the cause of the model underprediction of RO_2 species, as the inclusion of additional RO_2 production worsens the model's ability to predict OH and HO_2. If there is missing RO_2 production, the rate of propagation of these species to HO_2 would need to be slower than currently assumed in the model to reconcile the observations of OH, HO_2 and RO_2.

The small decrease in modelled HO_2 by heterogeneous uptake contrasts with the recent work from Li et al. (2019) that has shown, using GEOS-Chem, that the observed increasing ozone trend in North

China Plain is caused by reduced uptake of HO_2 onto aerosol due to reduction in $PM_{2.5}$ by ~40% between 2013 – 2017.

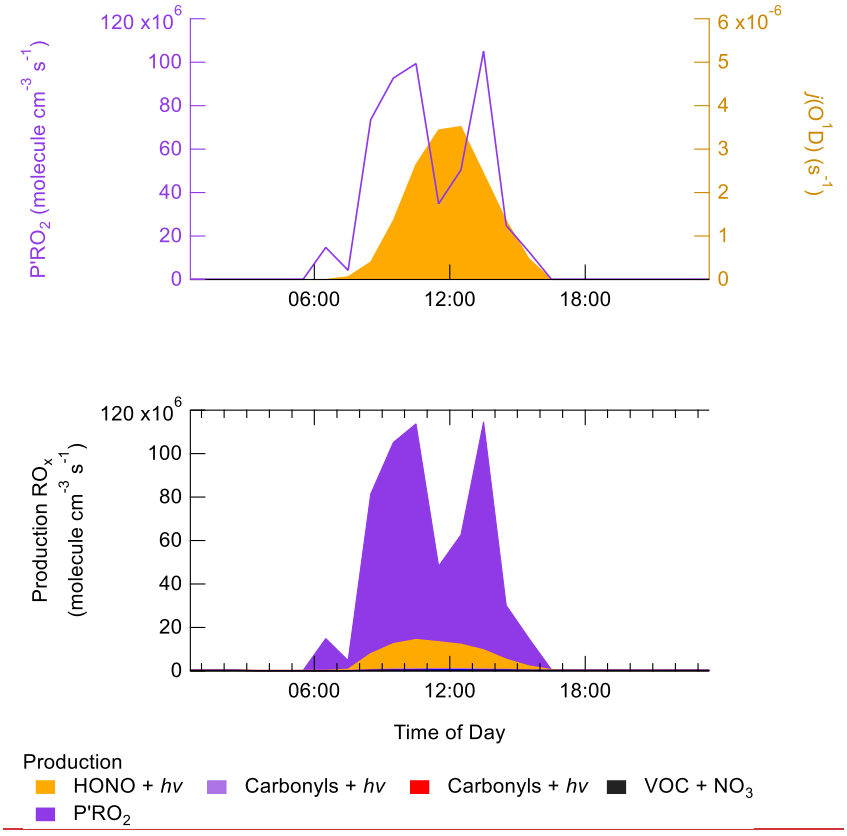

775

~~**Figure 12.** a- Average diel profile of the additional rate of primary production (P'RO_x) (blue) required to reconcile the model with the measurements of total RO_2), and j(O^1D) average diel profile (yellow). b- Breakdown of the rate of primary production of RO_x showing the contribution made by this additional rate of RO_2 production, P'(RO2) (shaded purple).~~

780

785

MCM Name	Structure	MCM Name	Structure
HOCH2CH2O2	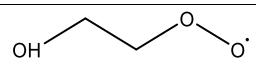	BUTDBO2	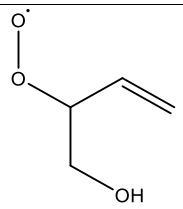
HYPROPO2	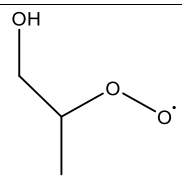	OXYBIPERO2	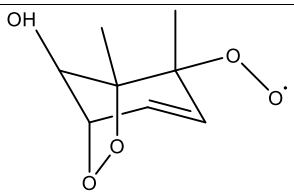
IBUTOLBO2	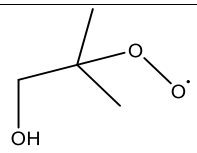	CH3O2	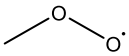
BUT2OLO2	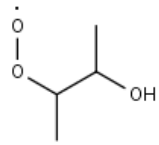	NBUTOLAO2	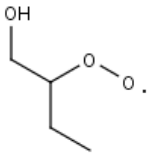

Table 4. The names and associated structures of the RO_2 species used to add additional primary production of RO_2 species into MCM-PRO2 and MCM-PRO2-SA. See http://mcm.leeds.ac.uk/MCMv3.3.1/home.htt for more details.

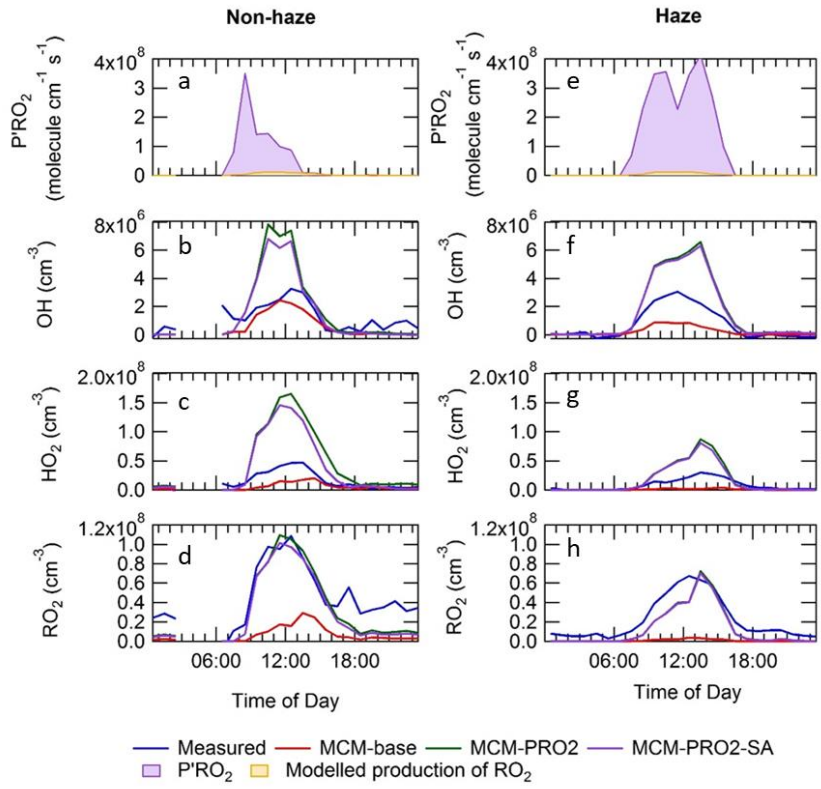

Figure 12. Average diel comparison of measurements of P'RO_2, OH, HO_2 and sum of RO_2 with the MCM-base, MCM-PRO2 and MCM-PRO2-SA box-model runs inside (e – h) and outside (a – d) of haze events. The average diel is from the entire APHH winter campaign. See text and Table 2 for definitions of each of the model runs.

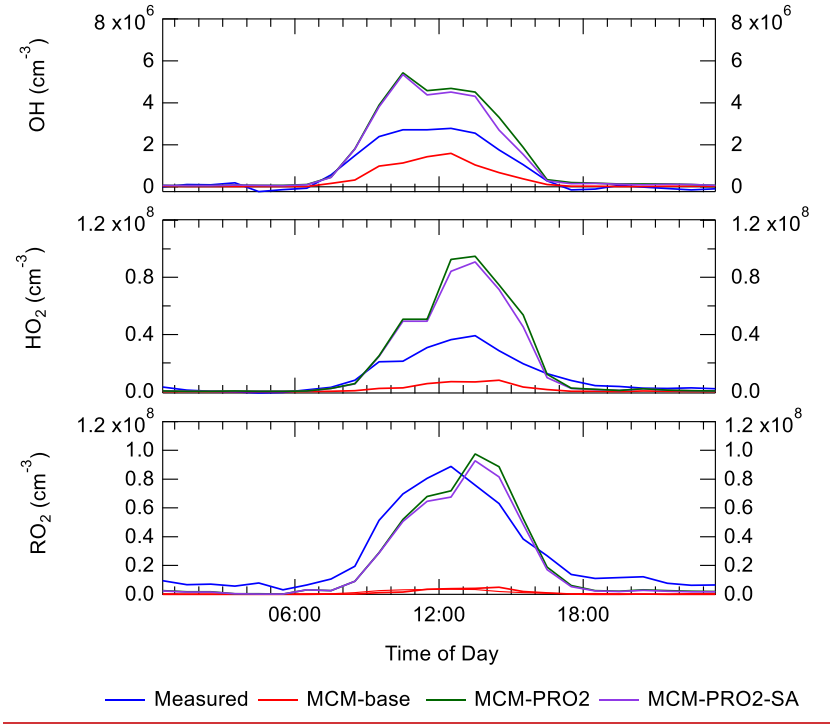

~~**Figure 13.** Average diel comparison of measurements of OH, HO_2 and sum of RO_2 with the MCM base, MCM-PRO2 and MCM-PRO2-SA box model runs. The average diel is from the entire APHH winter campaign. See text and Table 2 for definitions of each of the model runs.~~

4.3 Chemistry of radicals under haze conditions ~~and the rate of oxidation of NO_2 and SO_2 to form nitrate and sulphate aerosol~~

The observed concentrations of OH during the APHH campaign are much higher than those predicted by global models (~0.4 x 10^5 cm^{-3}, for a 24 hr period average during summertime) in the north China plane (NCP) (Lelieveld et al., 2016), and the OH concentration in and outside of haze events are comparable, despite the lower light levels during these events (on average up to 50% less $j(O^1D)$ during the haze events) as shown in Figure 5. The levels of OH are partly sustained during haze events owing to a significant increase in [HONO] in haze (see Figure 5), with HONO being a major source of OH, despite the reduction in *j*(HONO) in haze. The average midday OH reactivity measurements in and out of haze were 47 (s^{-1}) and 17 (s^{-1}), respectively, and since the OH concentrations are comparable in and out of haze, this implies there is a larger turnover rate (defined as the product of [OH] and *k*(OH)), or rate of chemical oxidation initiated by OH radicals, within haze, to balance this. The radical chain

length, ChL, is defined by the rate of radical propagation divided by the rate of radical production, and is given by Eq. 4:

$$\mathrm{ChL} = [\mathrm{OH}] \times k_{\mathrm{voc}}/\mathrm{P}(\mathrm{RO_x}) \quad \text{Eq. 4}$$

where k_{VOC} is the total OH reactivity with VOCs and $P(RO_x)$ is the primary production of RO_x radicals. As shown in Table 7 the average of ChL calculated using Eq. 4 during the APHH campaign was ~5.9. This large value indicates that radical propagation during the APHH campaign is very efficient; this ChL is higher than calculated for previous winter campaigns that had OH radical and OH reactivity measurements available, together with VOCs. The large chain length comes from the product of large OH concentrations and high OH reactivity measurements.

Campaign	OH 10^6 cm^{-3}	P(RO_x) (ppbv h^{-1})	kOH (s^{-1})	NO_2 (ppbv)	Chainlength ChL	Reference
PUMA, Birmingham	1.7	2.8	30	9.3	2.1	Emmerson et al. (2005) [a]
NY NYC, US	1.4	1.4	27	15	3.3	Ren et al. (2006)
IMPACT Tokyo	1.5	1.4	23	12	3.1	Kanaya et al. (2007) [a]
Boulder	2.7	0.7	5	5	2.0	Kim et al. (2014)
BEST-ONE, Suburban Beijing	2.8	0.9	12	6	4.7	Tan et al. (2017)
APHH, Central Beijing	2.7	1.6	47	30	5.9	This work.

Table 5. Comparison of OH concentration, primary production of RO_x radicals ($P(RO_x)$), OH reactivity (kOH), NO_2 concentration and chain length defined by Eqn (4) for various campaigns. The values are a noon-time average. Table modified from Tan et al. (2018). [a] OH reactivity is calculated only.

The average diel profiles of radical concentrations, both measured and calculated by the model, inside and outside of haze periods are presented in Figure 13: the maximum average OH concentration observed is almost the same in and out of haze (~2.7 x 10^6 molecule cm^{-3}) whilst the concentrations of the observed peroxy radicals decrease in haze. The model can replicate OH (within 20%) outside of haze but significantly underpredicts OH inside of haze events. The model also underpredicts HO_2 and RO_2 during haze, but over-predicts HO_2 under the non-haze conditions. The measured complex RO_2 radical species peak at similar concentrations inside (4.3 x 10^7 molecule cm^{-3}) and outside (4.6 x 10^7

molecule cm^{-3}) of haze. Interestingly, unlike the complex RO_2, the simple RO_2 concentration peaks at a lower concentration inside of haze (3.4 x 10^7 molecule cm^{-3}) compared with outside of haze (5.5 x 10^7 molecule cm^{-3}). The complex RO_2 is undepredicted by the model by a factor of ~48 and ~12 inside and outside of haze, respectively, whilst the simple RO_2 is undepredicted by a factor of ~66 and ~5.7 inside and outside of haze, respectively. The sharp increase for the underprediction of both simple and complex RO_2 inside haze events highlights the need of a large additional primary source of both simple and complex RO_2. The OH reactivity is replicated well by the model both in haze and non-haze conditions. The increased contribution to kOH (s^{-1}) from VOCs going from non-haze to haze conditions is a factor of: ~10 for aromatics, ~8 for alkenes and alkynes , ~6 for alkanes, ~9 for alcohols and ~2 for aldehydes. The large increase in the relative contribution to kOH from aromatics, alkenes and alkynes is consistent with the observation of higher complex RO_2 (compared to simple RO_2) during haze periods compared to non-haze periods. Figure 13 shows the OH concentration observed both in and outside of haze events is significant and indictates that gas-phase oxidation is taking place, and hence the formation of secondary oxidation products, even within haze conditions. Secondary oxidation products, such as nitric acid and sulphuric acid, which partition to the aerosol phase, are major contributors towards the formation of secondary particulate matter (Huang et al., 2014). A discussion on the impact of similar OH concentration inside and outside of haze on the oxidation of SO_2 and NO_2 can be found in the supplementary section S1.3 ~~The OH measurements enable calculation of the rate of SO_2 and NO_2 oxidation *via* reaction with OH, to form gas-phase phase HNO_3 and H_2SO_4. Figure 16 shows that on average 1.5 ppbv/h and 0.03 ppbv/h of gas-phase NO_2 and SO_2 are oxidised to form acidic species, and that the oxidation increases in these haze periods caused by comparable OH concentration in and out of haze and, as shown in Figure 5, an increase in local NO_2 and SO_2 concentrations. NO_x can also be lost in the atmosphere by the formation of N_2O_5 (Evans, 2005) and subsequent hydrolysis, but this is uninportant in Beijing during winter due to the low levels of O_3. The reaction of OH + SO_2 in the gas-phase is the rate-determining step in the formation SO_4^{-2}, so the H_2SO_4 formed in the gas-phase will partition in the aerosol phase (Barth et al., 2000). H_2SO_4 is effectively a non-volatile gas at atmospheric temperatures, and H_2SO_4 condensation onto pre-exsisiting particles is an irreversible kinetic process (Zaveri et al., 2008). Whilst HNO_3 is a semivolatile species and the gas-particle partitioning is highly sensitive to to meteorological conditions including: temperature, RH, particle size distribution, pH and particle composition. If the realtive humidity is lower than the deliquescence relative humidity (RH_d), then the HNO_3 that is formed in the gas phase reacts with NH_3 to form ammonium nitrate aersol (NH_4NO_3):~~

~~$HNO_3(g) + NH_3(g) \rightleftharpoons NH_4NO_3(s)$~~ ~~R1~~

If the ambient RH exceeds the RH_d then HNO_3 and NH_3 dissolve into the aqueous phase (aq):

$$HNO_3(g) + NH_3(g) \rightleftharpoons NO_3^-(aq) + NH_4^+(aq) \quad \text{R2}$$

To take into account the reversible process, knowledge of the RH_d that marks the transition between the solid and the aqueous phase, and the equilibrium constant, K_p, for the two phase is required (Ackermann et al., 1998). The MADE module (modal aerosol dynamics model for europe) uses these thermodynamic parameters as given by (Mozurkewich, 1993), resulting in:

$$\ln\left(\frac{RH_d}{100}\right) = \frac{618.3}{T} - 2.551 \quad \text{Eq. 5}$$

for RH_d and:

$$\ln\left(K_p\right) = 118.87 - \frac{24084}{T} - 6.025 \ln\left(T\right) \quad \text{Eq. 6}$$

for K_p. Eq. *5* and Eq. *6* shows that nitrate formation is favoured thermodynamically at low temperatures and high relative humidties (Ge et al., 2017). Previous measurements of SO_4^{-2} and NO_3^-

~~made in wintertime Beijing suggests that photochemstry is important in the formation of nitrate aersol, but not the formation of sulphate (Ge et al., 2017; Sun et al., 2013).~~

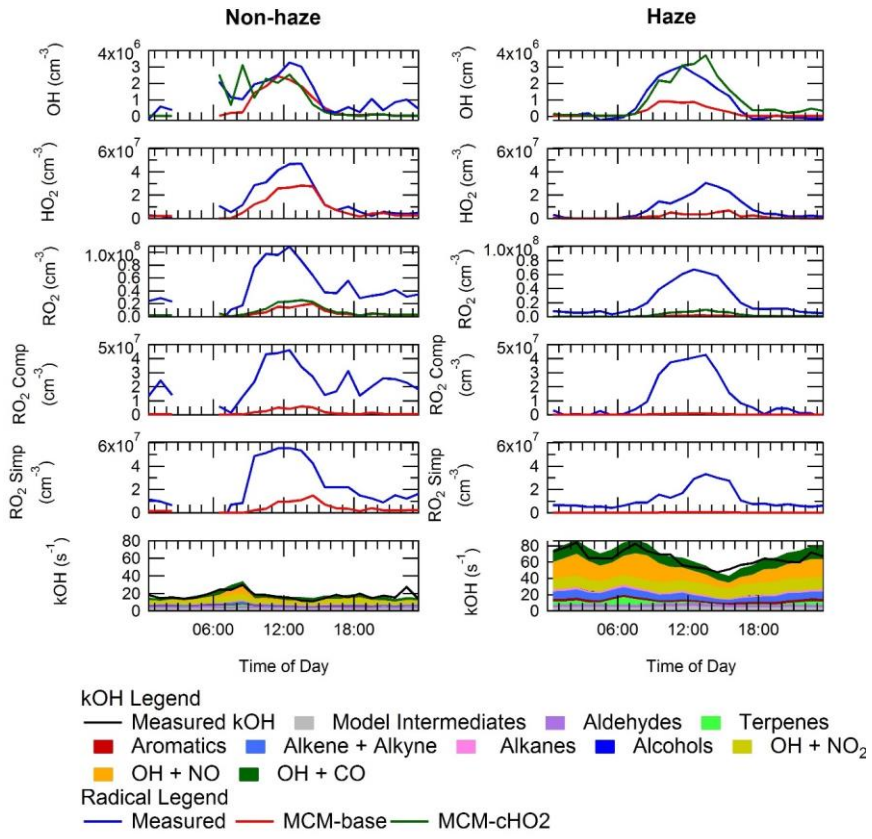

880

Figure 13. Average diel profiles for measured and modelled OH, HO_2, total RO_2, complex RO_2 (RO_2 comp), simple RO_2 (RO_2 simp) and kOH separated into haze (right) and non-haze (left) periods.

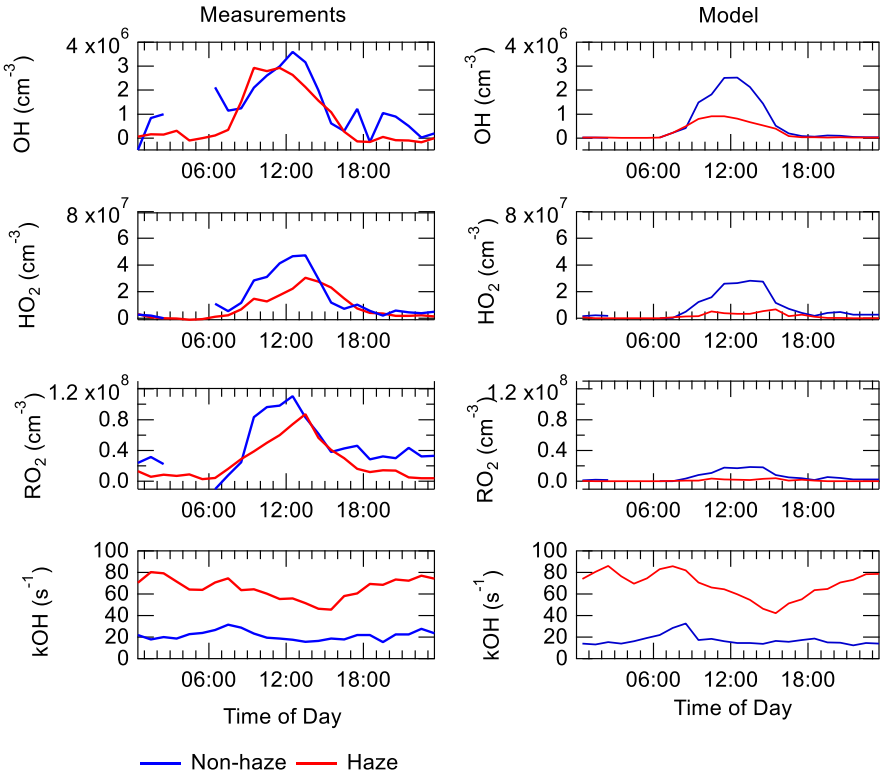

~~**Figure 14.** Average diel profiles for OH, HO_2, RO_2 and kOH for measurements (left) and model (right) separated into haze (red) and non-haze (blue) periods.~~

~~The average diel profiles for the measurements of NO_3^- and SO_4^- made during the APHH separated into haze and non-haze periods are shown in Figure 15. The average diurnal of NO_3^- shows a peak at midday, suggesting photochemistry is important in its formation, whilst the SO_4^- diurnal shows an anti-correlation with photolysis rates. As shown in Figure 15, the SO_4^- tracks the RH very well suggesting that the dominant path for sulphate formation during winter time in Beijing is through the aqueous processing of SO_2. The shape of the average diurnal of NO_3^- and SO_4^- is consistent with studies made by Sun et al. (2013) and Ge et al. (2017). Figure 16 also shows that the gas-phase oxidation of NO_2 increases under haze conditions, showing that nitrate formation is driven by photochemistry in haze events despite the lower photolysis rates. Similar conclusions have been made in Lu et al. (2019) from measurements during the BEST-ONE campaign; with SO_4^- aerosol predominantly driven by aqueous-phase chemistry whilst the production of NO_3^- aerosol from gas-phase oxidation of NO_2 with OH is important. The maximum production rate of HNO_3 observed during the BEST-ONE campaign is the~~

same as the one calculated for the APHH campaign (3 ppbv hr^{-1}). The BEST-ONE campaign assumed all the gas-phase HNO_3 formed partitioned into the aerosol phase due to the high relative humidity observed during the campaign.

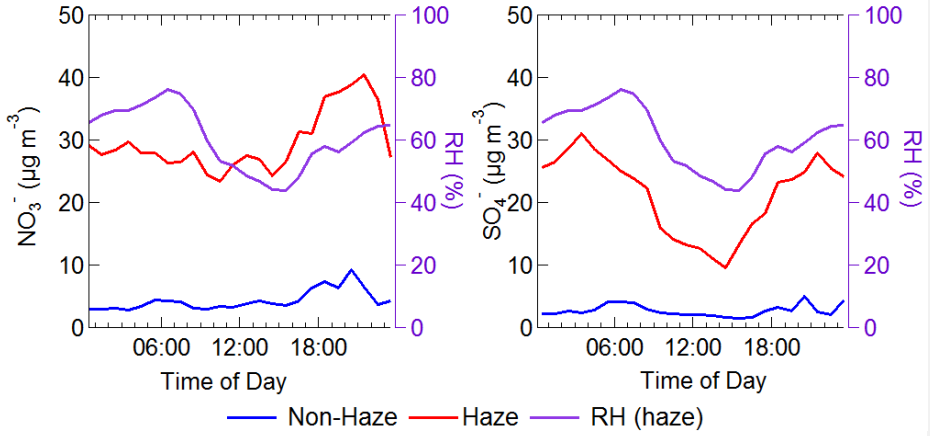

Figure 15. Average diel profiles of NO_3^- and SO_4^- made during the APHH winter campaign separated into haze and non-haze conditions. And the relative humidity (RH) measured during haze periods. Haze = $PM_{2.5}$ > 75 μg m^{-3}.

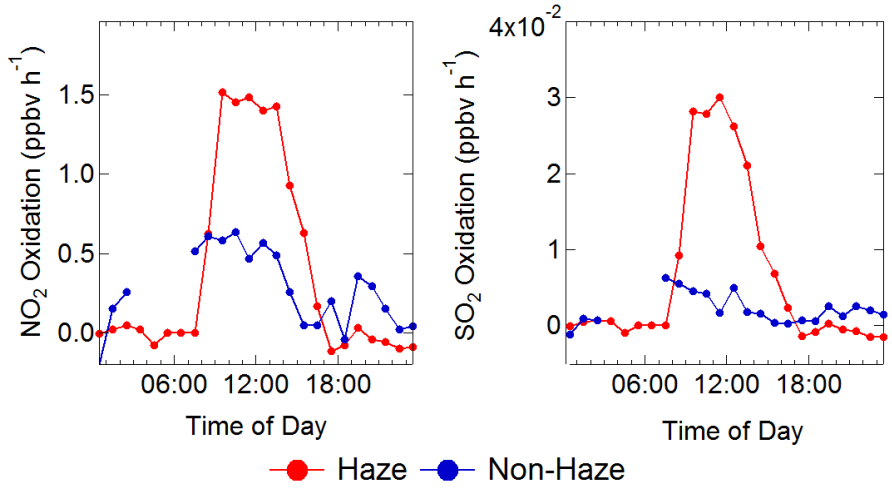

Figure 16. Average diel profiles of the rate of oxidation of NO_2 (left) and SO_2 (right) via reaction with OH in non-haze (blue) and haze (red) conditions.

4.4 Implications of model under-prediction of RO_2 radicals on the calculated rate of ozone production

Although ozone pollution is generally not considered a wintertime phenomenon in Beijing, the elevated levels of RO_2 observed under high NO_x conditions suggests that ozone could be produced rapidly, but then is rapidly titrated to NO_2 by reaction with NO. As well as being an important greenhouse gas, O_3 has a negative impact on both human health and crop yields (Lin et al., 2018), and in China led to 74,200 premature deaths and a cost to the economy of 7.6 billion US$ in 2016 (Maji et al., 2019).

The RO_2 radicals are under-predicted in the model, especially under the higher NO_x conditions, and as shown in Figure 14, this has an implication for the model's ability to predict the rate of *in situ* O_3 production. The rate of O_3 production is assumed to be equal to the net rate of NO_2 production Eq.5:

$$\mathrm{P(O_3)} = k_{\mathrm{HO_2+NO}}[\mathrm{HO_2}][\mathrm{NO}] + k_{\mathrm{RO_2+NO}}[\mathrm{RO_2}][\mathrm{NO}] - k_{\mathrm{OH+NO_2+M}}[\mathrm{OH}][\mathrm{NO_2}][\mathrm{M}] - k_{\mathrm{HO_2+O_3}}[\mathrm{HO_2}][\mathrm{O_3}] - \mathrm{P(RONO_2)} \quad \text{Eq. 5}$$

where RO_2 represents the sum of RO_2, and the last three terms allow for the reduction of ozone production owing to reactions that remove NO_2 or its precursors. The $P(RONO_2)$ term is the net rate of formation of organic nitrate, $RONO_2$, species, for example peroxy acetyl nitrates (PANs).

When the rate of O_3 production is calculated using the measured values of HO_2 and RO_2, there is a positive trend with increasing NO. However, when the modelled concentrations of HO_2 and RO_2 are used, there is a constant $P(O_3)$ across the whole NO range, leading to a large underestimation of O_3 production by the model at higher values of NO. At ~2.5 ppbv and ~177 ppbv of NO the model underestimates the O_3 production by 1.8 and 66, respectively. Figure 14 also shows that there is a high rate of *in situ* ozone production in Beijing in winter and, as shown in Table 8, the maximum rate of ozone production calculated from observed HO_2 and RO_2 is higher for Beijing winter than the corresponding values during the summer-time ClearfLo campaign in London. However, because of the very high NO in Beijing campaign, immediate titration of the O_3 formed results in very low ambient amounts, see Figure 5. As shown in Table 8, the average of the rate of ozone production calculated from observations of HO_2 and RO_2 between 08:00 and 17:00 during our APHH campaign (71 ppbv hr^{-1}, at 40 ppbv of NO) was higher than those calculated using observations during the BEST-ONE campaign (10 ppbv hr^{-1}, at 8 ppbv of NO) and calculated from the measured HO_2 and modelled RO_2 in the PKU campaign (43 ppbv hr^{-1}, at 39 ppbv of NO). An isopleth for ozone showing production as a function of NO_x and VOC for the BEST-ONE campaign (Lu et al., 2019) showed that a reduction in NO_x alone would lead to an increase in O_3 production, and an increase in the amount of secondary organic aerosol produced.

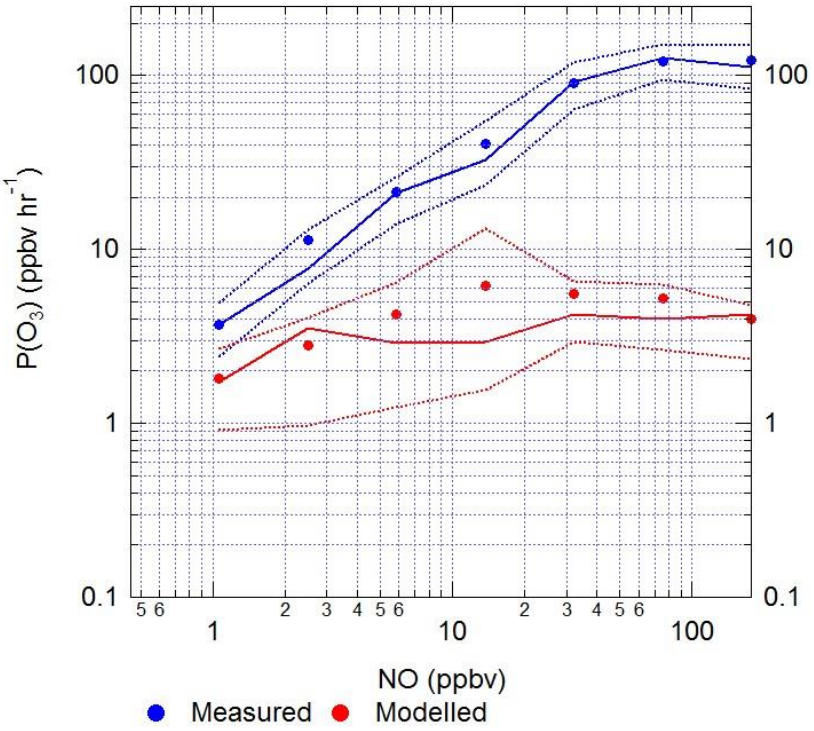

940 **Figure 14.** The calculated rate of *in situ* ozone production as a function of [NO] for Eq. 7 using modelled (red) and measured (blue) values of HO_2 and the sum of RO_2 radicals.

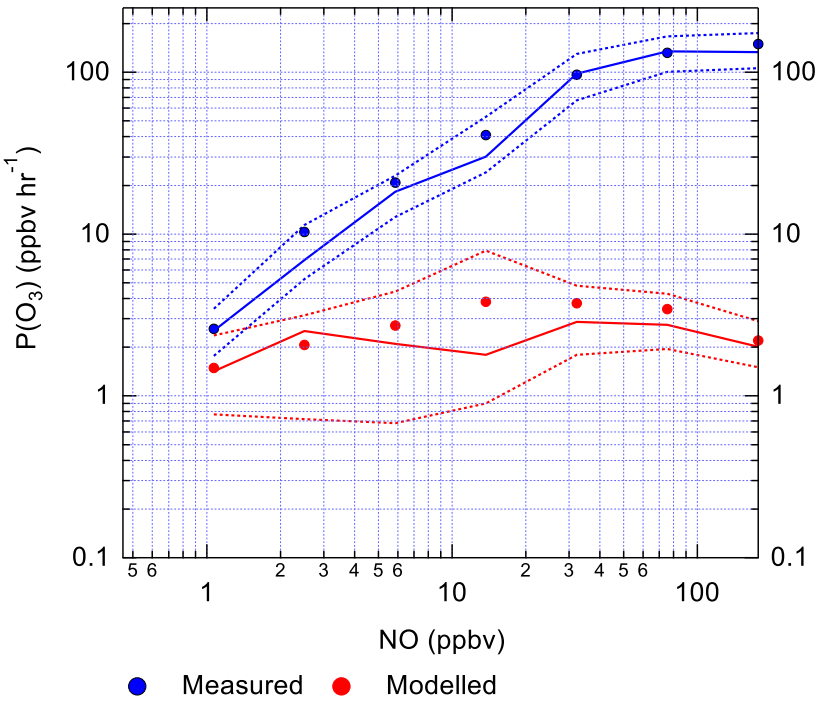

~~**Figure 17.** The calculated rate of *in situ* ozone production as a function of [NO] for Eq. 7 using modelled (red) and measured (blue) values of HO_2 and the sum of RO_2 radicals.~~

The top ten RO_2 species that react with NO to form NO_2 are shown in Figure 15, the top ten RO_2 only contribute to 65.8% of the ozone formed whilst the other 34.2% is from different RO_2's that individually contribute less than 1.5% each. It shows that simple RO_2 species (CH_3O_2 and $C_2H_5O_2$) contribute 26.8% of the total ozone production from RO_2 species.

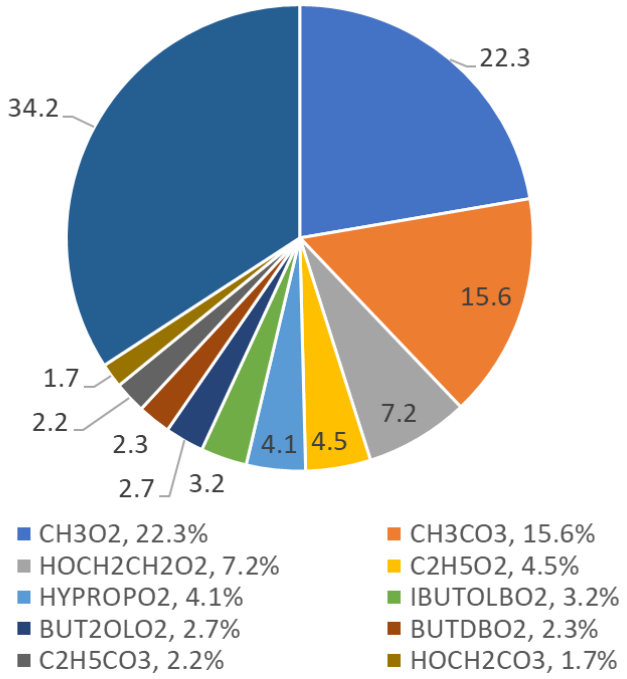

Figure 15. Pie chart showing the top ten RO_2 species that form ozone in the MCM-base model. These top ten RO_2 only contribute to a total of 65.8% of the ozone production, the rest coming from other RO_2 species (34.2%), each with less than a 1.5% contribution to the total production. The names for the RO_2 species are from the MCM, the related structures can be found http://mcm.leeds.ac.uk/MCM/.

Campaign	Dates	NO	$P(O_3)$ (ppbv hr^{-1})	Notes	Reference
APHH	Nov – Dec 2016	40	71	Rate average for the daytime periods between 08:00 and 17:00	This work.
		177	~~132~~123	Maximum ozone production.	
BEST-ONE	Jan – Feb, 2016	8.0	10	Rate average for the daytime periods between 08:00 and 17:00	Tan et al. (2018)
PKU	Nov – Dec 2017	43	39	Rate average for the daytime periods between 08:00 and 17:00	Ma et al. (2019)
ClearfLo	July – Aug 2012	52	41	Maximum ozone production.	Whalley et al. (2018)

Table 6. The rate of *in situ* ozone production averaged between 08:00 – 17:00 for the APHH, BEST-ONE and PKU campaigns and the associated NO concentration. Also shown is the maximum rate of ozone production calculated from measured HO_2 and RO_2 during the APHH and ClearFLo campaigns.

5. Summary

The APHH ~~AIRPRO~~ campaign took place in central Beijing at the Institute for Atmospheric Physics (IAP) in November and December 2016, with detailed measurements of OH, HO_2, sum of RO_2 and OH reactivity made using the FAGE technique. High radical concentrations were measured both inside and outside of haze events, despite the lower intensity of solar radiation and therefore photolysis rates in haze. The daily maxima for the radical species varied day-to-day from 1 to 8 x 10^6 cm^{-3}, 0.7 to 1.5 x 10^8 cm^{-3} and 1 to 2.5 x 10^8 cm^{-3} for OH, HO_2 and RO_2 respectively. Partial speciation of RO_2 was achieved, with the sum of simple RO_2 deriving from $<C_4$ saturated VOCs reaching a daily maximum concentration between 0.2-1.3 x 10^8 cm^{-3}, and the complex RO_2 deriving from larger alkyl, unsaturated and aromatic VOCs reaching a daily maximum concentration between 0.2 and 0.6 x 10^8 cm^{-3}. The partially speciated RO_2 measurements showed on average almost 50:50 ratio between the two. The complex RO_2 species have higher mixing ratios under high NO (>40 ppbv) conditions whilst simple RO_2 have higher mixing ratio at lower NO (<40 ppbv). The average daytime maximum of the radical species was 2.7~~0 x 10~~$\times 10^6$ cm^{-3}, 0.39 x 10^8 cm^{-3} and 0.88 x 10^8 cm^{-3} for OH, HO_2 and total RO_2, respectively. The OH radical concentrations are higher than previous winter campaigns outside of China, and comparable to the BEST-ONE campaign that took place in suburban Beijing (60 km northeast of Beijing). The OH reactivity was very high, and showed a significant day to day variability from 10 s^{-1} up to 150 s^{-1} in the most polluted periods. The major contribution to reactivity came from CO (17.3%), NO (24.9%), NO_2

(22.1%), alkanes (3.0%), alkynes and alkenes (10.8%), carbonyls (5.7%), terpenes (3.7%) and model intermediates (6.77%). A steady state calculation for OH showed that the OH budget can be closed using measured HO_2, HONO and *k*(OH).

The primary production of new radicals by initiation reactions, as opposed to formation via propagation reactions, was dominated (>83%) by the photolysis of HONO, consistent with other winter campaigns. The rate of primary radical production from HONO was observed to increase during haze events, due to the large increase in HONO concentration, even though photolysis rates were considerably lower in haze. Radical termination was dominated by the reaction of OH with NO and NO_2, although under non-haze conditions, when $PM_{2.5}$ < 75 µg m^{-3}, the contribution from net-PAN formation became important (~19%).

The comparison of the measurements with a box-model utilising the detailed Master Chemical Mechanism generally showed an underestimation of OH, HO_2 and RO_2. The MCM was able to replicate OH and HO_2 concentrations quite well when [NO] was around 3 ppbv. The model underestimation occurred at [NO] > 2.5 ppbv for OH, HO_2 and RO_2. The underprediction of the radicals reached a measured:modelled ratio of 3, 20 and 91 at 177 ppbv of NO. The under prediction of the peroxy radicals (HO_2 and RO_2) by the model leads to an underestimation of in situ O_3 production under high NO_x conditions. When the MCM is constrained to the measured HO_2, the model can replicate measured OH, and the measured OH reactivity is captured well by the model. This suggests that under high NO_x and haze conditions there is either an additional source of the peroxy radicals or unknown recycling chemistry of RO_2 to HO_2. The OH concentrations inside and outside of haze events were very similar, on average 2.7 x 10^6 molecule cm^{-3}, which suggests that rapid gas-phase oxidation, generating secondary species such as secondary nitrate, sulphate and organic aerosol still occurs in haze events.

Data availability. Data presented in this study are available from the authors upon request (l.k.whalley@leeds.ac.uk and d.e.heard@leeds.ac.uk).

Author contributions. ES, LW, RWM, CY and DH carried out the measurements; ES and LW developed the model and performed the calculations; JL, S, JH, RD, MS, JH, AL, LC, LK, WB, TV, YS, WX, PF, SY, LR, WA, CH and XW provided logistical support and supporting data to constrain the model; ES, LW and DH prepared the manuscript; with contributions from all co-authors.

Competing interests. The authors declare that they have no conflict of interest.

Acknowledgements – We are grateful to the Natural Environment Research Council for funding via the Newton Fund Atmospheric Pollution and Human Health in Chinese Megacity Directed International Program (grant number NE/N006895/1) and the National Natural Science Foundation of China (Grant No.41571130031). Eloise Slater and Freya Squires acknowledge NERC SPHERES PhD studentships. We acknowledge the support from Zifa Wang and Jie Li from the Institute of Applied Physics (IAP), Chinese Academy of Sciences for hosting the APHH-Beijing campaign. We thank Liangfang Wei, Hong Ren, Qiaorong Xie, Wanyu Zhao, Linjie Li, Ping Li, Shengjie Hou and Qingqing Wang from IAP, Kebin He and Xiaoting Cheng from Tsinghua University, and James Allan from the University of Manchester for providing logistic and scientific support for the field campaigns. We would also like to thank other participants in the APHH field campaign.

References

Ackermann, I. J., Hass, H., Memmesheimer, M., Ebel, A., Binkowski, F. S., and Shankar, U.: Modal aerosol dynamics model for Europe: Development and first applications, Atmospheric environment, 32, 2981-2999, 1998.

Barth, M., Rasch, P., Kiehl, J., Benkovitz, C., and Schwartz, S.: Sulfur chemistry in the National Center for Atmospheric Research Community Climate Model: Description, evaluation, features, and sensitivity to aqueous chemistry, Journal of Geophysical Research: Atmospheres, 105, 1387-1415, 2000.

Chan, C. K. and Yao, X.: Air pollution in mega cities in China, Atmospheric environment, 42, 1-42, 2008.

Cheng, N., Li, Y., Zhang, D., Chen, T., Sun, F., Chen, C., and Meng, F.: Characteristics of ground ozone concentration over Beijing from 2004 to 2015: Trends, transport, and effects of reductions, Atmos. Chem. Phys, 2016. 2016.

Commane, R., Floquet, C., Ingham, T., Stone, D., Evans, M., and Heard, D.: Observations of OH and HO_2 radicals over West Africa, Atmospheric Chemistry and Physics, 10, 8783-8801, 2010.

Crilley, L. R., Karmer, L. J., Ouyang, B., Duan, J., Zhang, W., Tong, S., Ge, M., Ge, K. T., Qin, M., Xie, P., Shaw, M. D., Lewis, A. C., Mehra, A., Bannan, T. J., Worrall, S. D., Priestley, M., Bacak, A., Coe, H., Allan, J., Percival, C. J., Popoola, O. A. M., Jones, R. L., and Bloss, W. J.: Intercomparison of nitrous acid (HONO) measurement techniques in a megacity (Beijing), AMT, 2019. 2019.

Dunmore, R., Hopkins, J., Lidster, R., Lee, J., Evans, M., Rickard, A., Lewis, A., and Hamilton, J.: Diesel-related hydrocarbons can dominate gas phase reactive carbon in megacities, Atmospheric Chemistry and Physics, 15, 9983-9996, 2015.

Ehhalt, D. H. and Rohrer, F.: Dependence of the OH concentration on solar UV, Journal of Geophysical Research: Atmospheres, 105, 3565-3571, 2000.

Emmerson, K., Carslaw, N., and Pilling, M.: Urban atmospheric chemistry during the PUMA campaign 2: Radical budgets for OH, HO 2 and RO 2, Journal of atmospheric chemistry, 52, 165-183, 2005.

Finlayson-Pitts, B., Wingen, L., Sumner, A., Syomin, D., and Ramazan, K.: The heterogeneous hydrolysis of NO 2 in laboratory systems and in outdoor and indoor atmospheres: An integrated mechanism, Physical Chemistry Chemical Physics, 5, 223-242, 2003.

Ge, X., He, Y., Sun, Y., Xu, J., Wang, J., Shen, Y., and Chen, M.: Characteristics and formation mechanisms of fine particulate nitrate in typical urban areas in China, Atmosphere, 8, 62, 2017.

Heard, D. E. and Pilling, M. J.: Measurement of OH and HO2 in the troposphere, Chemical Reviews, 103, 5163-5198, 2003.

Hollaway, M., Wild, O., Yang, T., Sun, Y., Xu, W., Xie, C., Whalley, L., Slater, E., Heard, D., and Liu, D.: Photochemical impacts of haze pollution in an urban environment, Atmos. Chem. Phys. Discuss., https://doi. org/10.5194/acp-2019-29, in review, 2019. 2019.

Hopkins, J. R., Jones, C. E., and Lewis, A. C.: A dual channel gas chromatograph for atmospheric analysis of volatile organic compounds including oxygenated and monoterpene compounds, Journal of Environmental Monitoring, 13, 2268-2276, 2011.

Hu, J., Wang, Y., Ying, Q., and Zhang, H.: Spatial and temporal variability of PM2. 5 and PM10 over the North China Plain and the Yangtze River Delta, China, Atmospheric Environment, 95, 598-609, 2014.

Huang, R.-J., Zhang, Y., Bozzetti, C., Ho, K.-F., Cao, J.-J., Han, Y., Daellenbach, K. R., Slowik, J. G., Platt, S. M., and Canonaco, F.: High secondary aerosol contribution to particulate pollution during haze events in China, Nature, 514, 218, 2014.

Jacob, D. J.: Heterogeneous chemistry and tropospheric ozone, Atmospheric Environment, 34, 2131-2159, 2000.

Jenkin, M. E., Valorso, R., Aumont, B., and Rickard, A. R.: Estimation of rate coefficients and branching ratios for reactions of organic peroxy radicals for use in automated mechanism construction, Atmospheric Chemistry and Physics, 19, 7691-7717, 2019.

Kanaya, Y., Cao, R., Akimoto, H., Fukuda, M., Komazaki, Y., Yokouchi, Y., Koike, M., Tanimoto, H., Takegawa, N., and Kondo, Y.: Urban photochemistry in central Tokyo: 1. Observed and modeled OH and HO2 radical concentrations during the winter and summer of 2004, Journal of Geophysical Research: Atmospheres, 112, 2007.

Kim, S., VandenBoer, T. C., Young, C. J., Riedel, T. P., Thornton, J. A., Swarthout, B., Sive, B., Lerner, B., Gilman, J. B., and Warneke, C.: The primary and recycling sources of OH during the NACHTT-2011 campaign: HONO as an important OH primary source in the wintertime, Journal of Geophysical Research: Atmospheres, 119, 6886-6896, 2014.

Lang, J., Zhang, Y., Zhou, Y., Cheng, S., Chen, D., Guo, X., Chen, S., Li, X., Xing, X., and Wang, H.: Trends of PM2. 5 and chemical composition in Beijing, 2000–2015, Aerosol Air Qual. Res, 17, 412-425, 2017.

Lee, J., Whalley, L., Heard, D., Stone, D., Dunmore, R., Hamilton, J., Young, D., Allan, J., Laufs, S., and Kleffmann, J.: Detailed budget analysis of HONO in central London reveals a missing daytime source, Atmospheric Chemistry and Physics Discussions, 15, 22097-22139, 2015.

Lelieveld, J., Gromov, S., Pozzer, A., and Taraborrelli, D.: Global tropospheric hydroxyl distribution, budget and reactivity, Atmospheric Chemistry and Physics, 16, 12477, 2016.

Li, K., Jacob, D. J., Liao, H., Shen, L., Zhang, Q., and Bates, K. H.: Anthropogenic drivers of 2013–2017 trends in summer surface ozone in China, Proceedings of the National Academy of Sciences, 116, 422-427, 2019.

Li, X., Brauers, T., Häseler, R., Bohn, B., Fuchs, H., Hofzumahaus, A., Holland, F., Lou, S., Lu, K., and Rohrer, F.: Exploring the atmospheric chemistry of nitrous acid (HONO) at a rural site in Southern China, Atmospheric Chemistry and Physics, 12, 1497-1513, 2012.

Lin, Y., Jiang, F., Zhao, J., Zhu, G., He, X., Ma, X., Li, S., Sabel, C. E., and Wang, H.: Impacts of O3 on premature mortality and crop yield loss across China, Atmospheric environment, 194, 41-47, 2018.

Lu, K., Fuchs, H., Hofzumahaus, A., Tan, Z., Wang, H., Zhang, L., Schmitt, S., Rohrer, F., Bohn, B., and Broch, S.: Fast photochemistry in wintertime haze: Consequences for pollution mitigation strategies, Environmental science & technology, 2019. 2019.

Lu, K., Hofzumahaus, A., Holland, F., Bohn, B., Brauers, T., Fuchs, H., Hu, M., Häseler, R., Kita, K., and Kondo, Y.: Missing OH source in a suburban environment near Beijing: observed and modelled OH and HO 2 concentrations in summer 2006, Atmospheric Chemistry and Physics, 13, 1057-1080, 2013.

Lu, X., Wang, Y., Li, J., Shen, L., and Fung, J. C.: Evidence of heterogeneous HONO formation from aerosols and the regional photochemical impact of this HONO source, Environmental Research Letters, 13, 114002, 2018.

Ma, X., Tan, Z., Lu, K., Yang, X., Liu, Y., Li, S., Li, X., Chen, S., Novelli, A., and Cho, C.: Winter photochemistry in Beijing: Observation and model simulation of OH and HO_2 radicals at an urban site, Science of The Total Environment, 685, 85-95, 2019.

Maji, K. J., Ye, W.-F., Arora, M., and Nagendra, S. S.: Ozone pollution in Chinese cities: Assessment of seasonal variation, health effects and economic burden, Environmental pollution, 247, 792-801, 2019.

Mozurkewich, M.: The dissociation constant of ammonium nitrate and its dependence on temperature, relative humidity and particle size, Atmospheric Environment. Part A. General Topics, 27, 261-270, 1993.

Qi, Y., Stern, N., Wu, T., Lu, J., and Green, F.: China's post-coal growth, Nature Geoscience, 9, 564, 2016.

Ren, X., Brune, W. H., Mao, J., Mitchell, M. J., Lesher, R. L., Simpas, J. B., Metcalf, A. R., Schwab, J. J., Cai, C., and Li, Y.: Behavior of OH and HO2 in the winter atmosphere in New York City, Atmospheric Environment, 40, 252-263, 2006.

Saunders, S. M., Jenkin, M. E., Derwent, R., and Pilling, M.: Protocol for the development of the Master Chemical Mechanism, MCM v3 (Part A): tropospheric degradation of non-aromatic volatile organic compounds, Atmospheric Chemistry and Physics, 3, 161-180, 2003.

Shi, Z., Vu, T., Kotthaus, S., Grimmond, S., Harrison, R. M., Yue, S., Zhu, T., Lee, J., Han, Y., and Demuzere, M.: Introduction to Special Issue-In-depth study of air pollution sources and processes within Beijing and its surrounding region (APHH-Beijing), Atmospheric Chemistry and Physics Discussions, 2018. 2018.

Stone, D., Whalley, L. K., and Heard, D. E.: Tropospheric OH and HO_2 radicals: field measurements and model comparisons, Chemical Society Reviews, 41, 6348-6404, 2012.

Stone, D., Whalley, L.K., Ingham, T., Edwards, P., Cryer, D.R., Brumby, C.A., Seakins, P.W. and Heard, D.E., 2016. Measurement of OH reactivity by laser flash photolysis coupled with laser-induced fluorescence spectroscopy. *Atmospheric Measurement Techniques*, pp.2827-2844.

Sun, Y., Wang, Z., Fu, P., Yang, T., Jiang, Q., Dong, H., Li, J., and Jia, J.: Aerosol composition, sources and processes during wintertime in Beijing, China, Atmospheric Chemistry and Physics, 13, 4577-4592, 2013.

Tan, Z., Fuchs, H., Lu, K., Hofzumahaus, A., Bohn, B., Broch, S., Dong, H., Gomm, S., Häseler, R., and He, L.: Radical chemistry at a rural site (Wangdu) in the North China Plain: observation and model calculations of OH, HO 2 and RO 2 radicals, Atmospheric Chemistry and Physics, 17, 663-690, 2017.

Tan, Z., Rohrer, F., Lu, K., Ma, X., Bohn, B., Broch, S., Dong, H., Fuchs, H., Gkatzelis, G. I., and Hofzumahaus, A.: Wintertime photochemistry in Beijing: observations of RO x radical concentrations in the North China Plain during the BEST-ONE campaign, Atmospheric Chemistry and Physics, 18, 12391-12411, 2018.

Formatted: Font: (Default) +Body (Calibri), 11 pt

Formatted: Font: (Default) +Body (Calibri)

Tang, G., Zhao, P., Wang, Y., Gao, W., Cheng, M., Xin, J., Li, X., and Wang, Y.: Mortality and air pollution in Beijing: The long-term relationship, Atmospheric Environment, 150, 238-243, 2017.

Wang, X., Wang, H., Xue, L., Wang, T., Wang, L., Gu, R., Wang, W., Tham, Y.J., Wang, Z., Yang, L. and Chen, J., 2017. Observations of N_2O_5 and $ClNO_2$ at a polluted urban surface site in North China: High N2O5 uptake coefficients and low ClNO2 product yields. *Atmospheric environment*, *156*, pp.125-134.

~~Wang, X., Wang, H., Xue, L., Wang, T., Wang, L., Gu, R., Wang, W., Tham, Y.J., Wang, Z., Yang, L. and Chen, J., 2017. Observations of N_2O_5 and $ClNO_2$ at a polluted urban surface site in North China: High N2O5 uptake coefficients and low ClNO2 product yields. *Atmospheric environment*, *156*, pp.125-134.~~

Wang, Z., Li, Y., Chen, T., Zhang, D., Sun, F., Wei, Q., Dong, X., Sun, R., Huan, N., and Pan, L.: Ground-level ozone in urban Beijing over a 1-year period: Temporal variations and relationship to atmospheric oxidation, Atmospheric Research, 164, 110-117, 2015.

Whalley, L., Blitz, M., Desservettaz, M., Seakins, P., and Heard, D.: Reporting the sensitivity of laser-induced fluorescence instruments used for HO2 detection to an interference from RO2 radicals and introducing a novel approach that enables HO2 and certain RO2 types to be selectively measured, Atmospheric Measurement Techniques, 6, 3425-3440, 2013.

Whalley, L. K., Stone, D., Dunmore, R., Hamilton, J., Hopkins, J. R., Lee, J. D., Lewis, A. C., Williams, P., Kleffmann, J., and Laufs, S.: Understanding in situ ozone production in the summertime through radical observations and modelling studies during the Clean air for London project (ClearfLo), Atmospheric Chemistry and Physics, 18, 2547-2571, 2018.

Whalley, L.K., Slater, E.J., Woodward-Massey, R., Ye, C., Lee, J. D., Squires, F., Hopkins, J. R., Dunmore, R. E., Shaw, M., Hamilton, J. F., Lewis, A. C., Mehra, A., Worrall, S. D., Bacak, A., Bannan, T. J., Coe, H., Ouyang, B., Jones, R. L., Crilley, L. R., Kramer, L. J., Bloss, W. J., Vu, T., Kotthaus, S., Grimmon, S., Sun, Y., Xu, Weiqi., Yue, S., Ren, L., Acton, W. J. F., Hewitt, C. N., Wang, X., Fu, P. and Heard, D. E : Evaluating the sensitivity of radical chemistry and ozone formation to ambient VOCs and NOx in Beijing, *Atmos. Chem. Phys Disc*, 2020

Whalley, L. K., Stone, D., Dunmore, R., Hamilton, J., Hopkins, J. R., Lee, J. D., Lewis, A. C., Williams, P., Kleffmann, J., and Laufs, S.: Understanding in situ ozone production in the summertime through radical observations and modelling studies during the Clean air for London project (ClearfLo), Atmospheric Chemistry and Physics, 18, 2547-2571, 2018.

Woodward-Massey, R., Slater, E. J., Alen, J., Ingham, T., Cryer, D. R., Stimpson, L. M., Ye, C., Seakins, P. W., Whalley, L. K., and Heard, D. E.: Implementation of a chemical background method for atmospheric OH measurements by laser-induced fluorescence: characterisation and observations from the UK and China, Atmos. Meas. Tech., 13, 3119–3146, https://doi.org/10.5194/amt-13-3119-2020, 2020.~~Woodward-Massey, R., Slater, E. J., Allen, J., Ingham, T., Cryer, D. R., Stimpson, L. M., Ye, C., Seakins, P. W., Whalley, L. K., and Heard, D. E.: Implementation of a chemical background method for atmospheric OH measurements by laser-induced fluorescence: characterisation and observations from the UK and China, Atmos. Meas. Tech, to be submitted 2019, 2019. 2019.~~

Zaveri, R. A., Easter, R. C., Fast, J. D., and Peters, L. K.: Model for simulating aerosol interactions and chemistry (MOSAIC), Journal of Geophysical Research: Atmospheres, 113, 2008.

Zhang, H., Wang, S., Hao, J., Wang, X., Wang, S., Chai, F., and Li, M.: Air pollution and control action in Beijing, Journal of Cleaner Production, 112, 1519-1527, 2016a.

Zhang, L., Wang, T., Zhang, Q., Zheng, J., Xu, Z., and Lv, M.: Potential sources of nitrous acid (HONO) and their impacts on ozone: A WRF-Chem study in a polluted subtropical region, Journal of Geophysical Research: Atmospheres, 121, 3645-3662, 2016b.

Formatted: Normal, Space After: 0 pt

Zhou, X., Gao, H., He, Y., Huang, G., Bertman, S. B., Civerolo, K., and Schwab, J.: Nitric acid photolysis on surfaces in low-NOx environments: Significant atmospheric implications, Geophysical Research Letters, 30, 2003.

Supplementary Material

1.1 Effect of deposition rate on the radical concentration and OH reactivity.

The MCM-base model, which uses a deposition rate of 0.1/MH, has been run again using several different deposition rates for the model generated intermediates. The effect of changing the deposition rate on the concentration of OH, HO_2 and RO_2, and also on the OH reactivity, kOH, is shown in Figure S1. Figure S1 shows that changing the deposition rate does not change the radical concentration significantly (less than 5%), and for the OH reactivity the maximum difference is 10%. The small changes in OH reactivity when the deposition rate is changed by a factor of 10 shows that the model intermediates do not contribute significantly to the OH reactivity, rather the OH reactivity is dominated by measured, primary emissions. It also shows that the deposition rate used in the MCM-base model run is appropriate as the OH reactivity is replicated well, and changes in the deposition rate do not change the total radical concentration significantly.

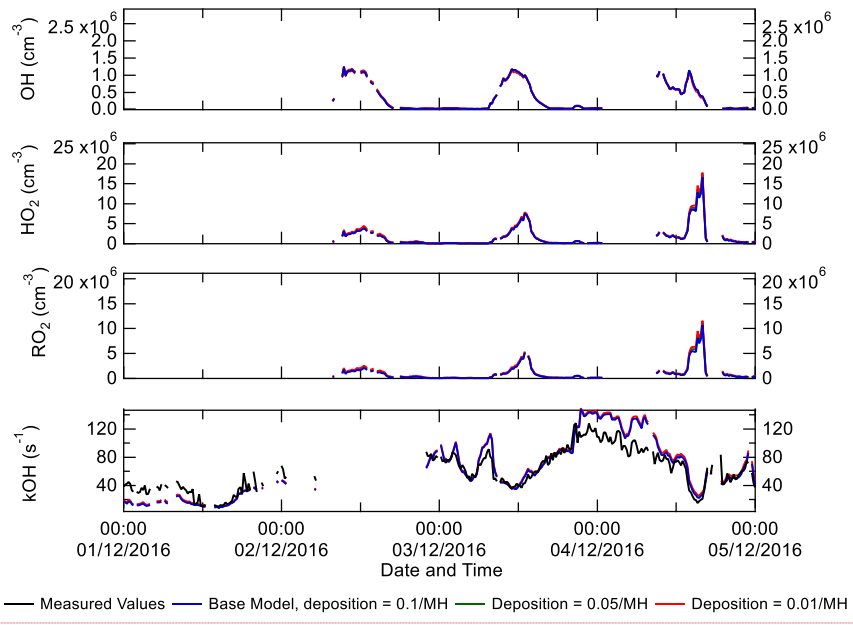

Figure S1. Effect of changing the deposition rate for model generated intermediates on the concentrations of OH, HO2 and RO2, and the OH reactivity, together with a comparison with the measurements.

For the winter campaign only, VOC species up to C7 were measured by the DC-GC-FID, but to test the sensitivity of the model to higher weight VOCs, measurements from a PTR-MS were incorporated into the MCM-base model to include C2 and C3 aromatic species. The species measured by the PTR-MS

Formatted: Font: (Default) +Body (Calibri)

Formatted: Subscript

Formatted: Subscript

Formatted: Font: (Default) +Body (Calibri)

Formatted: Font: (Default) +Body (Calibri)

Field Code Changed

and used in this model run, MCM-fVOC, were ethyl benzene(C2), propyl benzene(C3), isopropyl benzene(C3), 2-Ethyltoluene(C3), 3- Ethyltoluene(C3), 4-Ethyltoluene(C3), 1,3,5-trimethylbenzene(C3), 1,2,4- trimethylbenzene(C3) and 1,2,3-trimethylbenzene (C3). Since the DC-GC-FID measured three C2 aromatic species (o-xylene, m-xylene and p-xylene) the concentration of ethyl benzene was calculated through the difference between the PTR C2 and the DC-GC-FID C2 measurements. The model comparison between MCM-base and MCM-fVOC model runs is shown in Figure S2, and shows that introducing higher weight VOCs does not effect the radical concentration significantly, with the largest difference observed on the 5/12/2016 of ~7%.

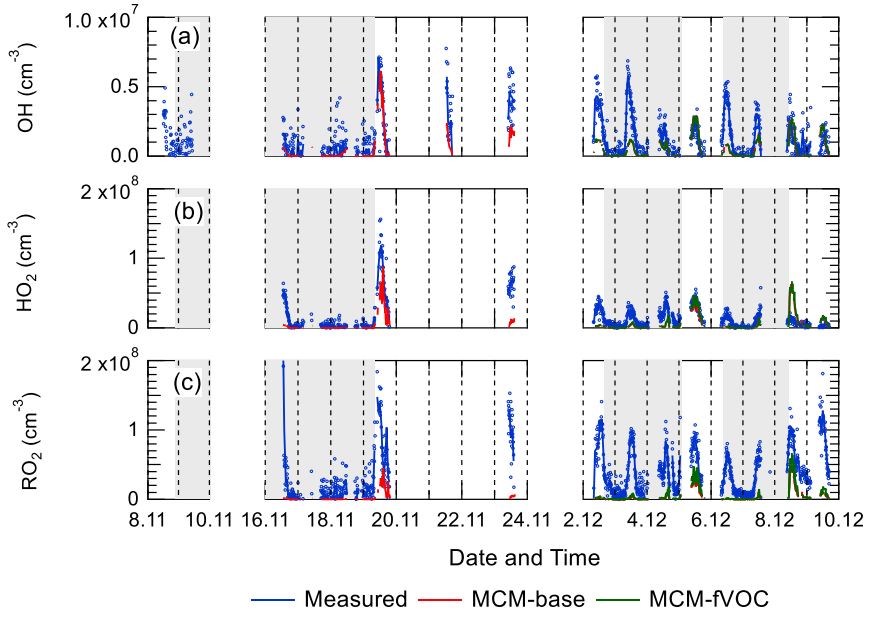

Figure S2. a) Comparison of measured OH with modelled OH from MCM-base and MCMfVOC. b) Comparison of measured HO2 with modelled HO2 from MCM-base and MCM-fVOC. c) Comparison of measured total RO2 with modelled total RO2 from MCM-base and MCMfVOC. It should be noted that PTR-MS data were only available from 24/11/2016 onwards, hence the data comparison is only between the 02/12/2016 – 10/12/2016.

The impact of the higher weight VOCs in the model on OH reactivity is shown in Figure S3, and shows that introducing the higher weight VOCs has a very small impact on modelled kOH, 3 Also the modelled kOH from the MCM-fVOC model run is in good agreement with measured kOH. These results show that the MCM-base model does not have a large sensitivity to the introduction of higher weight aromatic species.

Formatted: Font: (Default) +Body (Calibri)

Formatted: Font: (Default) +Body (Calibri)

Field Code Changed

Formatted: Font: (Default) +Body (Calibri)

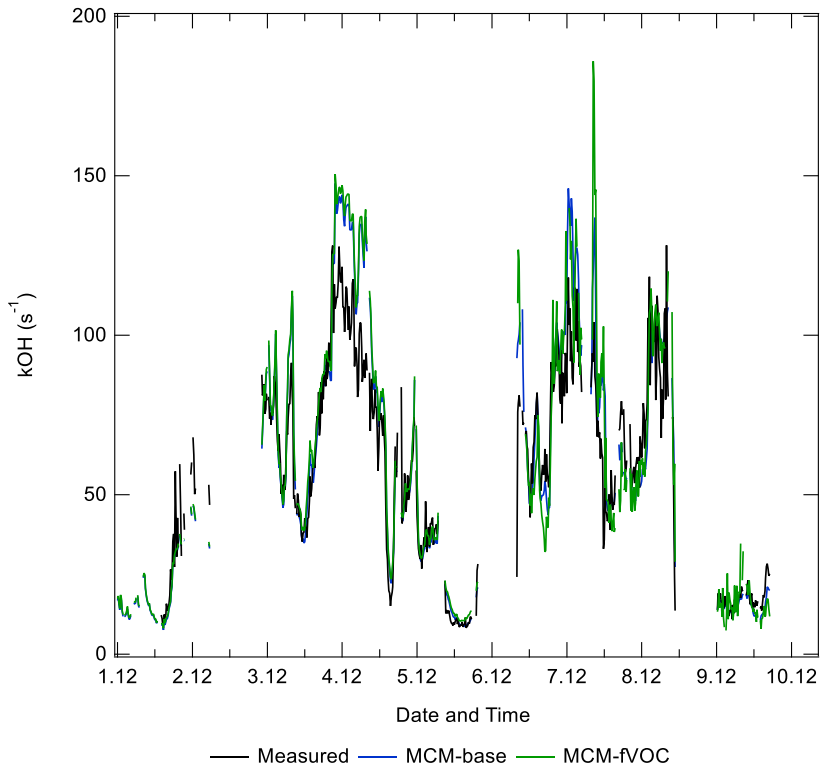

Figure S3. Comparison of measured OH reactivity (kOH) with modelled OH reactivity from the model runs MCM-base and MCM-fVOC.

S1.2 Primary radical production and comparison with previous campaigns.

As summarised in Table S1, several other winter-time campaigns have highlighted the importance of HONO, including the PUMA campaign (Emmerson et al., 2005) in Birmingham; the IMPACT campaign in Tokyo (Kanaya et al., 2007); the NACHTT campaign in Boulder (Kim et al., 2014) and the PMTACS-NY campaign in New York (Ren et al., 2006). These campaigns showed 36.2, 19, 80.4, and 46 % contribution to primary production of ROx from HONO. However, it should be noted that HONO was not measured during the PUMA campaign, so the percentage contribution to the primary production of radicals should be considered a lower limit as it is based upon modelled HONO (where only the reaction of OH + NO was considered), which is often an underestimate (Lee et al., 2015). As shown in Table 5, the Birmingham, Tokyo, New York and Surburban Beijing campaigns all show a high contribution towards RO_x production from ozonolysis, 63, 35, 42 and 28%, respectively, only the campaign in Boulder (5%) showed little contribution, which is similar to the observations made during APHH campaign. The Boulder campaign is the only one that showed a significant contribution (14.9 %)

Formatted: Font: (Default) +Body (Calibri)
Formatted: Font: (Default) +Body (Calibri)
Field Code Changed
Formatted: Justified
Formatted: Line spacing: 1.5 lines
Field Code Changed
Field Code Changed
Field Code Changed
Field Code Changed
Field Code Changed
Field Code Changed
Field Code Changed
Field Code Changed
Field Code Changed
Field Code Changed

to primary radical production from the reaction of $O(^1D) + H_2O$, whilst other winter campaigns show a contribution of less than 1%. The higher contribution from photolysis of O_3 during the Boulder campaign may be due to the campaign taking place in late February (spring) and, as shown in Table S1, photolysis rates, water vapour and temperature were all higher.

	PUMA, Birmingham, UK	**IMPACT, Tokyo, Japan**	**NACHTT, Boulder, USA**	**PMTACS-NY, New York, USA**	**BEST-ONE, Suburban Beijing, China**	**APHH, Central Beijing, China**	**PKU, Central Beijing, China**
Date	Jan – Feb 2000	Jan – Feb, 2004	Late Feb 2011	Jan – Feb, 2001	Jan – March 2016	Nov -Dec, 2016	Jan-Feb, 2017
OH (cm^{-3})	~1.7×10^6	~1.6×10^6	~2.7×10^6	~ 1.4×10^6	3×10^6	2.7×10^6	1.4×10^6
O_3 (ppbv)	37	20	40	20	30	15	10
$j(O^1D)$ (s^{-1})	~1×10^{-5}	~2.8 x 10-5	~1×10^{-5}	~5×10^{-6}	7×10^{-6}	~3×10^{-6}	-
$j(O_3)$ (%)	0.6	<1	14.7	1.1	<1	<1	<1
j(HONO) (%)	36.2[1]	19	80.4	65.5	46	68	86
Ozonolysis (%)	63.2	35	4.9	42.4	28	21	6
j(Carbonyls) (%)	22	23	-	-	9	8	7%[2]
j(HCHO) (%)	6	10	-	6	9	2	
Reference	Emmerson et al. (2005)	Kanaya et al. (2007)	Kim et al. (2014)	Ren et al. (2006)	Tan et al. (2018)	This work.	Ma et al. (2019)

Table S1. Summary of some previous measurements of OH, HO_2 and RO_2 that have taken place during the winter, and a summary of the major primary radical sources during these campaigns. All values are the noon average for each campaign. [1] This should be considered a lower limit due to no HONO measurements being made during the campaign. [2] Primary production from the sum of j(Carbonyls) and j(HCHO)."

S1.3 NO_2 and SO_2 oxidation during haze events

Secondary oxidation products, such as nitric acid and sulphuric acid, which partition to the aerosol phase, are major contributors towards the formation of secondary particulate matter (Huang et al., 2014). The OH measurements enable calculation of the rate of SO_2 and NO_2 oxidation *via* reaction with OH, to form gas-phase phase HNO_3 and H_2SO_4. Figure S4 shows that on average 1.5 ppbv/h and 0.03 ppbv/h of gas-phase NO_2 and SO_2 are oxidised to form acidic species, and that the oxidation increases in these haze periods caused by comparable OH concentration in and out of haze and, as shown in Figure S4, an increase in local NO_2 and SO_2 concentrations. NO_x can also be lost in the atmosphere by the formation of N_2O_5 (Evans, 2005) and subsequent hydrolysis, but this is uninportant in Beijing during winter due to the low levels of O_3. The reaction of OH + SO_2 in the gas-phase is the rate-

Formatted: Font: (Default) +Body (Calibri), 9 pt
Formatted: Justified
Formatted Table
Formatted: Font: (Default) +Body (Calibri), 9 pt
Formatted: Font: (Default) +Body (Calibri), 9 pt
Formatted: Font: (Default) +Body (Calibri), 9 pt
Formatted: Font: (Default) +Body (Calibri), 9 pt
Formatted: Font: (Default) +Body (Calibri), 9 pt
Formatted: Font: (Default) +Body (Calibri), 9 pt
Formatted: Font: (Default) +Body (Calibri), 9 pt
Formatted: Font: (Default) +Body (Calibri), 9 pt
Formatted: Font: (Default) +Body (Calibri), 9 pt
Formatted: Font: (Default) +Body (Calibri), 9 pt
Formatted: Font: (Default) +Body (Calibri), 9 pt
Formatted: Font: (Default) +Body (Calibri), 9 pt
Formatted: Font: (Default) +Body (Calibri), 9 pt
Formatted: Font: (Default) +Body (Calibri), 9 pt
Formatted: Font: (Default) +Body (Calibri), 9 pt
Formatted: Font: (Default) +Body (Calibri), 9 pt
Formatted: Font: (Default) +Body (Calibri), 9 pt
Formatted: Font: (Default) +Body (Calibri), 9 pt
Formatted: Font: (Default) +Body (Calibri), 9 pt
Formatted: Font: (Default) +Body (Calibri), 9 pt
Formatted: Font: (Default) +Body (Calibri), 9 pt
Formatted: Font: (Default) +Body (Calibri), 9 pt
Formatted: Font: (Default) +Body (Calibri), 9 pt
Formatted: Font: (Default) +Body (Calibri), 9 pt
Formatted: Font: (Default) +Body (Calibri), 9 pt
Field Code Changed
Formatted: Justified, Line spacing: 1.5 lines
Formatted: Font: (Default) +Body (Calibri)
Formatted: Line spacing: 1.5 lines
Formatted: Font: (Default) +Body (Calibri)
Formatted: Font: (Default) +Body (Calibri)
Formatted: Font: (Default) +Body (Calibri)
Formatted: Font: (Default) +Body (Calibri)

determining step in the formation SO_4^{-2}, so the H_2SO_4 formed in the gas-phase will partition in the aerosol phase (Barth et al., 2000). H_2SO_4 is effectively a non-volatile gas at atmospheric temperatures, and H_2SO_4 condensation onto pre-exsisiting particles is an irreversible kinetic process (Zaveri et al., 2008). Whilst HNO_3 is a semivolatile species and the gas-particle partitioning is highly sensitive to to meteorological conditions including: temperature, RH, particle size distribution, pH and particle composition. If the realtive humidity is lower than the deliquescence relative humidity (RH_d), then the HNO_3 that is formed in the gas phase reacts with NH_3 to form ammonium nitrate aersol (NH_4NO_3):

$$HNO_3(g) + NH_3(g) \rightleftharpoons NH_4NO_3(s) \qquad \text{S R1}$$

If the ambient RH exceeds the RH_d then HNO_3 and NH_3 dissolve into the aqueous phase (aq):

$$HNO_3(g) + NH_3(g) \rightleftharpoons NO_3^-(aq) + NH_4^+(aq) \qquad \text{S R2}$$

To take into account the reversible process, knowledge of the RH_d that marks the transition between the solid and the aqueous phase, and the equilibrium constant, K_p, for the two phase is required (Ackermann et al., 1998). The MADE module (modal aerosol dynamics model for europe) uses these thermodynamic parameters as given by (Mozurkewich, 1993), resulting in:

$$\text{In}\left(\frac{RH_d}{100}\right) = \frac{618.3}{T} - 2.551 \qquad \text{S E1}$$

for RH_d and:

$$\text{In}\left(K_p\right) = 118.87 - \frac{24084}{T} - 6.025\ \ln\left(T\right) \qquad \text{S E2}$$

for K_p. SE1 and SE2 shows that nitrate formation is favoured thermodynamically at low temperatures and high relative humidties (Ge et al., 2017). Previous measurements of SO_4^{-2} and NO_3^- made in wintertime Beijing suggests that photochemstry is important in the formation of nitrate aersol, but not the formation of sulphate (Ge et al., 2017; Sun et al., 2013).

Figure S4 also shows that the gas-phase oxidation of NO_2 increases under haze conditions, showing that nitrate formation is driven by photochemistry in haze events despite the lower photolysis rates. Similar conclusions have been made in Lu et al. (2019) from measurements during the BEST-ONE campaign; with SO_4^- aerosol predominantly driven by aqueous-phase chemistry whilst the production of NO_3^- aerosol from gas-phase oxidation of NO_2 with OH is important. The maximum production rate of HNO_3 observed during the BEST-ONE campaign is the same as the one calculated for the APHH campaign (3 ppbv hr^{-1}). The BEST-ONE campaign assumed all the gas-phase HNO_3 formed partitioned into the aerosol-phase due to the high relative humidity observed during the campaign.

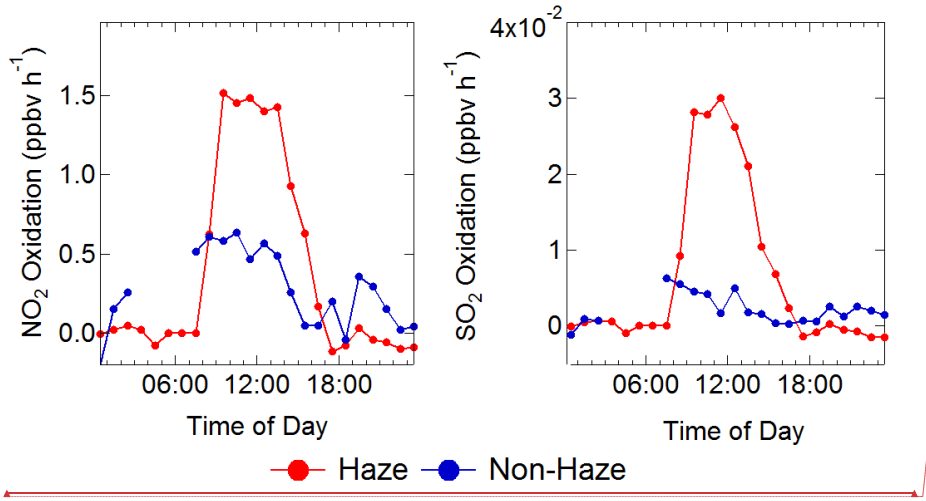

Figure S1. Average diel profiles of the rate of oxidation of NO_2 (left) and SO_2 (right) via reaction with OH in non-haze (blue) and haze (red) conditions.

S1.4 Estimating the contribution of HO_2NO_2 and $CH_3O_2NO_2$ to the RO_2 signal

In the main paper we do not apply a correction for a possible contribution of pernitric acid (PNA, HO_2NO_2) and methyl peroxy nitric acid (MPNA, $CH_3O_2NO_2$). The MPNA decomposition will contribute to the simple RO_2 and total RO_2 whilst the PNA contributes to the complex and total RO_2 measurements. The concentration of HO_2NO_2 and $CH_3O_2NO_2$ was modelled using the MCM-base model, then in agreement with the work by Fuchs et al.(2008) 0.43 % and 9 % of the HO_2NO_2 and $CH_3O_2NO_2$ is calculated to decompose and contribute to the RO_2 signal. The rate of decomposition in the Julich and Leeds RO_xLIF reactors is expected since the design and residence time (~1 second) are similar. The comparison of the measured total, simple and complex RO_2 with the corrected values is shown in Figure S5. Figure S5 shows that the correction from the decomposition of HO_2NO_2 and $CH_3O_2NO_2$ is ~6 %, ~8 % and 4 % for total, complex and simple RO_2, respectively.

Formatted: Font: (Default) +Body (Calibri)
Formatted: Font: (Default) +Body (Calibri)
Formatted: Font: 11 pt, Not Italic, Font color: Auto
Formatted: Caption, Justified
Formatted: Font: 11 pt, Not Italic, Font color: Auto
Formatted: Line spacing: 1.5 lines

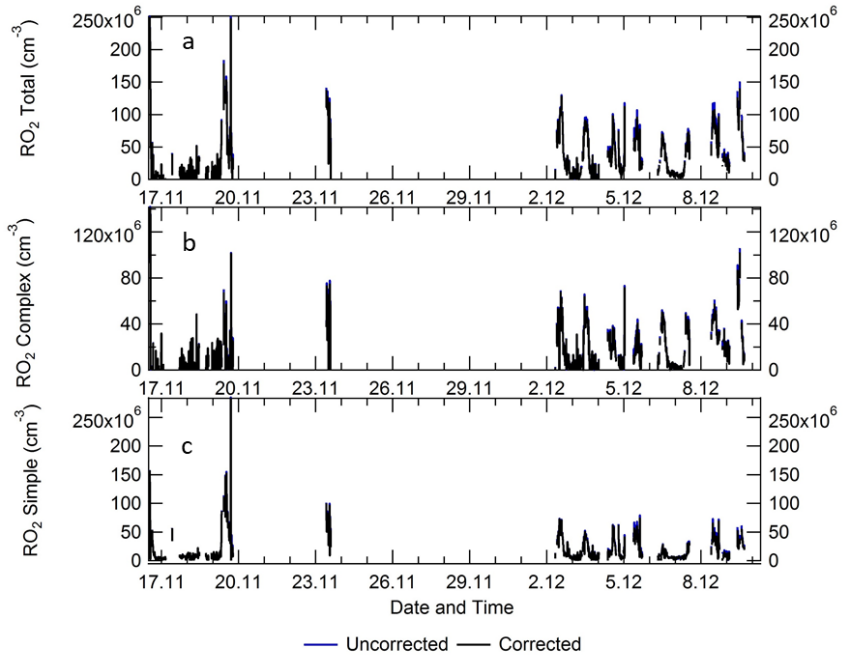

Figure S2. a) Timeseries comparison for measured total RO_2 (blue) and total RO_2 corrected (black) for the decomposition from HO_2NO_2 and $CH_3O_2NO_2$. b) Timeseries comparison for measured complex RO_2 (blue) and complex RO_2 corrected (black) for the decomposition from HO_2NO_2. c) Timeseries comparison for measured simple RO_2 (blue) and simple RO_2 corrected (black) for the decomposition from $CH_3O_2NO_2$.

S1.5 Exploring the sensitivity of the photostationary steady-state OH calculation to the HONO concentration.

The HONO concentration used to constrained both the model and the photostationary steady-state calculation was the suggested value by Crilley et al.(2019). During the campaign there was several HONO measurement present and, although the measurements agreed on temporal trends and variability (r^2>0.97), the absolute concentration diverged between 12 – 39%, the value suggested by Crilley et al. (2019) was the mean of the measurements. Since HONO is a primary source of OH the impact of the variable HONO concentration has been explored by increasing and decreasing the HONO by 40%, the results are shown in Figure S6. Figure S6 shows that the variation observed in the HONO measurements can increase/decrease the PSS up to 17% which is smaller than the error on the measured OH of ~26%.

Formatted: Line spacing: 1.5 lines

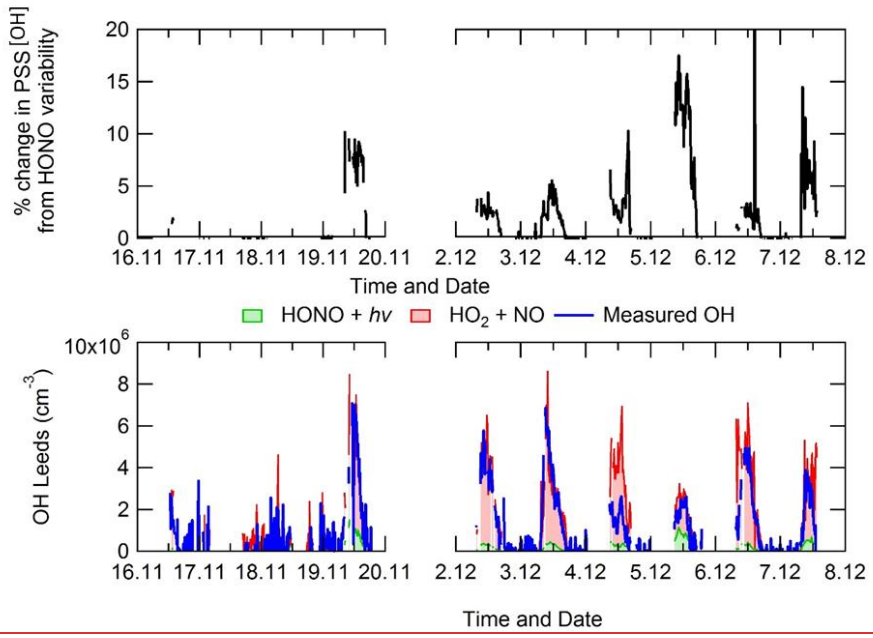

Figure S3. Top – Percentage change in the OH calculated from the PSS when the HONO is varied by 40%. Bottom – Comparison of the measured OH and the OH calculated from the PSS using the mean suggested value by Crilley et al. (2019).

S1.6 In-depth comparison of measured OH and OH calculated from the PSS on the 04/12 using measured and modelled OH reactivity.

On the 04/12/2016 the PSS calculation for OH is overpredicted by ~2.5 and the modelled OH reactivity is higher than the measured OH reactivity by an average of ~14 s^{-1}. The modelled OH reactivity was used in the PSS calculation for OH and a comparison between the PSS calculation using measured and modelled kOH and measured OH is shown in Figure S7. Figure S7 shows that whilst using the modelled OH reactivity does reduce the calculated PSS OH, the PSS using modelled kOH still overpredicts the measured OH by a factor of ~2.4. The large overprediction by the PSS suggests the differences between the PSS and measured OH on the 04/12/2016 stems from measurement problems and could be derived from issues with the OH, HO_2, HONO or NO measurements on this day.

Formatted: Caption

Formatted: Font: Not Bold

Formatted: Justified

Formatted: Line spacing: 1.5 lines

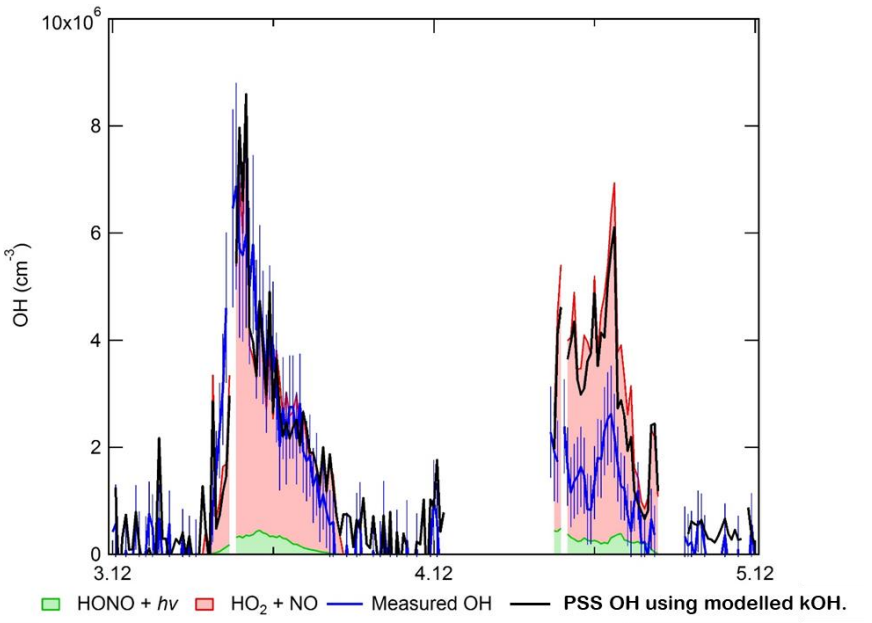

Figure S4. Comparison of measured OH (with errors, blue bars) with OH calculated from a photostationary steady-state (PSS) calculation using measured OH reactivity. The contributions towards OH production from HONO + hv (green) and HO_2 + NO (red) are shown, as well as the OH calculated using the PSS but with modelled OH reactivity (black)."

S1.7 The effects of the kRO2 + NO rate constant on the modelled radical species

Other than CH_3O_2 and $C_2H_5O_2$, rate constants for the reaction of many other RO_2 + NO is based on structure activity relationships (SARs) in the MCM and is lumped to kRO2NO and kAPNO (http://mcm.leeds.ac.uk/MCM/). The lumped rate constants kRO2NO and kAPNO were both decreased by a factor of 2 and 10 to investigate the effects on modelled OH, HO_2 and RO_2. The model where the rate constant for RO_2 + NO was decreased by a factor of 2 is titled MCM-kRO2-2, whilst the model where the rate constant was decreased by a factor of 10 is titled MCM-kRO2NO-10.

The comparison of measured values with modelled values (MCM-base, MCM-kRO2-2 and MCM-kRO2-10) is shown in Figure S8. Figure S8 shows that on certain days (e.g. 19/11, 5/12 and 9/12) when the model (MCM-base) could not reproduce the measured values of RO_2 the discrepancy between the measurements and the MCM-kRO2NO-10 model is almost reconciled. On these days the MCM-kRO2NO-10 does not really change the OH or HO_2 concentration from the base model. Onall days the MCM-base underpredicts the RO_2 concentration, and MCM-kRO2NO-10 does decrease the gap between measurements and modelled, compared to MCM-base. MCM-kRO2NO-2 does not significantly increase the total RO_2 concentration from MCM-base, unlike MCM-kRO2NO-10. Since

Formatted: Centered

Field Code Changed

Formatted: Line spacing: 1.5 lines

changing the rates of RO_2 + NO will be very dependent on the NO concentration, the ratio of measured:modelled radical concentration has been binned against the log of NO for MCM-base, MCM-kRO2NO-2 and MCM-kRO2NO-10 in Figure S9. Figure S9 shows similar results to the timeseries where at the lower concentration of NO (19/11, 5/12 and 9/12) the MCM-kRO2NO-10 can reproduce the RO_2 concentration. The results at higher [NO] show that decreasing the rate of RO_2 + NO improves the agreement between measured:modelled RO_2, especially for MCM-kRO2NO-10, but the observed RO_2 concentration is still underpredicted beyond 30 ppbv.

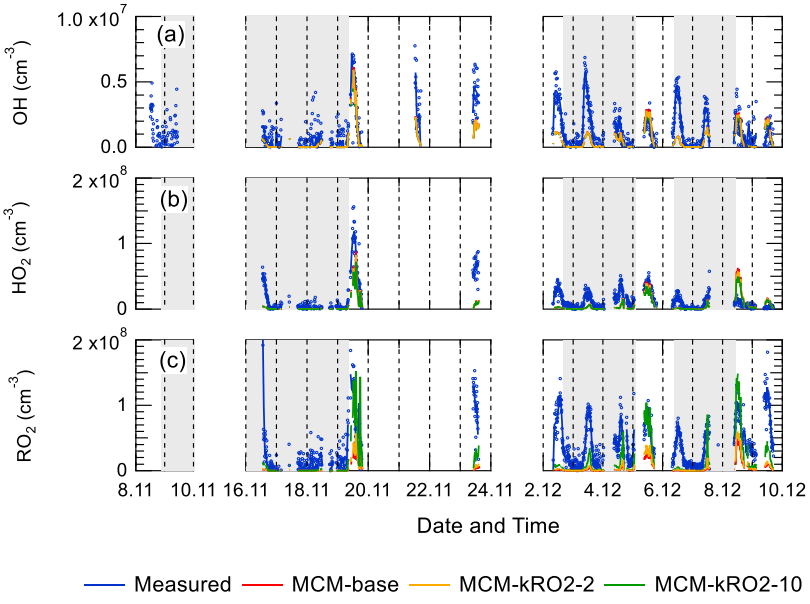

Figure S5. (a) Time-series comparison of measured values of OH with modelled OH concentrations from MCM-base, MCM-kRO23NO-2 and MCM-kRO2-10. (b) Time-series comparison of measured values of HO_2 with modelled HO_2 concentrations from MCM-base, MCM-kRO23NO-2 and MCM-kRO2-10. (c) Time-series comparison of measured values of total RO_2 with modelled total RO_2 concentrations from MCM-base, MCM-kRO23NO-2 and MCM-kRO2-10. The data sets are 15-minutes averaged.

The fact that the OH and HO_2 modelled concentrations do not change significantly for the models with reduced RO_2 + NO rate constant highlights that the enhanced RO_2 radicals (in MCM-kRO2-10) are not recycling into HO_2 or OH, even though the agreement for the RO_2 concentration is improved for these models (MCM-kRO2NO-2 and MCM-krO2NO-10). The lack of RO_2 recycling highlights that the RO_2 and RO radicals are terminating rather than propagating in the model.

This work highlights alternative chemistry and solutions must be applied for the two different NO regimes observed during the Beijing wintertime campaign. At high [NO] (above 10 ppbv) further

Formatted: Line spacing: 1.5 lines

reductions in the RO_2+NO rate constant would be required to reconcile the model with observations. However, at NO mixing ratios below 10 ppbv, further reductions in the RO_2+NO rate constant would lead to the model overpredicting the RO_2 concentration.

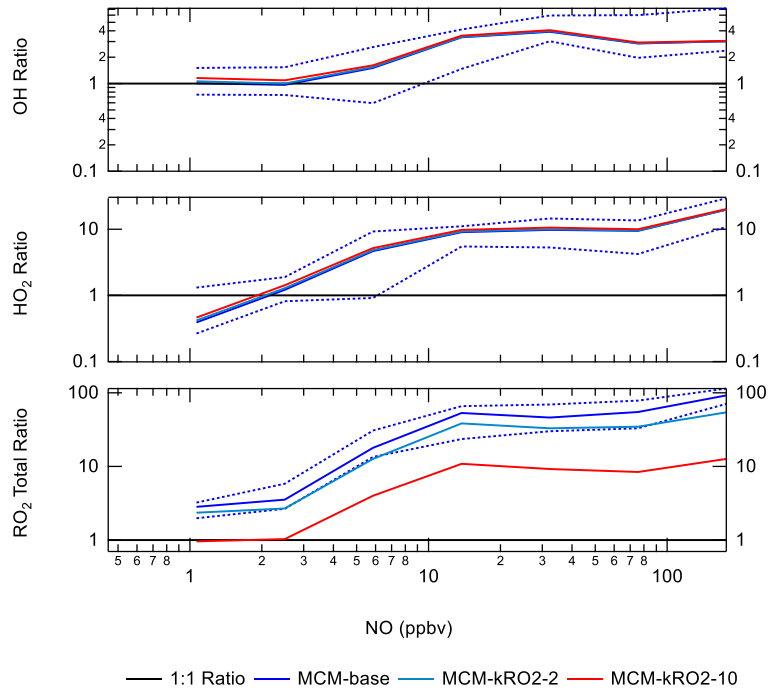

Figure S6. The ratio of measurement/model for OH (a), HO_2 (b) and RO_2 (c) across various NO concentrations for daytime values only ($j(O^1D) > 1 \times 10^{-6}$ s^{-1}). Light blue represents for results from MCM-kRO2NO-2, dark blue represents results from MCM-base and red represents results from MCM-kRO2NO-10.

S1.8 $ClNO_2$ and Cl concentration required to bridge the gap between measured and modelled total RO_2

Unfortunately, there were no $ClNO_2$ measurements during the winter campaign, and hence it was not possible to calculate a time series for Cl atoms formed from photolysis of $ClNO_2$ and to assess any additional RO_2 radicals generated. Using the model run where additional RO_2 source was added to reconcile the measurements and the model a rough calculation has shown that the $ClNO_2$ concentration would have to be on average ~5800 ppbv in order to close the gap between modelled and measured RO_2. Figure S10 shows the average diel of the calculated $ClNO_2$ and Cl concentration with peak at 1.4×10^4 ppbv and 1.6×10^6 molecule cm^{-3}, respectively. The $ClNO_2$ and Cl concentration have been calculated using SE3 – SE5:

Formatted: Caption

Formatted: Font: Not Bold, Pattern: Clear

Formatted: Line spacing: 1.5 lines

$$P'RO_2 = k_{VOC+Cl}[VOC][Cl] \quad \text{S E3}$$

$$[Cl] = \frac{P'RO_2}{k_{VOC+Cl}[VOC][Cl]} \quad \text{S E4}$$

$$[ClNO_2] = \frac{k_{VOC+Cl}[VOC][Cl]}{jClNO_2} \quad \text{S E5}$$

where k_{VOC+Cl} is a generic rate constant to represents the reaction of all VOCs with Cl which in this case is 4 x 10^{-12} molecule^{-1} cm^3 s^{-1}, [VOC] is the sum of the measured VOC concentration for the campaign and P'RO_2 is the calculated additional RO_2 used in MCM-PRO2 (see main paper section 4.2 for more details). The $ClNO_2$ required to bridge the gap between measured and modelled of RO_2 is ~3 orders of magnitude greater than the peak $ClNO_2$ concentration measured in suburban Beijing (2.9 ppbv) by Wang et al. (2018) suggesting that other additional primary source are needed in the model besides Cl chemistry .

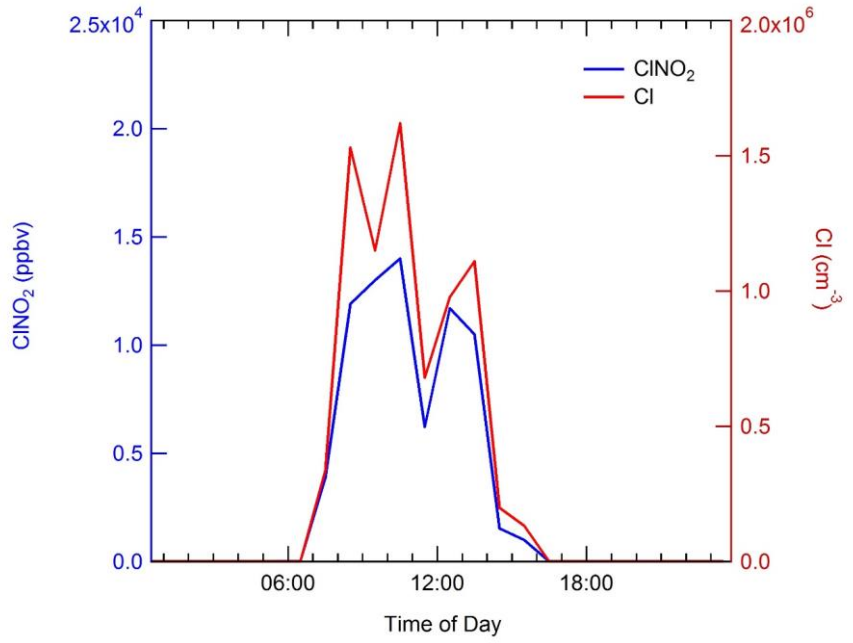

Figure S7. Average diel of the $ClNO_2$ and Cl atom concentration required to bridge the gap between measured and modelled RO_2. The $ClNO_2$ and Cl concentrations have been calculated from the additional primary source of RO_2 added to the MCM-PRO2 model run, see section 4.2 in the main paper for more details.

Formatted: Line spacing: 1.5 lines

Formatted: Line spacing: 1.5 lines

Formatted: Line spacing: 1.5 lines

References

Ackermann, I. J., Hass, H., Memmesheimer, M., Ebel, A., Binkowski, F. S., and Shankar, U.: Modal aerosol dynamics model for Europe: Development and first applications, Atmospheric environment, 32, 2981-2999, 1998.

Barth, M., Rasch, P., Kiehl, J., Benkovitz, C., and Schwartz, S.: Sulfur chemistry in the National Center for Atmospheric Research Community Climate Model: Description, evaluation, features, and sensitivity to aqueous chemistry, Journal of Geophysical Research: Atmospheres, 105, 1387-1415, 2000.

Crilley, L. R., Karmer, L. J., Ouyang, B., Duan, J., Zhang, W., Tong, S., Ge, M., Ge, K. T., Qin, M., Xie, P., Shaw, M. D., Lewis, A. C., Mehra, A., Bannan, T. J., Worrall, S. D., Priestley, M., Bacak, A., Coe, H., Allan, J., Percival, C. J., Popoola, O. A. M., Jones, R. L., and Bloss, W. J.: Intercomparison of nitrous acid (HONO) measurement techniques in a megacity (Beijing), AMT, 2019. 2019.

Emmerson, K., Carslaw, N., and Pilling, M.: Urban atmospheric chemistry during the PUMA campaign 2: Radical budgets for OH, HO 2 and RO 2, Journal of atmospheric chemistry, 52, 165-183, 2005.

Fuchs, H., Holland, F. and Hofzumahaus, A., 2008. Measurement of tropospheric RO 2 and HO 2 radicals by a laser-induced fluorescence instrument. *Review of Scientific Instruments*, *79*(8), p.084104.

Ge, X., He, Y., Sun, Y., Xu, J., Wang, J., Shen, Y., and Chen, M.: Characteristics and formation mechanisms of fine particulate nitrate in typical urban areas in China, Atmosphere, 8, 62, 2017.

Huang, R.-J., Zhang, Y., Bozzetti, C., Ho, K.-F., Cao, J.-J., Han, Y., Daellenbach, K. R., Slowik, J. G., Platt, S. M., and Canonaco, F.: High secondary aerosol contribution to particulate pollution during haze events in China, Nature, 514, 218, 2014.

Kanaya, Y., Cao, R., Akimoto, H., Fukuda, M., Komazaki, Y., Yokouchi, Y., Koike, M., Tanimoto, H., Takegawa, N., and Kondo, Y.: Urban photochemistry in central Tokyo: 1. Observed and modeled OH and HO2 radical concentrations during the winter and summer of 2004, Journal of Geophysical Research: Atmospheres, 112, 2007.

Kim, S., VandenBoer, T. C., Young, C. J., Riedel, T. P., Thornton, J. A., Swarthout, B., Sive, B., Lerner, B., Gilman, J. B., and Warneke, C.: The primary and recycling sources of OH during the NACHTT-2011 campaign: HONO as an important OH primary source in the wintertime, Journal of Geophysical Research: Atmospheres, 119, 6886-6896, 2014.

Lee, J., Whalley, L., Heard, D., Stone, D., Dunmore, R., Hamilton, J., Young, D., Allan, J., Laufs, S., and Kleffmann, J.: Detailed budget analysis of HONO in central London reveals a missing daytime source, Atmospheric Chemistry and Physics Discussions, 15, 22097-22139, 2015.

Lu, K., Fuchs, H., Hofzumahaus, A., Tan, Z., Wang, H., Zhang, L., Schmitt, S., Rohrer, F., Bohn, B., and Broch, S.: Fast photochemistry in wintertime haze: Consequences for pollution mitigation strategies, Environmental science & technology, 2019. 2019.

Ma, X., Tan, Z., Lu, K., Yang, X., Liu, Y., Li, S., Li, X., Chen, S., Novelli, A., and Cho, C.: Winter photochemistry in Beijing: Observation and model simulation of OH and HO_2 radicals at an urban site, Science of The Total Environment, 685, 85-95, 2019.

Mozurkewich, M.: The dissociation constant of ammonium nitrate and its dependence on temperature, relative humidity and particle size, Atmospheric Environment. Part A. General Topics, 27, 261-270, 1993.

Ren, X., Brune, W. H., Mao, J., Mitchell, M. J., Lesher, R. L., Simpas, J. B., Metcalf, A. R., Schwab, J. J., Cai, C., and Li, Y.: Behavior of OH and HO2 in the winter atmosphere in New York City, Atmospheric Environment, 40, 252-263, 2006.

Formatted: Font: Bold

Sun, Y., Wang, Z., Fu, P., Yang, T., Jiang, Q., Dong, H., Li, J., and Jia, J.: Aerosol composition, sources and processes during wintertime in Beijing, China, Atmospheric Chemistry and Physics, 13, 4577-4592, 2013.

Tan, Z., Rohrer, F., Lu, K., Ma, X., Bohn, B., Broch, S., Dong, H., Fuchs, H., Gkatzelis, G. I., and Hofzumahaus, A.: Wintertime photochemistry in Beijing: observations of RO x radical concentrations in the North China Plain during the BEST-ONE campaign, Atmospheric Chemistry and Physics, 18, 12391-12411, 2018.

Wang, X., Wang, H., Xue, L., Wang, T., Wang, L., Gu, R., Wang, W., Tham, Y.J., Wang, Z., Yang, L. and Chen, J., 2017. Observations of N_2O_5 and $ClNO_2$ at a polluted urban surface site in North China: High N2O5 uptake coefficients and low ClNO2 product yields. *Atmospheric environment*, *156*, pp.125-134.

Zaveri, R. A., Easter, R. C., Fast, J. D., and Peters, L. K.: Model for simulating aerosol interactions and chemistry (MOSAIC), Journal of Geophysical Research: Atmospheres, 113, 2008.

Formatted: Normal, Left

Formatted: Normal, Justified, Tab stops: 4.13 cm, Left